UiT THE ARCTIC UNIVERSITY OF NORWAY

Department of Geosciences

U-Pb zircon provenance of metamorphosed clastic sediments in the Brusque Metamorphic Complex, Dom Feliciano Belt, southeastern Brazil

—

Ragnhild Eiesland

Master's thesis in geology, GEO-3900

May 2018

UiT The Arctic University of Norway

Faculty of Science and Technology

Department of Geosciences

GEO-3900

Master thesis in Hard Rock Geology

U-Pb zircon provenance of metamorphosed clastic sediments in the Brusque Metamorphic Complex, Dom Feliciano Belt, southeastern Brazil

Submitted by : Ragnhild Eiesland

Primary supervisor : Prof. Jiří Konopásek

Co-supervisor : Prof. Maria de Fátima Bitencourt

Tromsø, May 2018

Acknowledgements

This work was supported by the Norwegian Centre for International Cooperation in Education (SIU) and the Coordenação de Aperfeicoamento de Pessoal de Nível Superior (CAPES) in Brazil through the grant project no. UTF-2016-CAPES-SIU10024.

To Jiří Konopásek, thank you for your guidance and supervision during the past year. I am grateful for the opportunity you gave me to work with such an interesting project, and for introducing me to the geology of Brazil. I am thankful to Jack James Percival, for always being positive and taking his time to answer all of my questions. You rock!

To Maria de Fátima Bitencourt, Luana Moreira Florisbal, Roberto Sacks de Campos, Giuseppe Betino de Toni and Matheus Battisti, thank you for making the field trip in Brazil so wonderful! Giuseppe, thank you for all the fun conversations and for always sharing your *mate*.

To Jiří Sláma, thank you for your warm welcome in Prague and for your help with the LA-ICP-MS analysis. To Kai Neufeld, thank you for your help with the CL imaging. To Trine Merete Dahl and Karina Monsen at the laboratory at the Department of Geosciences in Tromsø, thank you for your expertise. To Martina Suppersberger Hamre at the University of Bergen, thank you for your contribution during the mineral separation process.

I am grateful to all the amazing people I have got to known during these five years as a student, and I will always look fondly on my time in Sogndal and Tromsø. Elizabeth Joa, Katrine Eliassen, Sigrid Klakken, Birgitte Andrea Fagerheim and Anne Paavilainen, thank you for all the laughs and beautiful hikes in the mountains. To my fellow master students, thank you for the cozy coffee breaks and late night talks towards the end. I am grateful to Caroline Asvald, for her good hugs and kind words. I am glad that I got to experience Brazil and Prague with you. Marius Jenssen, thank you for being a great office-mate!

To Kristin Norman Tønsberg, thank you for always being there for me. To my ever-loving family and boyfriend, Bjørn Ola Sveen Volden, thank you for all your encouragement and support through this adventure. I am forever grateful!

To Profs. Stein Bondevik and Winfried Dallmann, thank you for inspire me to keep on following the rocky path of geology.

Tromsø, May 2018

Ragnhild Eiesland

Abstract

The Brusque Metamorphic Complex is situated in the northern part of the Dom Feliciano Belt in the state of Santa Catarina, southeastern Brazil. The complex is composed of Neoproterozoic sequences of volcanic and sedimentary rocks, which were folded and metamorphosed at greenschist to low-amphibolite facies conditions. U-Pb dating of detrital zircon grains in five samples of clastic metasedimentary rocks in the Brusque Metamorphic Complex has revealed a mixed source for the detritus in the sedimentary succession. Two quartzite samples, suggested as representing the lower part of the succession related to early Neoproterozoic rifting, show detrital zircon ages consistent with erosion of the Paleoproterozoic-Archean basement of the Río de la Plata and Congo cratons, as well as erosion of an inferred Mesoproterozoic volcano-sedimentary cover of these cratonic units. Two other quartzite samples, suggested as representing the upper part of the succession, yielded predominantly Paleoproterozoic zircon ages with affinity to the Congo and Río de la Plata cratons, as well as the Luís Alves Microplate. The suppression of Mesoproterozoic detrital zircons towards higher stratigraphic level in the sedimentary succession of the Brusque Metamorphic Complex is suggested to reflect gradual erosion of the Mesoproterozoic cover. A phyllite sample, containing mostly late Neoproterozoic and only small number of Paleoproterozoic zircons, is interpreted as being a part of the adjacent Itajaí Basin molasse sediments rather than the Brusque Metamorphic Complex. While the Neoproterozoic zircons in this sample are suggested as derived from the Coastal-Punta del Este Terrane and the Florianópolis Batholith, the Paleoproterozoic zircons probably represent second-cycle grains derived from erosion of the Brusque Metamorphic Complex itself. Detrital zircon grains in the metasedimentary succession of the Central Kaoko Zone in the Kaoko Belt in northern Namibia, at the opposite side of the South Atlantic Ocean, reveal very similar age signals as those observed in the studied samples of the Brusque Metamorphic Complex. Such similarity suggests an origin in a common sedimentary basin, where the Brusque Metamorphic Complex represented a western margin and the Central Kaoko Zone an eastern margin of a developing early Neoproterozoic rift system.

Contents

1 Introduction

The Brusque Metamorphic Complex in the Dom Feliciano Belt (South America) and the Central Kaoko Zone in the Kaoko Belt (Africa) (Fig. 3) both represent early Neoproterozoic rift basins filled with volcanic and sedimentary rocks, which subsequently have been metamorphosed and deformed during the Brasiliano/Pan-African orogeny (Basei et al., 2000; Goscombe et al., 2003a, b). While Konopásek et al. (2014, 2017) have suggested possible sources for the clastic material in the Central Kaoko Zone, questions still remain regarding the source of the sedimentary succession in the Brusque Metamorphic Complex. Such questions could be answered by a provenance study, by which the source, as well as the transport and depositional history of the original sediments, may be recognized (Košler et al., 2002).

This study presents new geochronological data obtained for metamorphosed clastic sediments in the Brusque Metamorphic Complex, with the aim to investigate possible source regions for the detrital material available for sedimentation of the complex. To address this problem, metasedimentary rocks have been collected from different parts of the Brusque Metamorphic Complex. Detrital zircon grains have been extracted and dated by the Laser Ablation-Inductively Coupled Plasma-Mass Spectrometry (LA-ICP-MS) method. This method is a popular analytical technique used for U-Pb isotopic dating in sedimentary provenance studies. It is often applied on heavy minerals like zircon ($ZrSiO_4$), which is a highly refractory mineral and common as detrital grains in sedimentary rocks (Deer et al., 2013).

Besides interpreting the provenance of the sampled metasedimentary rocks, a new lithostratigraphy of the Brusque Metamorphic Complex is proposed. A tectonic model of evolution of the area between the Brusque Metamorphic Complex (eastern Río de la Plata Craton margin, South America) and the Central Kaoko Zone (western Congo Craton margin, Africa), with emphasis on evolution of sedimentary rocks, is also suggested.

1.1 Previous geochronology in the study area

Hartmann et al. (2003) analyzed 27 zircon grains from a quartzite sample collected in the northern part of the Brusque Metamorphic Complex. The detrital zircon grains yielded 25 concordant U-Pb dates between ca. 2.22 and 2.02 Ga, with clusters around 2.17, 2.14 and 2.10 Ga.

Basei et al. (2006) dated detrital zircons from a garnet-biotite schist sample in the southern part of the Brusque Metamorphic Complex and yielded ages between ca. 1.90 and 1.00 Ga, with maxima around 1.85, 1.50 and 1.05 Ga. They also dated a sample from a level of sedimentary rocks with mafic tuff contribution which contained ca. 2.20-1.80 Ga detrital zircon grains.

Basei et al. (2008b) obtained 22 zircon dates for a mica schist sample with volcanogenic contribution, and from a garnet-biotite schist sample, collected in the southern and northern part of the Brusque Metamorphic Complex, respectively. The samples yielded ages between 2.25 and 1.70 Ga (eight grains), 1.50 and 1.30 Ga (six grains) and 1.30 and 1.10 Ga (four grains), with clusters around 2.25, 2.05, 1.85, 1.50, 1.40 and 1.20 Ga. Also, two zircon grains revealed Neoproterozoic ages of ca. 570 and 540 Ma.

Basei et al. (2008a) pointed out that the typical age signal for detrital zircons in the sedimentary succession of the Brusque Metamorphic Complex is in the time interval of 1.99-2.14 Ga. Based on previous geochronological studies of metasedimentary rocks in the complex, it has been suggested that the Archean-Paleoproterozoic detrital zircon grains are sourced in the Río de la Plata Craton and Luís Alves Microplate, whereas those of Mesoproterozoic age are derived from the African continent (Basei et al., 2008b, 2018).

1.2 Geological setting

The formation of the supercontinent Rodinia occurred in the late Mesoproterozoic at ca. 1100 Ma, and there is general agreement that this supercontinent included about all the Earth's continental crust at that time (e.g. Pisarevsky et al., 2003; Li et al., 2008; Evans, 2009). In the period between ca. 800 and 700 Ma, Rodinia underwent rifting and fragmented into different continental terranes, including the Congo-São Francisco, Kalahari and Río de la Plata cratons which most likely occupied a marginal position of the supercontinent (Oriolo et al., 2017; Konopásek et al., in press) (Fig. 1). However, based on paleomagnetic data, it is suggested that the Congo-São Francisco and Río de la Plata cratons never completely separated, but remained in contact along the São Francisco-Congo cratonic bridge (Porada, 1989).

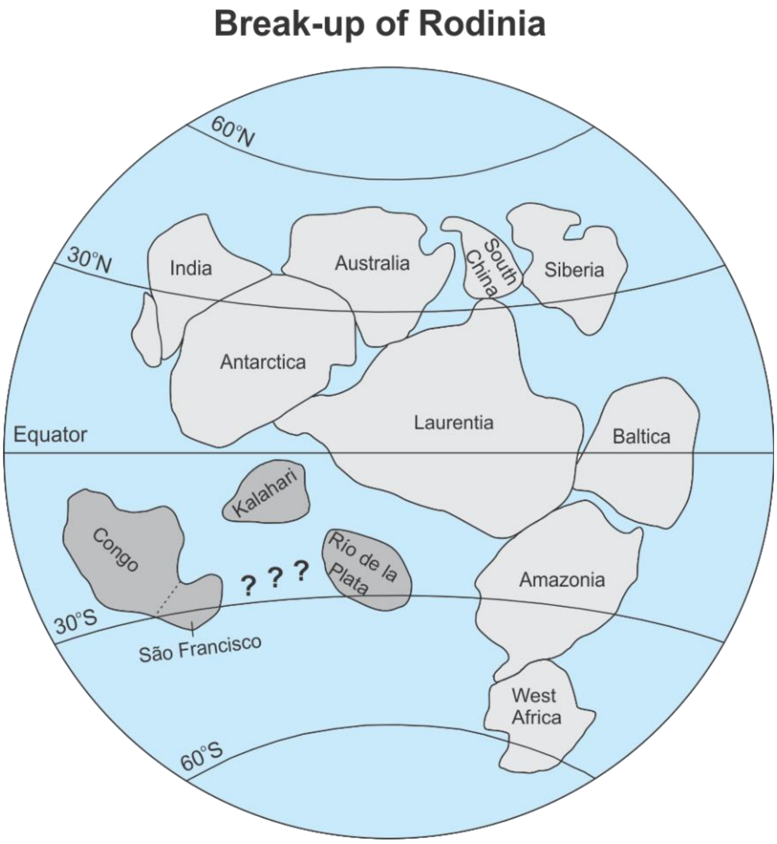

Fig. 1. Model of the supercontinent Rodinia during its rifting process, with the Congo-São Francisco, Kalahari and Río de la Plata cratons (dark gray) situated at the margin. The question marks represent the uncertainty wether the Congo-São Francisco and Río de la Plata cratons were completely separated during the rifting. Modified after Meert and Torsvik (2003) and Oriolo et al. (2017).

The rifting between the Congo and Kalahari cratons (part of present Africa) and the Río de la Plata Craton (part of present South America) is evident by the occurrence of rift-related volcanism and associated sedimentation along the opposite margins of the South Atlantic Ocean. The rift-related volcanic rocks at the African side are dated between ca. 840 and 710 Ma (Frimmel et al., 1996, 2001; Konopásek et al., 2014), and similar ages were obtained on the South American side (Basei et al., 2008a; Saalmann et al., 2011). Rift-related igneous rocks in the Coastal-Punta del Este Terrane have been dated at ca. 820-770 Ma (Konopásek et al., 2008, in press; Oyhantçabal et al., 2009; Lenz et al., 2011), and Konopásek et al. (in press) interpreted the terrane as being the axial part of the rift between the present day South America and Africa. Hoffman et al. (1996) dated rift-related magmatic rocks along the southern Congo Craton margin at ca. 746 and 756 Ma, which they suggested to reflect about 10 Ma of rifting between the Congo and Kalahari cratons.

Konopásek et al. (2017) suggested that the potential oceanic domain, the proto-South Atlantic Ocean of Porada (1979) or the Adamastor Ocean of Hartnady et al. (1985), that formed between Africa and South America after continental break-up, must have been narrow as the time of opening and closure of the ocean is assumed to be less than 25 Ma. The closure of the Neoproterozoic ocean was due to the convergence of the West Africa, Amazonia, Río de la Plata, Kalahari and Congo-São Francisco cratons, which started to collide at ca. 650 Ma and led to the assembly of western Gondwana (Fig. 2a). Consequently, several

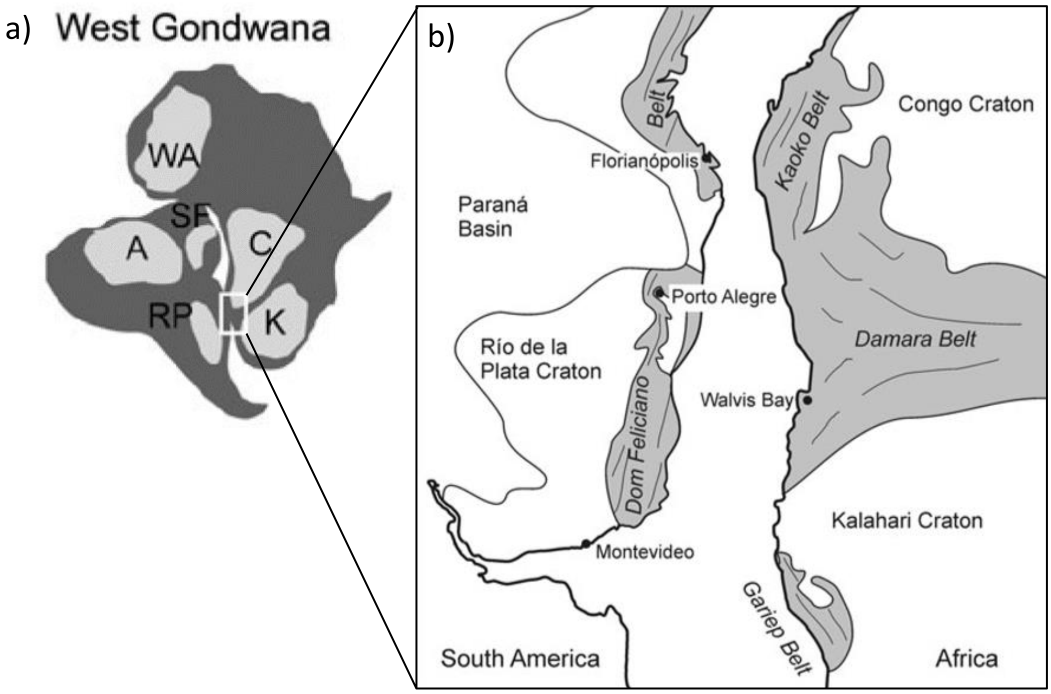

Fig. 2. a) Illustration of the West Africa (WA), Kalahari (K) and Congo (C) cratons of the African continent and the Amazonia (A), Río de la Plata (RP) and São Francisco (SF) cratons of the South American continent, making up the western Gondwana. b) Position of the cratons and extent of the orogenic belts (dark grey) after the opening of the South Atlantic Ocean. Modified after Oyhantçabal et al. (2011) and Ulrich et al. (2011).

orogenic belts formed along the borders of the cratons and among these are the Kaoko, Damara and Gariep belts in southern Africa (Pan-African orogeny) and the Dom Feliciano Belt in South America (Brasiliano orogeny) (Porada, 1989) (Fig. 2b). Goscombe and Gray (2007, 2008) suggested that the Coastal Terrane acted as an arc/back-arc system along the western margin of the Congo Craton at ca. 650-630 Ma. Collisional evolution in the Kaoko and Dom Feliciano belts at ca. 580-550 Ma led to the thrusting of the Coastal Terrane over the Congo Craton margin (Goscombe and Gray, 2007).

The Coastal-Punta del Este Terrane occurs in the center of the Kaoko-Dom Feliciano-Gariep orogenic system. After the opening of the South Atlantic Ocean, the Coastal Terrane represents the westernmost unit of the Kaoko Belt and the Punta del Este Terrane is the easternmost unit of the Dom Feliciano Belt (Konopásek et al., in press) (Fig. 3).

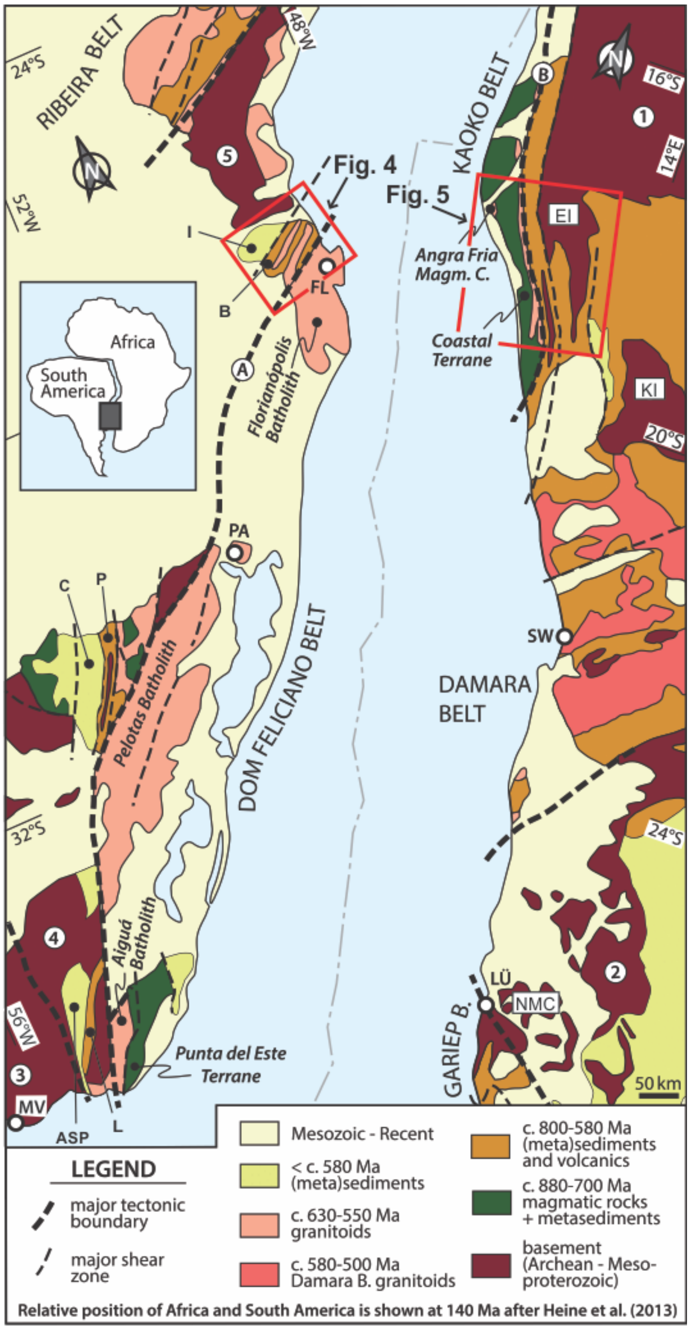

Fig. 3. Simplified geological map of the central part of the Dom Feliciano-Gariep-Kaoko orogeny, exposed along the coasts of the South Atlantic Ocean. 1 - Congo Craton; 2 - Kalahari Craton; 3 - Río de la Plata Craton – Piedra Alta Terrane; 4 - Río de la Plata Craton – Nico Pérez Terrane; 5 - Luís Alves Microplate. EI - Epupa Inlier; KI - Kamanjab Inlier; NMC - Namaqua Metamorphic Complex. Basins: ASP - Arroyo del Soldado-Piriápolis; C – Camaquã; I – Itajaí. Metamorphic complexes: L – Lavalleja; P – Porongos; B – Brusque. (A) Sierra Ballena-Dorsal Canguçu-Major Gercino shear zone; (B) Village-Three Palm shear zone system. FL – Florianópolis; PA – Porto Alegre; MV – Montevideo; LÜ – Lüderitz; SW – Swakopmund. The red squares show the location of the Brusque Metamorphic Complex (Fig. 4) and the Kaoko Belt (Fig. 5). Modified after Konopásek et al. (2014, 2016) and Basei et al. (2000).

1.2.1 The Dom Feliciano Belt

The Dom Feliciano Belt, situated at the eastern margin of the Río de la Plata Craton, extends for ca. 1200 km along the coast of southeastern Brazil and eastern Uruguay (Basei et al., 2011a) (Fig. 3). The belt is divided into four geotectonic units. From southeast to northwest these are: the Punta del Este Terrane, Granite Belt, Schist Belt and Foreland Belt (Preciozzi et al., 1999; Basei et al., 2000).

The high-grade Punta del Este Terrane comprises orthogneisses, paragneisses, amphibolites and migmatites, and is separated from the Nico Pérez Terrane of the Río de la Plata craton by the Sierra Ballena Shear Zone (Oyhantçabal et al., 2010). Metaigneous rocks of the terrane provide protolith ages between ca. 800 and 770 Ma, and rims of protolith zircons representing recrystallization during metamorphism have been dated between ca. 670 and 620 Ma (Oyhantçabal et al., 2009; Basei et al., 2011b; Lenz et al., 2011; Masquelin et al., 2012).

The Granite Belt is an igneous complex, which is subdivided into the Florianópolis (Santa Catarina State, Brazil), the Pelotas (Rio Grande do Sul State, Brazil) and the Aiguá (Uruguay) batholiths. These Neoproterozoic batholiths consist of calc-alkaline to alkaline granitoid rocks and reveal a decrease in age from north to south, i.e. from the Florianópolis Batholith to the Aiguá Batholith (Basei et al., 2000). The Granite Belt is considered as being either roots of a magmatic arc (e.g. Porada, 1989) or the result of post-collisional magmatism (e.g. Bitencourt and Nardi, 2000).

The Schist Belt is subdivided into the Brusque (Santa Catarina State, Brazil), the Porongos (Rio Grande do Sul State, Brazil) and the Lavalleja (Uruguay) metamorphic complexes (Basei et al., 2000). The metamorphic complexes comprise pre-collisional Neoproterozoic sequences of volcanic and sedimentary rocks, which have been folded and metamorphosed at greenschist to low-amphibolte facies (Oyhantçabal et al., 2011). In addition, the sequences have been intruded by multiple post-tectonic granitoid rocks (Basei et al., 2008b).

The Foreland Belt is subdivided into the Itajaí (Santa Catarina State, Brazil), Camaquã (Rio Grande do Sul State, Brazil) and Arroyo del Soldado-Piriápolis (Uruguay) basins (Basei et al., 2000). The basins consist of sedimentary and volcanic rocks deposited in the Ediacaran and metamorphosed at low grade around 530 Ma (Gaucher et al., 2003; Basei et al., 2011a, c).

The Río de la Plata Craton is divided by the Saranda del Yi Shear Zone into the western Piedra Alta and eastern Nico Pérez terranes (Oyhantçabal et al., 2010). To the north of the Río de la Plata Craton, the Luís Alves Microplate is situated (Fig. 3). The Luís Alves Microplate have been suggested as representing an exotic terrane that was attached to the Río de la Plata Craton during the Neoproterozoic assembly of western Gondwana (e.g. Basei et al., 2009). However, it is also thought that the Luís Alves Microplate was already attached to the Río de la Plata Craton prior to the assembly (e.g. Guadagnin et al., 2010). In any case, the Río de la Plata Craton and Luís Alves Microplate served as a foreland of the Dom Feliciano Belt during its development. Both continental units are predominantly Paleoproterozoic in age, and their basement consist of gneissic and migmatitic rocks (Basei et al., 2000).

1.2.1.1 The Brusque Metamorphic Complex

The Brusque Metamorphic Complex constitutes the schist belt in the northern part of the Dom Feliciano Belt, and is predominantly trending NE-SW (Basei et al., 2011a) (Figs. 3 and 4). The complex is bounded to the northwest by the Itajaí-Perimbó Shear Zone (IPSZ), where it is in contact with rocks of the Itajaí Basin. To the southeast, the complex is bounded by the Major Gercino Shear Zone (MGSZ) along which the granitoids of the Florianópolis Batholith are intruded (de Campos et al., 2012).

The Brusque Metamorphic Complex comprises metamorphosed volcano-sedimentary sequences, deposited in a predominantly marine environment (Chemale et al., 1995). Basei et al. (2011a) proposed a division of the complex into the basal Rio do Oliveira (metavolcanosedimentary units), the intermediate Botuverá (metasedimentary units) and the upper Rio da Areia (metacarbonatic units) formations. The Brusque Metamorphic Complex have been intruded by post-collisional Neoproterozoic granitoids known as the São João Batista, Valsungana and Nova Trento suites (Basei et al., 2000; Florisbal et al., 2012b).

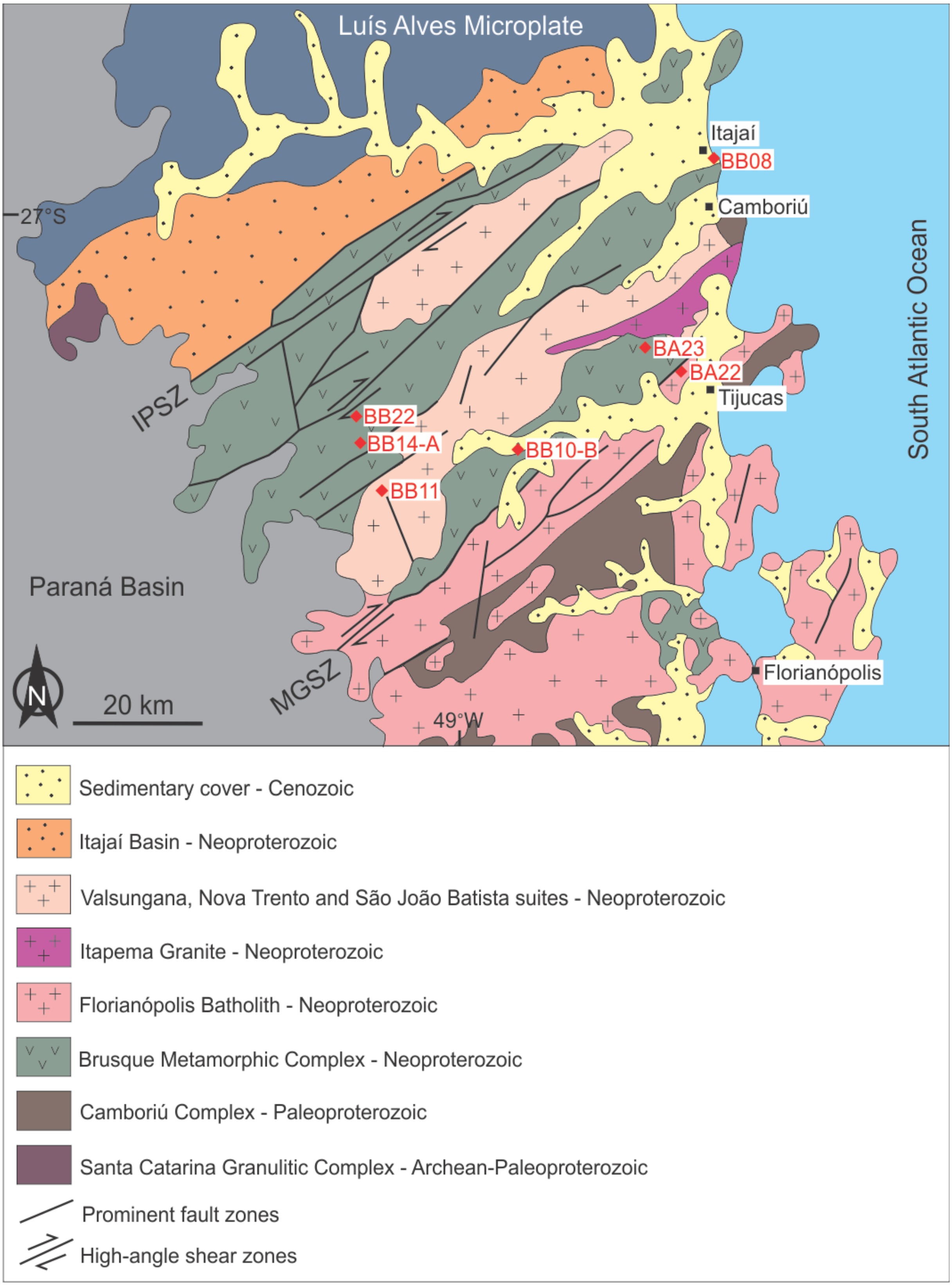

Fig. 4. Geological map of the Brusque Metamorphic Complex with its intrusive suites, the neighboring cratonic domain and ambient lithostratigraphic units. IPSZ - Itajaí-Perimbó Shear Zone; MGSZ – Major Gercino Shear Zone. The locations of the studied samples are shown as red diamonds. Modified after de Campos et al. (2012b) and Hueck et al. (2016).

The period of sedimentation, volcanism and metamorphism of the Brusque Metamorphic Complex occurred during the Neoproterozoic (de Campos et al., 2012). Hartmann et al. (2003) suggested that the Brusque Metamorphic Complex evolved as a rift basin, which formed during continental rifting. Basei et al. (2008a) dated A-type granites, that now occur within the metasedimentary rocks of the Brusque Metamorphic Complex, at 834.7 ± 8.7 and 843 ± 12 Ma and interpreted them as being related to the rifting and formation of the Brusque paleobasin. The timing of sedimentation of the Brusque Metamorphic Complex is poorly constrained. However, sedimentation is suggested between ca. 840 and 640 Ma, which represents the age of rifting of the Brusque paleobasin and the main metamorphism of the sediments in the complex, respectively (Basei et al., 2011a).

The basement of the basin is represented by the high-grade gneissic-migmatitic Camboriú Complex, which is exposed in the eastern part of the Brusque Metamorphic Complex (Hueck et al., 2016) (Fig. 4). The Camboriú Complex reveals a long polycyclic history and its provenance is uncertain (Basei et al., 2013). The gneissic-migmatitic complex is intruded by granitoid rocks of the Itapema Granite (Florisbal et al., 2012a).

1.2.2 The Kaoko Belt

The Kaoko Belt, situated at the Congo Craton margin, extends for more than 600 km along the coast of southern Angola and northern Namibia (Porada, 1989) (Figs. 3 and 5). The belt consists of two tectonic units represented by the Congo Craton margin with its Neoproterozoic sedimentary cover and the Coastal Terrane, where the latter is overriding the former (Konopásek et al., 2016). The Kaoko Belt is divided into three geotectonic zones, namely from west to east, these are the Western, Central and Eastern kaoko zones (Miller, 2008) (Fig. 5). Goscombe et al. (2005b) subdivided the Western Kaoko Zone into the westerly Coastal Terrane and the easterly Orogen Core domain, based on the exotic character of the Coastal Terrane compared to the Congo Craton margin.

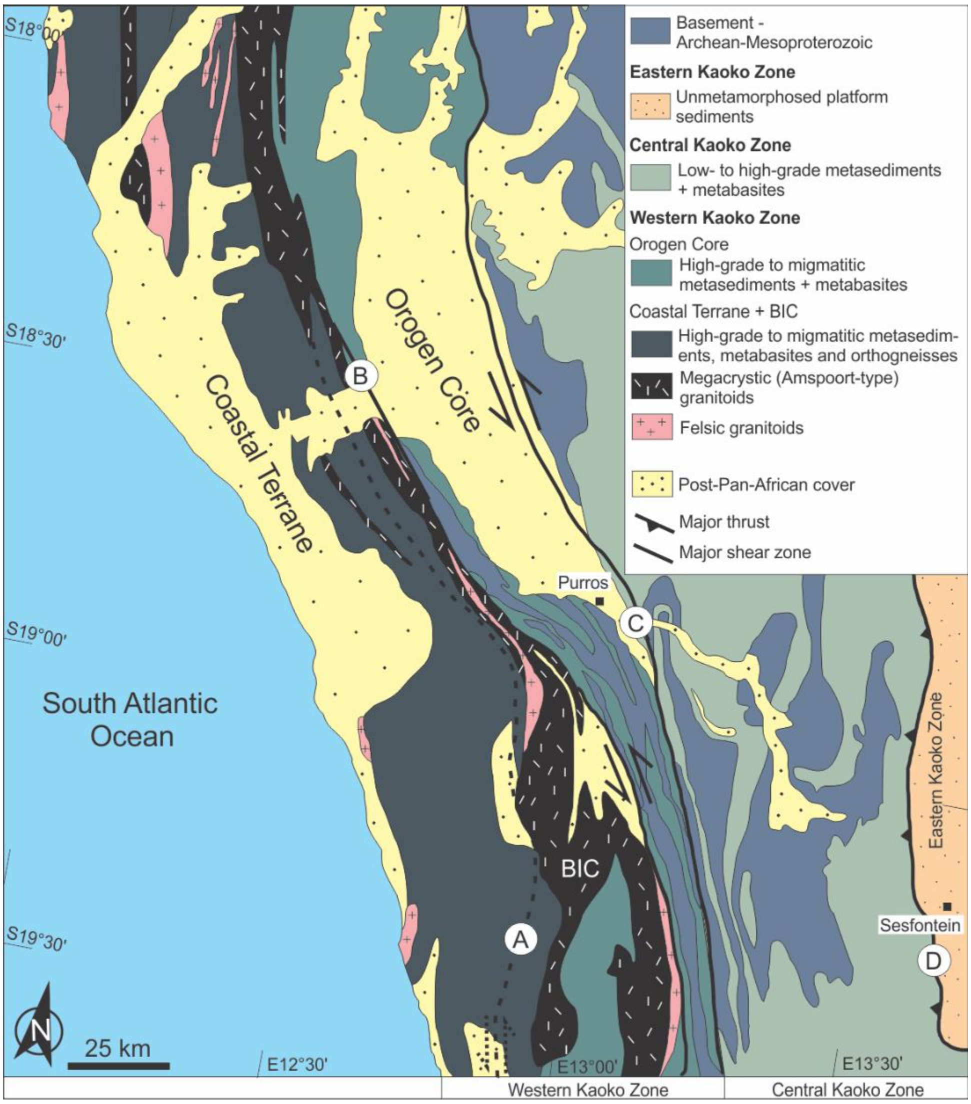

Fig. 5. Geological map of the central part of the Kaoko Belt. BIC – Boundary Igneous Complex. A - Three Palm Mylonite Zone; B - Village Mylonite Zone; C - Purros Shear Zone; D - Sesfontein Thrust. Modified after Konopásek et al. (2014).

The high-grade Coastal Terrane comprises metamorphosed sedimentary rocks with intercalated gneisses and amphibolites and its evolution differs from that of the Congo Craton margin (i.e. the Central Kaoko Zone and the Orogen Core; Konopásek et al., 2017). Unlike the Congo Craton margin rocks, the ages of the gneisses in the Coastal Terrane are typically around ca. 800 Ma, whereas the age of the migmatization of the unit was determined at ca. 650-630 Ma (Franz et al., 1999; Goscombe et al., 2005a; Konopásek et al., 2008, in press). Also, no pre-Neoproterozoic basement rocks have so far been detected in the Coastal Terrane (Konopásek et al., 2017). Two suites of intrusive rocks, referred to as the Angra Fria Magmatic Complex, crops out in the Coastal Terrane (Fig. 3) and have been dated at ca. 625-620 Ma and ca. 585-575 Ma (Konopásek et al., 2016). The Angra Fria Magmatic Complex are interpreted as representing a continuation of the Granite Belt in the Dom Feliciano Belt (Konopásek et al., 2016).

The boundary between the Coastal Terrane and the Orogen Core (and also the Congo Craton margin) has been defined by Konopásek et al. (2008) as the Boundary Igneous Complex, with magmatic activity dated between ca. 580 and 550 Ma (Seth et al., 1998; Konopásek et al., 2008). The Orogen Core domain consists of metasedimentary rocks with incorporated basement fragments of pre-Neoproterozoic age, which was migmatized at ca. 550 Ma (Goscombe et al., 2005a; Konopásek et al., 2008). The Orogen Core domain is in contact with the Central Kaoko Zone along the Purros Shear Zone (Ulrich et al., 2011). The Central Kaoko Zone, is a fold and thrust belt comprising a sequence of sedimentary and volcanic rocks, with exposures of the Congo Craton basement (Konopásek et al., 2014). This sequence shows inverted Barrovian metamorphism, which ranges in grade from lower-greenschist facies in the east to upper-amphibolite facies in the west (Oyhantçabal et al., 2011; Jung et al., 2014). The Central Kaoko Zone is thrust over the Eastern Kaoko Zone along the Sesfontein Thrust (Miller, 2008). The Eastern Kaoko Zone, in the foreland, comprises a low-grade sedimentary succession which is divided into a basal siliciclastic unit (Nosib Group), a middle carbonate unit (Otavi Group) and an upper siliciclastic molasses unit (Mulden Group) (Prave, 1996). The sedimentary succession overlies the Congo Craton margin represented by the Kamanjab Inlier in the south and Epupa Inlier in the north (Konopásek et al., 2014) (Fig. 3).

1.2.2.1 The Central Kaoko Zone

Konopásek et al. (2014) dated metamorphosed volcanic rocks from the lower part of the metasedimentary sequence covering the Congo Craton margin (Central Kaoko Zone and Orogen Core), which yielded U-Pb zircon ages between ca. 740 and 710 Ma. These rocks were interpreted as being related to continental rifting, reflecting a syn-rifting volcanic activity lasting for ca. 30 Ma (Fig. 6a). The sediments in the lower part of the metasedimentary sequence, associated with the rifting, is suggested to have its provenance in the Congo/Kalahari cratons (Konopásek et al., 2014).

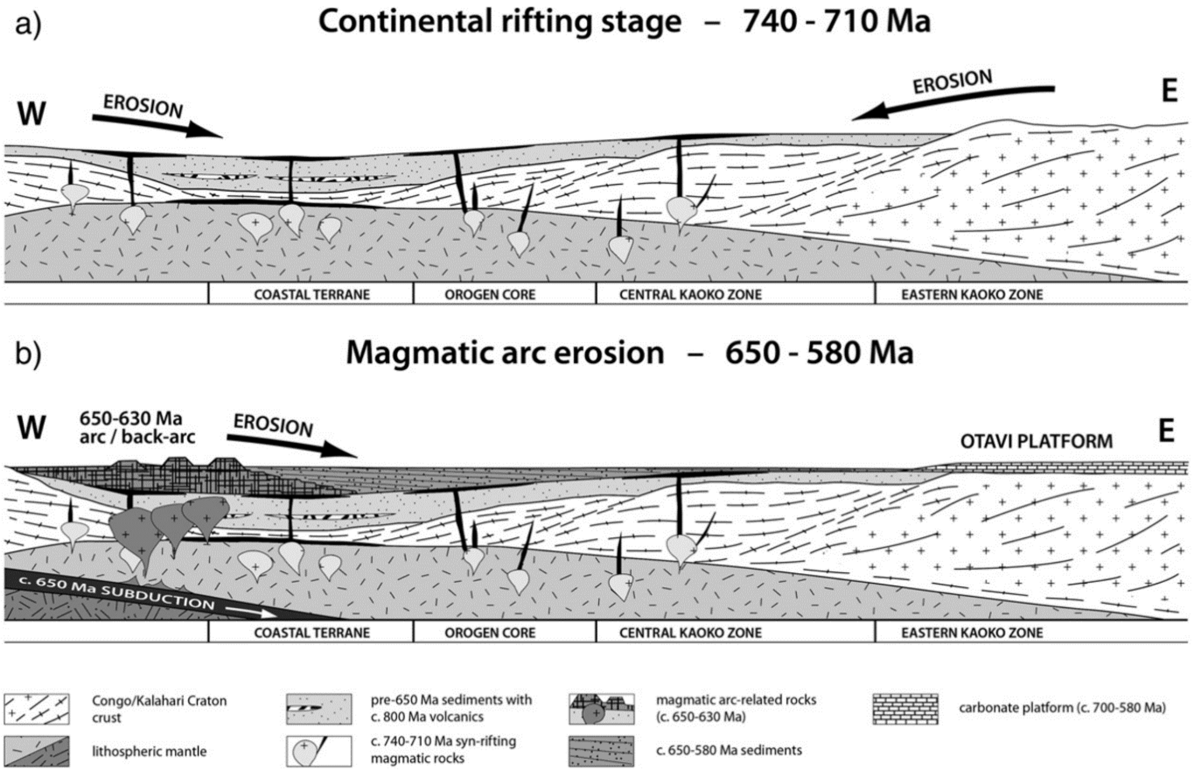

Fig. 6. Model of the pre-collisional position of the tectonic units of the Kaoko Belt. a) Continental rifting with volcanic activity (ca. 740-710 Ma), erosion of the Congo/Kalahari cratons and sedimentation of the lower part of the metasedimentary succession. b) Erosion of volcanic arc and underlying crust between ca. 650 and 580 Ma provides clastic material for the upper part of the metasedimentary succession. After Konopásek et al. (2014).

The age of deposition of the upper sedimentary sequence is constrained to be between ca. 650 and 580 Ma (Konopásek et al., 2014) (Fig. 6b). Such limits are estimated from the age of the youngest detrital zircon population (ca. 650) and the age of metamorphism of the samples due to the collision of the Coastal Terrane and the Congo Craton at ca. 580-550 Ma (Goscombe and Gray, 2007, 2008). The sediments in the upper part of the metasedimentary sequence is suggested to have derived from the Coastal-Punta del Este Terrane, as well as the underlying older crust (Konopásek et al., 2014). Konopásek et al. (2014) supports the interpretation of Goscombe and Gray (2007, 2008) that the Coastal Terrane may have acted as an arc/back-arc system along the western margin of the Congo Craton at ca. 650-630 Ma.

2 Methods

2.1 Field work

The field work was conducted between 9th and 23rd of June in 2017 together with supervisor Jiří Konopásek, Ph.D. student Jack James Percival and fellow student Caroline Asvald. The sampled area covered the entire Brusque Metamorphic Complex, with an emphasis on taking representative rock samples for provenance studies in its different parts. For this study, a total of seven samples were collected, named BB08, BB10-B, BB11, BB14-A, BB22, BA22 and BA23. Approximately 2-3 kg of rock for each of the samples were collected, by the use of hammer and chisel. Each sampling locality were marked with GPS coordinates (WGS 84), and field description together with pictures were made for the corresponding outcrops. The scarcity of outcrops made the sampling challenging to some extent, but finally the desired amount and quality of rock samples was collected.

2.2 Laboratory work

The laboratory work included mineral separation (crushing, milling, sieving, gravity shaking table, magnetic separation and heavy liquid separation), mount preparation, cathodoluminescence (CL) imaging and Laser Ablation-Inductively Coupled Plasma-Mass Spectrometry (LA-ICP-MS) analysis. All laboratory work, except heavy liquid separation and LA-ICP-MS analysis, were conducted at the University of Tromsø, Norway. The heavy liquid separation was done at the Mineral Separation Laboratory at the University of Bergen, Norway, whereas the LA-ICP-MS analysis was performed at the Institute of Geology of the Czech Academy of Sciences in Prague, Czech Republic.

2.2.1 Mineral separation

Prior to the laboratory work, the rock samples were washed clean and dried to prevent contamination. The rock samples were crushed manually with a hammer into grain fractions of ca. 50 mm, and further into ca. 10 mm fractions by a jaw crusher. To obtain fractions ≤ 0.3 mm, a hammer mill with aperture of 0.5 mm was used followed by manual sieving with aperture of 0.3 mm. Fractions ≤ 0.3 mm were kept for further mineral separation and introduced to the Holman-Wilfley gravity shaking table, in order to separate the minerals into heavy, middle and light fractions. The heavy fractions were kept for further zircon separation, while the middle fractions were saved for backup. Paramagnetic minerals in the heavy fractions were removed using a hand magnet, and the remaining magnetic minerals were removed by using the Frantz Magnetic Separator. The remaining non-magnetic minerals were loaded with diiodomethane (DIM) heavy liquids, to separate the zircons from the other heavy minerals. DIM heavy liquid has a high density (3.3 g/cm^3) (Chisholm et al., 2014), which causes the zircons (ρ = > 3.3 g/cm^3) (Deer et al., 2013) to sink to the bottom while other minerals (ρ = < 3.3 g/cm^3) float on top.

2.2.2 Mount preparation

The zircon concentrates were transferred to a petri dish with ethanol and studied under the Leica binocular microscope. Zircon grains were handpicked using a needle and transferred with the help of a pipette on a double-sided tape attached to a circular plastic plate. Zircons with different colours, shapes and sizes (to a certain degree) were selected in order to collect grains representing possible different age populations. Also, only transparent and apperantly non-metamict grains were chosen to minimize the chance to obtain misleading ages. Experiments performed by Košler et al. (2013) show that a minimum number of 60-100 zircon grains should be analysed in provenance studies to avoid loss of minor zircon populations. Vermeesch (2004) suggested that at least 117 grains should be dated, whereas Link et al. (2005) suggested that several hundred grains should be analysed, which is rarely possible, mainly for economic reasons. Considering previous studies, approximately 200 grains were picked for each sample, except for the samples BB08 and BA22, where only 114 and 22 zircon grains were found, respectively. The sample BB11 was not mounted due to the presence of only few zircons. Finally, the zircon grains were mounted in epoxy-filled blocks. After the mounts dried, they were grinded manually with an abrasive paper of 800 µm in order to expose central parts of the zircon grains. After grinding, the mounts were polished by a BUEHLER Phoenix Beta Grinder/Polisher by using a 6 µm diamond paste for 5 minutes and subsequently with 3 µm paste for another 5 minutes.

2.2.3 Cathodoluminescence (CL) imaging

Prior to the cathodoluminescence (CL) imaging of the zircon grains, the mounts were coated with carbon and attached to the stage of the electron microscope with a copper tape. The CL imaging was carried out using a Zeiss Merlin VP Compact Scanning Electron Microscope. For each sample, an overview picture was taken to localize the zircons and detailed images were taken to see the internal structure of the single grains. The CL images were taken in order to select the laser spots before performing the Laser Ablation Inductively Coupled Plasma Mass Spectrometry (LA-ICP-MS) analysis.

2.2.4 Laser Ablation-Inductively Coupled Plasma-Mass Spectrometry (LA-ICP-MS)

2.2.4.1 Instrumentation

The instrumentation of the Laser Ablation-Inductively Coupled Plasma-Mass Spectrometry (LA-ICP-MS) comprises a laser ablation (LA) system coupled to an inductively coupled plasma mass spectrometer (ICP-MS) equipment (Fig. 7). The LA system typically consists of a laser, a microscope, an optical lens, a charge-coupled device (CCD) camera, an ablation cell and an adjustable platform (Orellana et al., 2013). The mass spectrometry (MS) typically consist of an ion source (ICP), a mass filter, a detector and a vacuum system (Košler and Sylvester, 2003). The laser in the LA system produces a beam of radiation and is thus able to ablate particles from the sample surface (Darke and Tyson, 1993; Košler and Sylvester, 2003), creating an aerosol. The aerosol is further transported by a carrier gas (typically helium), which serves as an ion source for the MS (Košler and Sylvester, 2003). In the ICP, the particles are vaporized, atomized and ionized before they are transmitted to the MS, where the ions are separated according to their mass-to-charge ratio and finally analysed (Günther and Hattendorf, 2005).

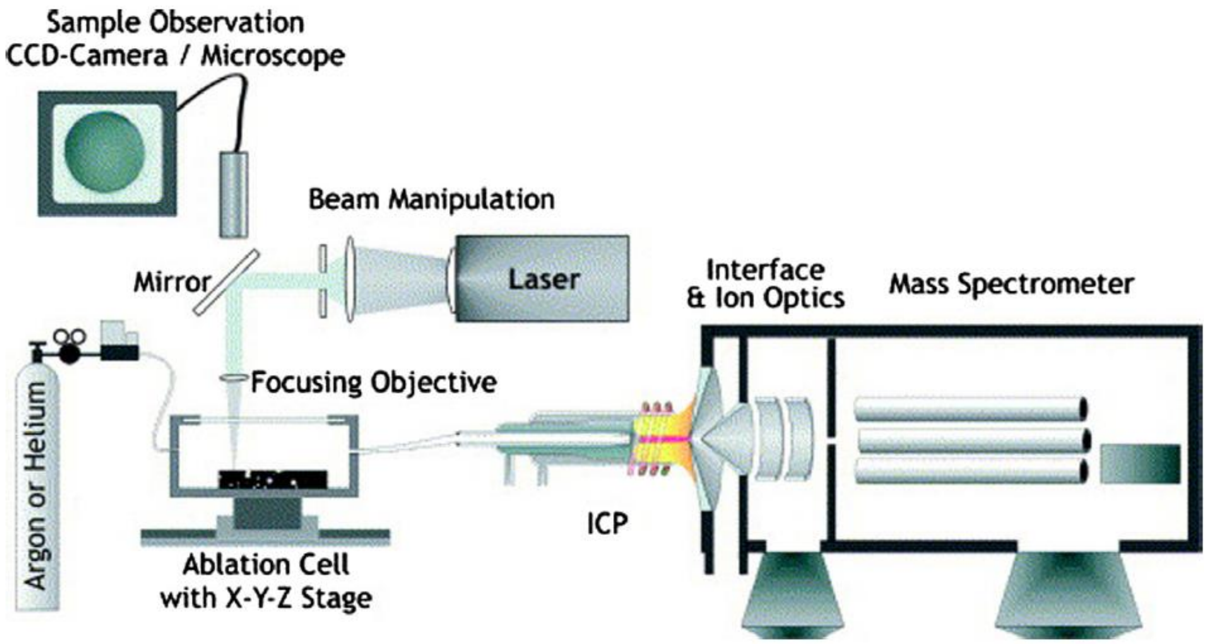

Fig. 7. Instrumentation of the Laser Ablation-Inductively Coupled Plasma-Mass Spectrometry (LA-ICP-MS). After Günther and Hattendorf (2005).

2.2.4.2 Analysis

Prior to the LA-ICP-MS analysis of the zircons, the mounts were re-polished and cleaned with 2 % nitric acid (HNO_3) to remove the carbon coating and then brought into ultrasonic bath of deionized water. To measure the U/Pb and Pb isotopic ratios of the zircons, a Thermo Scientific Element 2 sector field ICP-MS coupled to a 193 nm Ar-F excimer laser was used. The mounts were inserted in a sample cell mounted on a motorized stage of the laser ablation system, and the zircons were examined at a microscopic level through a viewing system including a camera to select the laser spots. One, occationally two, laser spots was chosen per zircon grain (Fig. 8). The laser was fired with a fluence (energy density) of 3.17 J/cm^2 at a repetition rate of 5 Hz. The spot size was chosen to be 25 microns, so that the beam diameter would fit within the smallest grains. First, 15 seconds of gas blank was measured followed by a 35 seconds measurement of U and Pb signals from the ablated zircon. In the transport of the ablated material to the inductively coupled plasma, a He carrier gas was used.

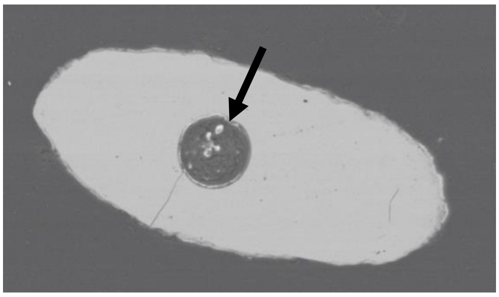

Fig. 8. Backscatter electron image of a zircon grain in the sample BB14-A showing the laser spot, as indicated by the black arrow.

Three external standards (natural zircon reference materials) were analysed together with the samples. These standards were the Plešovice, used as a primary standard, with a $^{207}Pb/^{206}Pb$ age of 337.13 ± 0.37 Ma (Sláma et al., 2008), the GJ-1 with a $^{207}Pb/^{206}Pb$ age of 608.53 ± 0.4 Ma (Jackson et al., 2004) and the 91500 with a $^{207}Pb/^{206}Pb$ age of 1065.4 ± 0.3 Ma (Wiedenbeck et al., 1995). The samples were analysed in sequences, where two measurements from each of the standards were analysed before and after every 14 measurements of the sampled zircons. The data were acquired in pulse counting mode, where one point was measured for each mass peak of ^{204}Pb + Hg, ^{206}Pb, ^{207}Pb, ^{208}Pb, ^{232}Th, ^{235}U and ^{238}U.

2.3 Data processing

Data reduction was carried out in Igor Pro version 6.37 by using the Iolite software. The instrument mass bias and residual elemental fractionation were corrected by normalizing to the Plešovice standard (Sláma et al., 2008), while the GJ-1 and 91500 standards (Wiedenbeck et al., 1995; Jackson et al., 2004) were applied for quality control. The three standards were all used for matrix-matched calibration. No corrections for common lead (^{204}Pb) was applied to the data. Background noise in the signals was reduced by subtracting the baseline from the total signal, giving only the signals obtained for the sampled material.

The reduced data were imported to Microsoft Excel for analysis. Isoplot version 4.15 (Ludwig, 2012) was used to present the U-Pb ages in Wetherill concordia diagrams, where the isotopic ratios of $^{207}Pb/^{235}U$ and $^{206}Pb/^{238}U$ ages were plotted with respect to their 2σ absolute error. Discordance of the $^{206}Pb/^{238}U$ and $^{207}Pb/^{206}Pb$ ages were calculated by the following equations, respectively:

$$^{206}Pb/^{238}U = (1-(^{206}Pb/^{238}U - {}^{207}Pb/^{235}U))*100$$

$$^{207}Pb/^{206}Pb = (1-(^{206}Pb/^{238}U - {}^{207}Pb/^{206}Pb))*100$$

producing a percentage value. Data with ≥ ± 10 % discordance were discarded and not used for further analysis. DensityPlotter (Vermeesch, 2012) was used to create histograms and Kernel Density Estimate (KDE) in order to display the detrital age distribution for each of the samples. The bin width of the histograms was chosen to be 30 Ma. $^{206}Pb/^{238}U$ ages were used for the data < 1.00 Ga, while $^{207}Pb/^{206}Pb$ ages were used for those > 1.00 Ga.

3 Results

3.1 Field work

Fig. 4 shows the locations of the rock samples collected for this study. Their respective WGS 84 coordinates are; S26°55.545', W48°38.061' (BB08), S27°16.967', W48°55.009' (BB10-B), S27°19.024', W49°07.533' (BB11), S27°15.130', W49°09.390' (BB14-A), S27°13.360', W49°09.841' (BB22), S27°12.195', W48°39.855' (BA22) and S27°10.512', W48°43.055' (BA23). The sampled outcrops are shown in Fig. 9. The sample BA23 was collected from a large loose block, while the other six samples were taken from in situ outcrops. The sampled outcrops were generally highly affected by weathering, as well as covered by vegetation. However, the sample BB08 was collected from an outcrop at a beach and was partly covered in sand.

In hand specimen, the sample BB08 had a fine-grained texture and contained mm-thick and discontinous light coloured bands of brown and gray. The rock sample was highly folded and foliated, and revealed a slightly shiny luster. The sample BB10-B was gray in colour, foliated and had a slightly shiny luster. The texture was fine-grained and mm-thick quartz lenses occurred occasionally. The sample BB11 revealed a shiny luster and was dark gray with thin, light layers. The rock sample was foliated and folded, and revealed a fine-grained texture with visible garnet crystals. The sample BB14-A was pink with a fine-grained texture and a dull luster. Mineral lineation was observed and the rock tended to break off as layers along these surfaces. The sample BB22 was gray-white in colour and had a dull luster. The rock sample was fine grained, and quartzporphyroclasts with diameter of ca. 1.0 mm occurred frequently. Occationally, the quartz grains formed cm-thick veins. The sample BA23 was dark gray, foliated and revealed a shiny luster. A preferred orientation of the micas was clear and mm-thick lenses of quartz occurred frequently. Garnet crystals was visible. The sample BA22 was gray-white in colour and revealed a slightly shiny luster. The rock sample had a very massive texture and no clear preferred orientation of the minerals was observed.

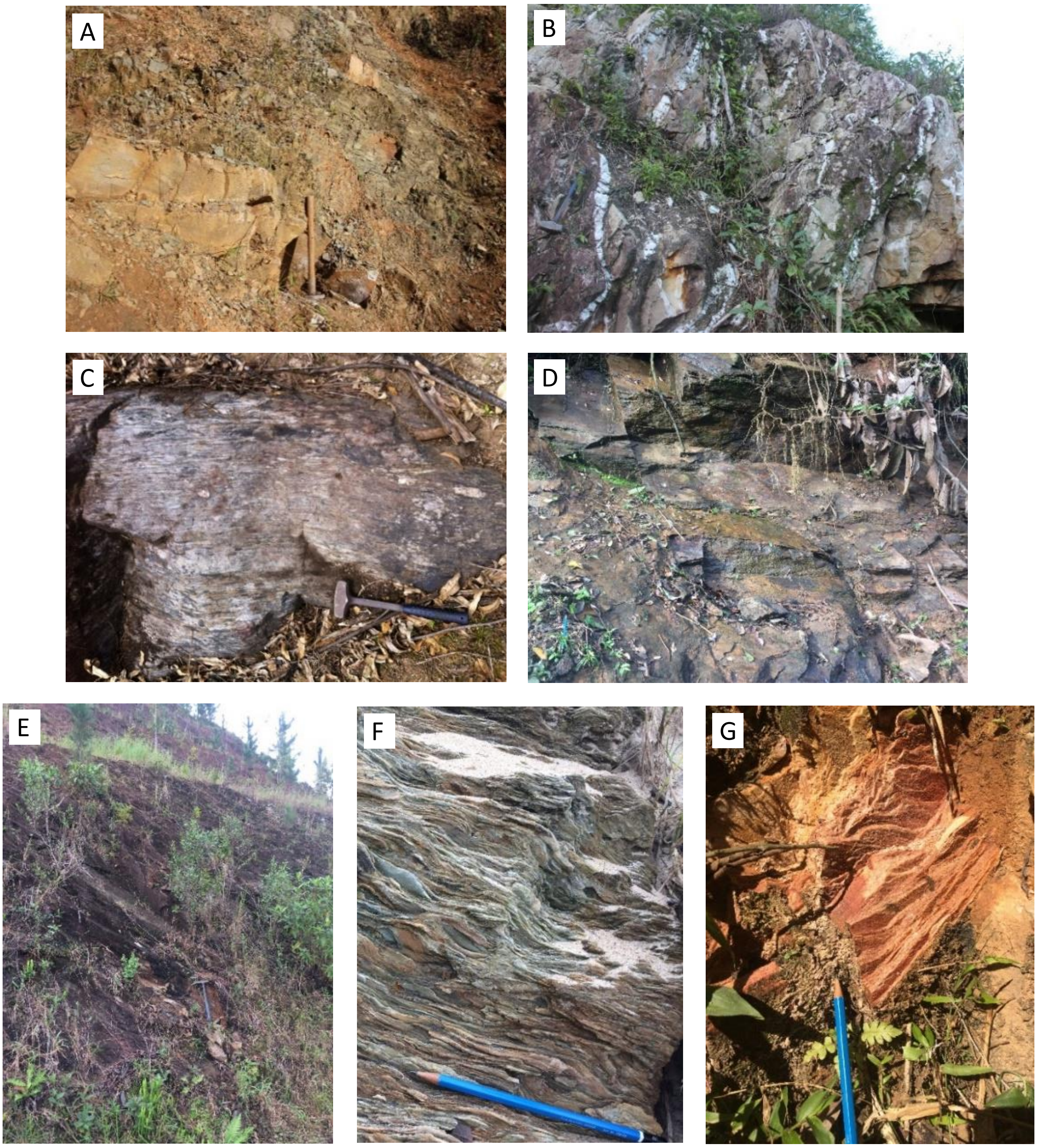

Fig. 9. Field photographs of the sampled outcrops. a) Sample BA22; b) Sample BB22; c) Sample BA23; d) Sample BB11; e) Sample BB10-B; f) Sample BB08; g) Sample BB14-A.

3.2 Laboratory work

The U/Pb isotopic ratios of the detrital zircon grains, measured by the Laser Ablation-Inductively Coupled Plasma-Mass Spectrometry (LA-ICP-MS), and their corresponding calculated ages are given in the Appendix A. The sample BB11, a garnet-mica schist, was not dated due to the lack of zircon grains and is therefore not further considered. For the remaining six samples thin section photographs, cathodoluminescence (CL) images and age spectrums were made and are presented in the following sections (3.2.1-3.2.6).

3.2.1 Sample BB08

Sample BB08 is a phyllite consisting of quartz, carbonate, plagioclase, chlorite, biotite and muscovite, with accessory amounts of zircon and opaque minerals (Fig. 10). Zircon grains in this sample are highly variable in size, with lengths between ca. 60 and 210 µm and widths between ca. 40 and 180 µm. Seen under the binocular microscope, the zircon grains appear pink or orange in colour and the shape of the grains ranges from nearly round through ovoid to elongate. Most of the grains are abraded on the edges, while some of the elongate grains tend to be prismatic. Cathodoluminescence (CL) images of the zircons (Fig. 11) revealed a majority of grains with oscillatory zoning, whereas some of the grains are overgrown by featureless rims. Sector or convolute zoning is present in some grains and a subordinate number of zircons show only faint zoning. Numerous zircons are relics of larger grains. A small number of grains contain inclusions and/or fractures.

Analysis of 101 zircon grains yielded 85 concordant U-Pb dates, which are presented as an age spectrum in Fig. 12. The dates show a bimodal distribution with distinct peaks at ca. 2.15 Ga and ca. 675 Ma within the groups of data between ca. 1.75 and 2.95 Ga and between ca. 500 and 750 Ma, respectively. In the former interval, one minor peak appears at ca. 2.20 Ga, whereas in the latter, two minor peaks form at ca. 565 and 625 Ma. Individual ages appear at ca. 85 Ma, 375 Ma, around 1.05 Ga and at ca. 1.35 Ga.

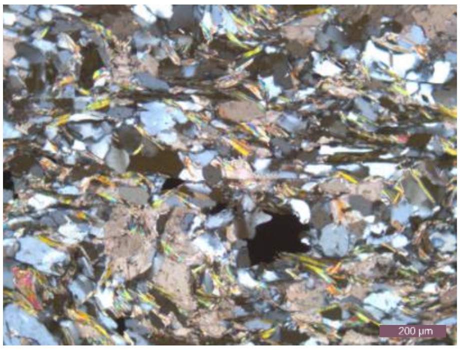

Fig. 10. Photomicrograph of the sample BB08 with crossed polarized light (XPL) and magnification 4x.

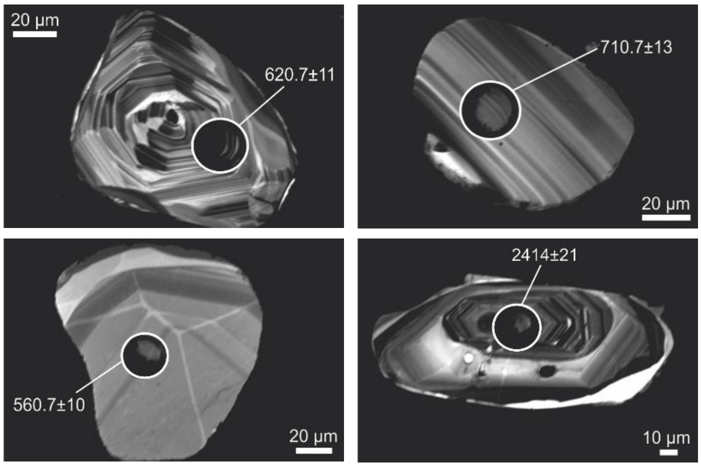

Fig. 11. Cathodoluminescence images of representative detrital zircon grains in the sample BB08. The circles represent the analyzed spots and the numbers refer to the yielded ages (Ma).

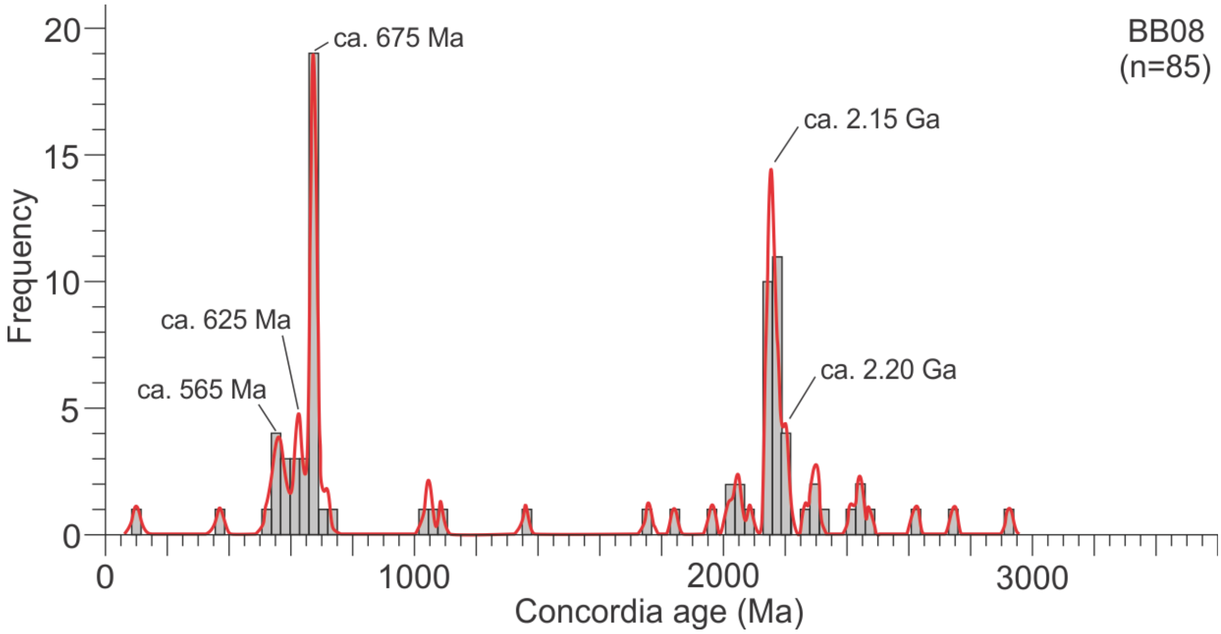

Fig. 12. Kernel density plot and histogram of detrital zircon age data from the sample BB08. The data show a bimodal distribution with major peaks at ca. 2.15 Ga and ca. 675 Ma, and minor peaks at ca. 2.20 Ga, 625 Ma and 565 Ma.

3.2.2 Sample BB10-B

The sample BB10-B is a mica-rich quartzite containing the mineral assemblage quartz-biotite-muscovite-chlorite, with accessory zircon, apatite and opaque minerals (Fig. 13). Zircon grains extracted from this sample are between ca. 50 and 120 µm in length and between ca. 30 and 50 µm in width, and significantly smaller than the zircons from the other samples. The zircons are light yellow or white and mostly elongate in shape. Numerous grains reveal a prismatic habit. Some grains are ovoid in shape. Cathodoluminescence (CL) images of the zircons (Fig. 14) reveal grains with sector or oscillatory zoning. Numerous grains show thin and homogenous CL-bright rims. Inclusions are common, while fractures are rare.

U-Pb dating of 182 zircon grains yielded 171 concordant dates. The corresponding age spectrum is presented in Fig. 15 and shows a broad range of data between ca. 1.00 and 2.20 Ga, with poorly defined peaks at ca. 1.25, 1.50, 1.80 and 2.00 Ga. A small number of individual data appear at ca. 2.55 and 2.70 Ga.

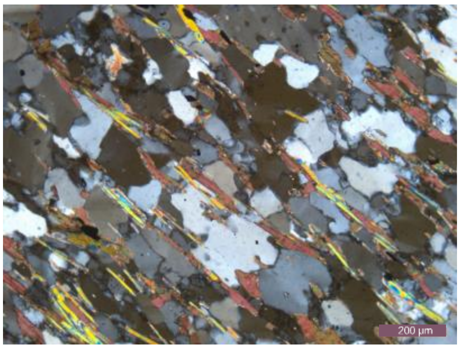

Fig. 13. Photomicrograph of the sample BB10-B with crossed polarized light (XPL) and magnification 10x.

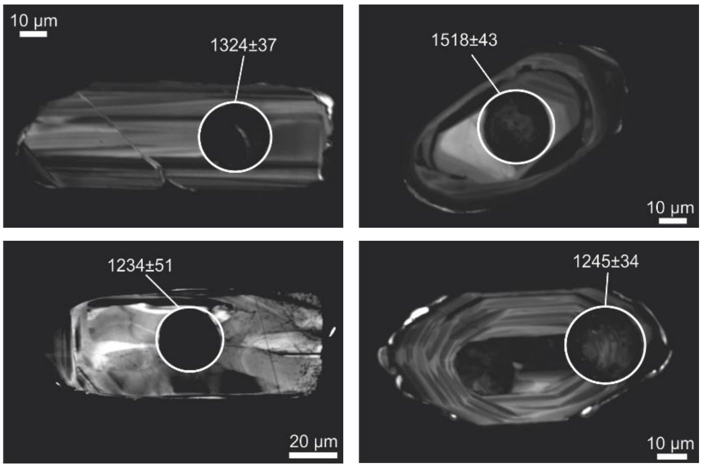

Fig. 14. Cathodoluminescence images of representative detrital zircon grains in the sample BB10-B. The circles represent the analyzed spots and the numbers refer to the yielded ages (Ma).

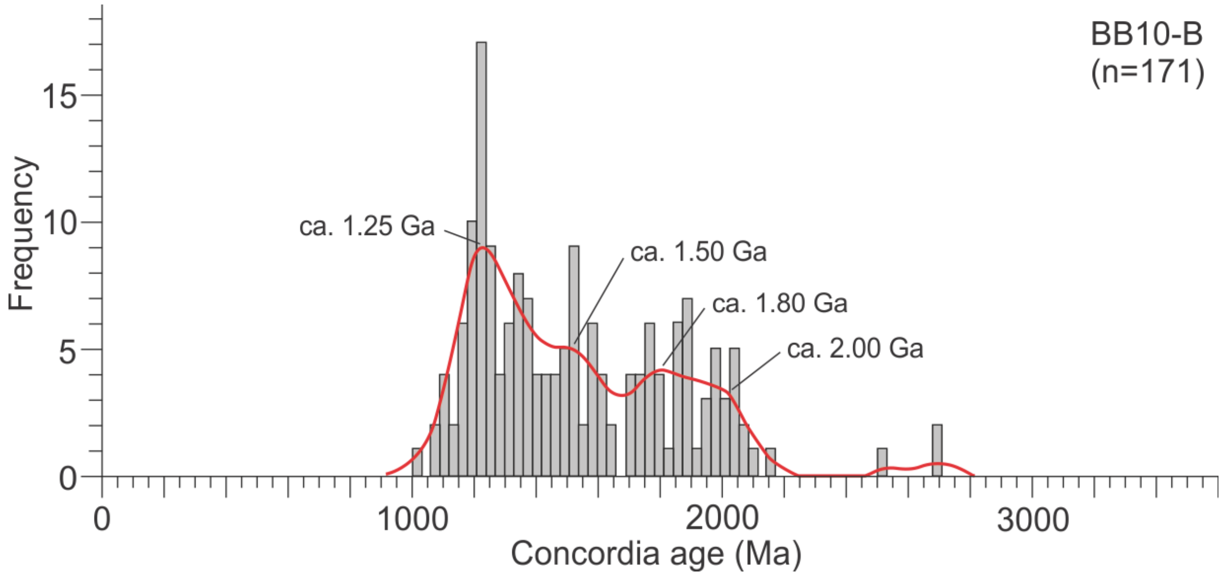

Fig. 15. Kernel density plot and histogram of detrital zircon age data from the sample BB10-B. Most of the data range in the interval between 1.00 and 2.20 Ga, with poorly defined peaks at ca. 1.25, 1.50, 1.80 and 2.00 Ga.

3.2.3 Sample BB14-A

The sample BB14-A is a quartzite comprising predominantly quartz with subordinate muscovite and biotite, as well as accessory zircon, rutile and opaque minerals (Fig. 16). Zircon grains extracted from this sample have lengths between ca. 80 and 200 µm and widths between ca. 40 and 80 µm. Seen under the binocular microscope, the zircons appear orange or pink in colour. The majority of the grains are elongate or ovoid, while some are nearly round in shape. The zircons are abraded on the edges, as seen by truncation of the oscillatory zoning and only few grains reveal relics of crystal faces. A substantial number of the grains appear to be relics of larger crystals. Cathodoluminescence (CL) images of the zircon grains (Fig. 17) reveal grains with predominantly oscillatory zoning and subordinate grains with sector zoning. Convolute zoning is apparent in some grains. Only few zircons show faint zoning or no zoning at all. Both inclusions and fractions are rare in zircons from this sample.

The analysis of 168 zircon grains yielded 166 concordant U-Pb dates, and the resulting age spectrum is presented in Fig. 18. The data cluster around several distinct peaks at ca. 2.15, 1.95, 1.80, 1.55 and 1.15 Ga, and individual dates appear between ca. 2.30 and 2.90 Ga and at ca. 3.40 Ga.

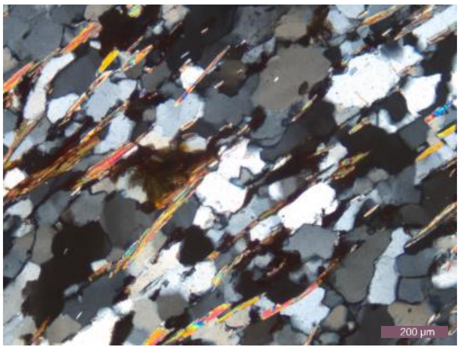

Fig. 16. Photomicrograph of the sample BB14-A with crossed polarized light (XPL) and magnification 10x.

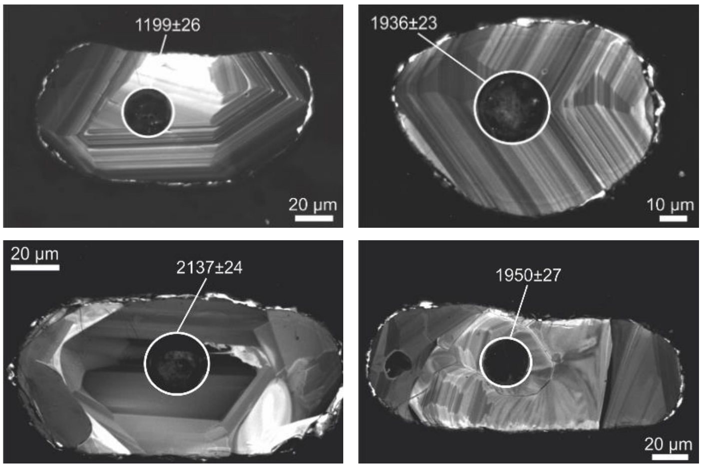

Fig. 17. Cathodoluminescence images of representative detrital zircon grains in the sample BB14-A. The circles represent the analyzed spots and the numbers refer to the yielded ages (Ma).

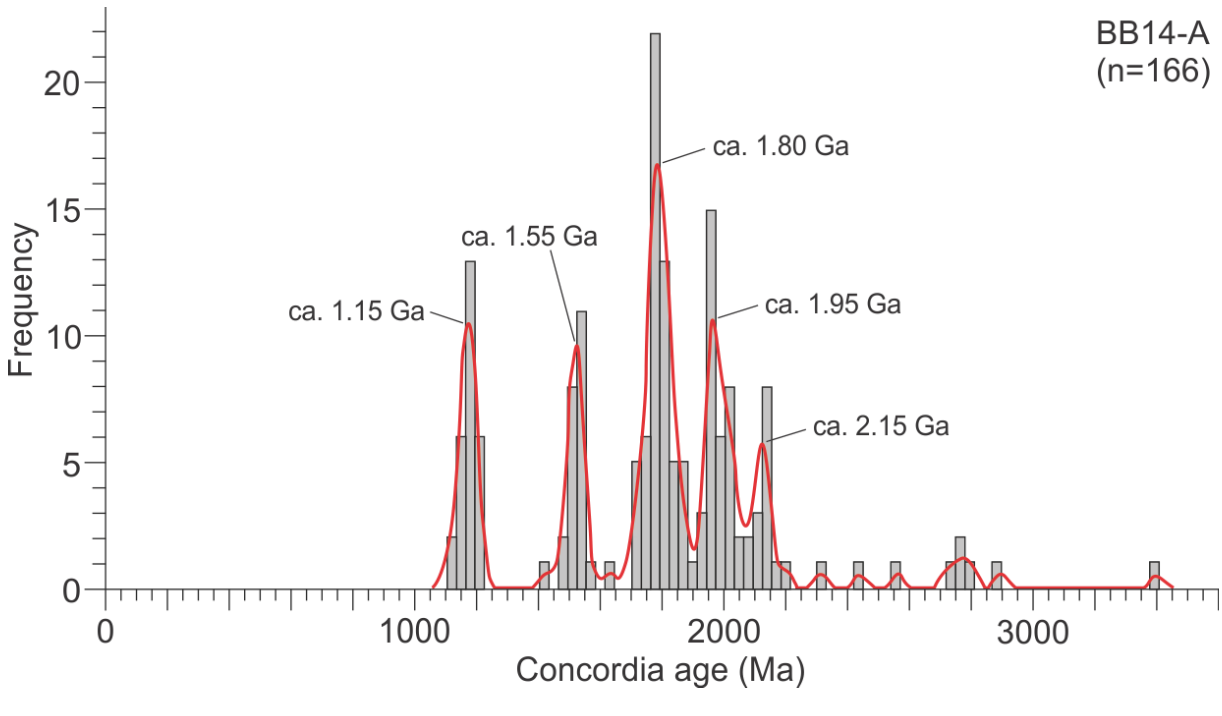

Fig. 18. Kernel density plot and histogram of detrital zircon age data from the sample BB14-A. The data show five distinct peaks at ca. 2.15, 1.95, 1.80, 1.55 and 1.15 Ga.

3.2.4 Sample BB22

The sample BB22 is a quartzite consisting of quartz with subordinate muscovite, and accessory amounts of zircon, titanite and opaque minerals (Fig. 19). Zircon grains extracted from this sample are ca. 70-250 µm long and ca. 30-130 wide. Seen under the binocular microscope, the zircons are pink and the shape of the grains are very similar to those observed in the sample BB14-A. Cathodoluminescence (CL) images of the zircons (Fig. 20) reveal a substantial number of oscillatory zoned grains, where some show a complex core. Some grains are sector-zoned, and some reveal a complex zoning pattern. Inclusions and fractures are present in some of the grains.

Out of the 154 zircon grains dated, 148 yielded concordant U-Pb dates. The age spectrum (Fig. 21) shows a majority of zircons between ca. 2.00 and 2.25 Ga, with one large peak at ca. 2.20 Ga and two minor peaks at ca. 2.10 and 2.05 Ga. A small number of individual data appear at ca. 1.60 Ga and in the interval between ca. 2.35 and 3.15 Ga.

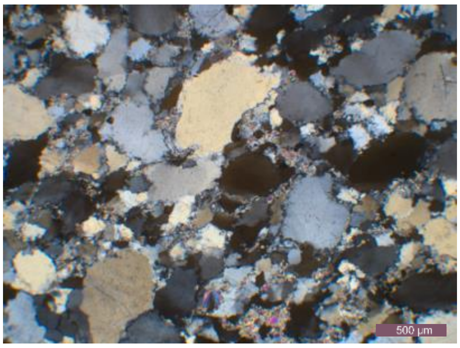

Fig. 19. Photomicrograph of the sample BB22 with crossed polarized light (XPL) and magnification 4x.

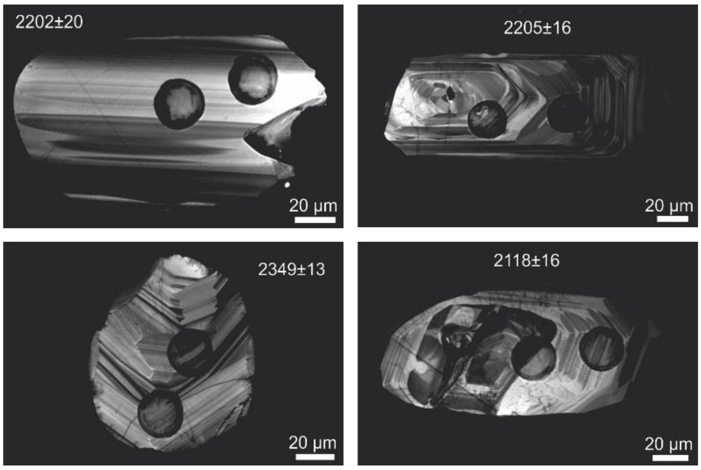

Fig. 20. Cathodoluminescence images of representative detrital zircon grains in the sample BB22. The circular craters shows the laser spots and the numbers in white represent the age (Ma) of the grains. The laser was fired twice per grain, but only one measurement was made for each zircon.

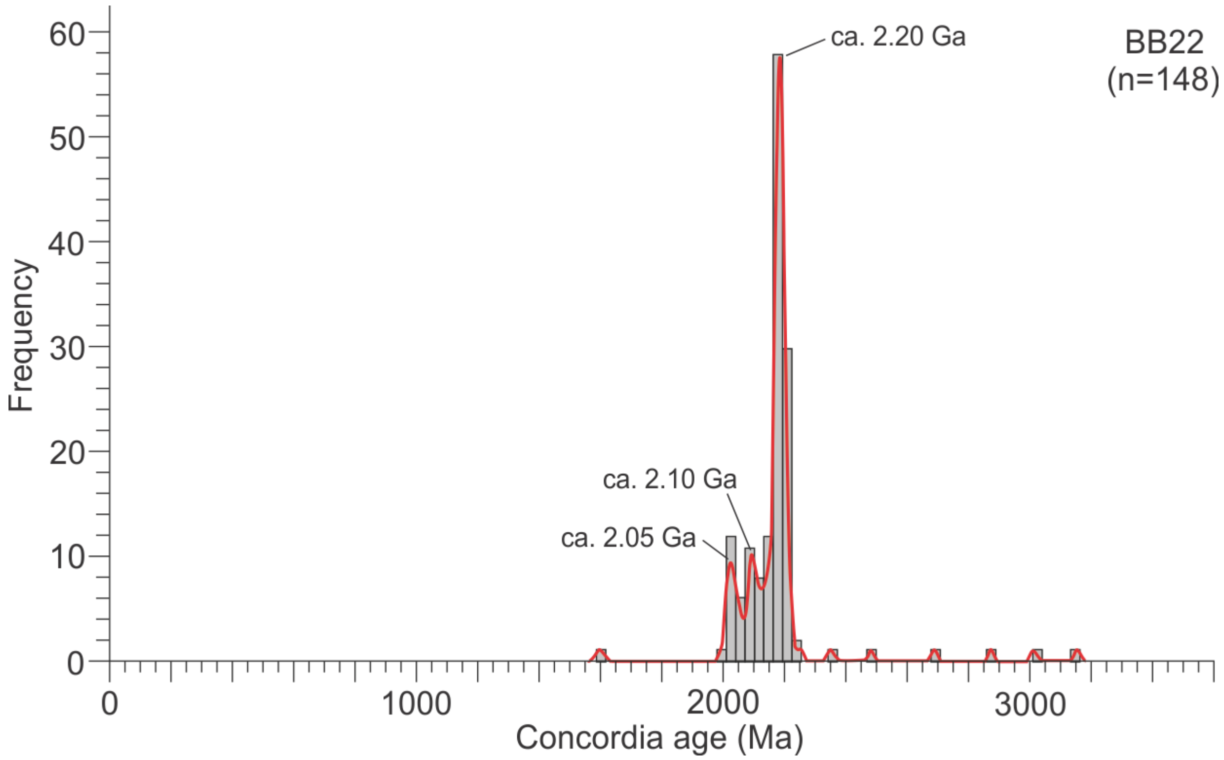

Fig. 21. Kernel density plot and histogram of detrital zircon age data from the sample BB22. The data form one large peak at ca. 2.20 Ga and smaller peaks at ca. 2.10 and 2.05 Ga.

3.2.5 Sample BA23

The sample BA23 is a quartzite containing the mineral assemblage quartz-muscovite-chlorite-biotite, with accessory amounts of zircon, apatite, garnet and opaque minerals (Fig. 22). Zircon grains in this sample vary between ca. 80 and 150 µm in length and between ca. 40 and 120 µm in width. The zircons are brown-orange in colour and mostly ovoid in shape. A subordinate number of grains are nearly round or only slightly elongated. A majority of the zircons are fragments of larger crystals and only a few grains show relics of crystal faces. Cathodoluminescence (CL) images of the zircons (Fig. 23) reveal grains with oscillatory or sector zoning, where many of the grains reveal the presence of featureless rims. A subordinate number of the grains reveal a complex zoning pattern, whereas some show only faint zoning. A substantial number of the zircon grains are fractured and/or contain inclusions.

U-Pb dating of 140 zircon grains yielded 136 concordant dates, where the resulting age spectrum is presented in Fig. 24. The highest proportion of dates cluster around one peak at ca. 2.00 Ga in a group of data between ca. 2.20 and 1.90 Ga. Individual ages appear at ca. 1.40, 1.50 and in the interval between ca. 2.30 and 3.15 Ga.

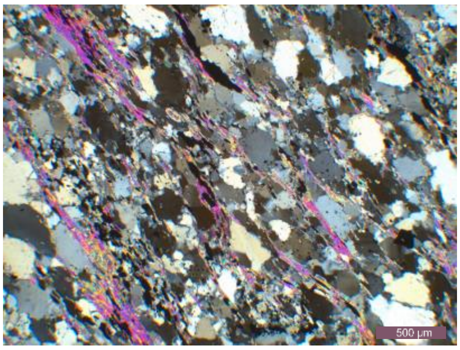

Fig. 22. Photomicrograph of sample BA23 in crossed polarized light (XPL) with magnification 4x.

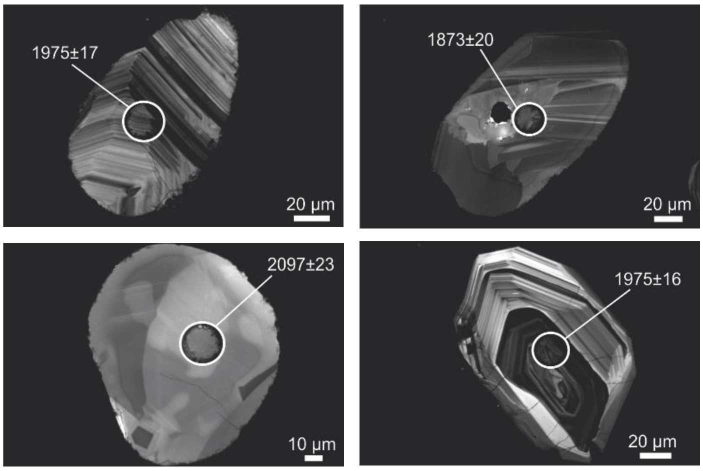

Fig. 23. Cathodoluminescence images of representative detrital zircon grains in the sample BA23. The circles represent the analyzed spots and the numbers refer to the yielded ages (Ma).

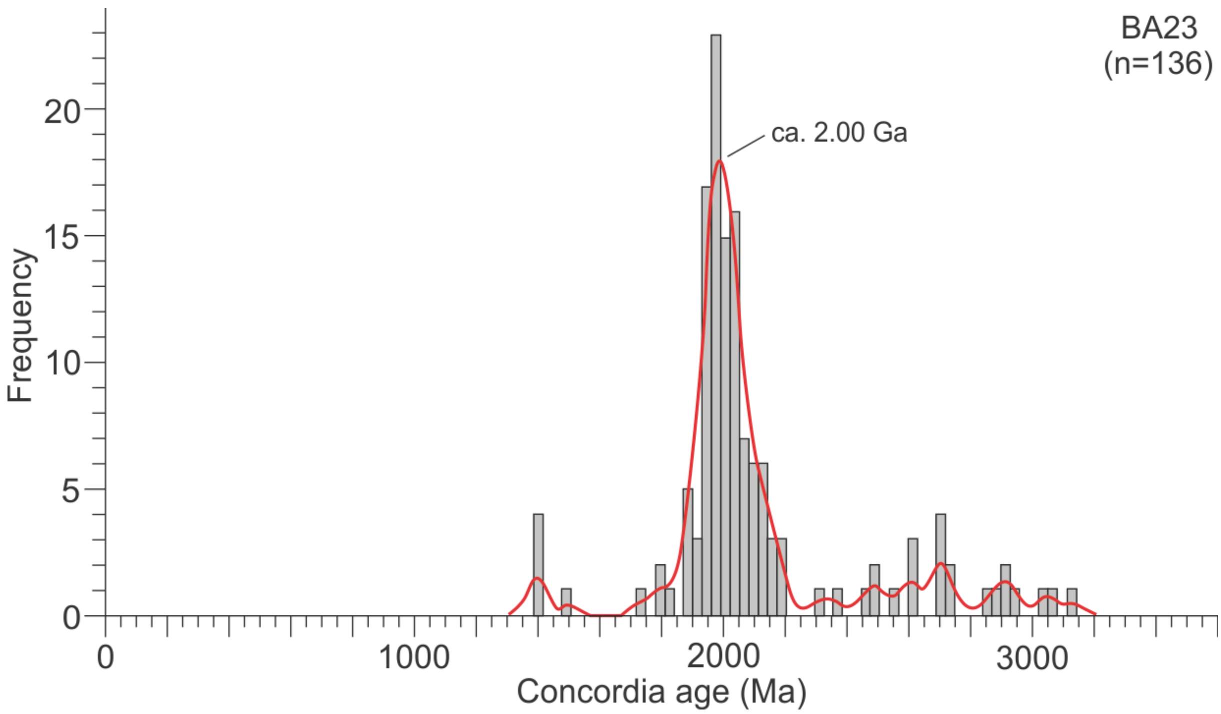

Fig. 24. Kernel density plot and histogram of detrital zircon age data from the sample BA23. The data show one broad peak at ca. 2.00 Ga within the interval of ca. 1.90-2.20 Ga.

3.2.6 Sample BA22

The sample BA22 is interpreted as a felsic volcanic rock. It consists predominantly of quartz, plagioclase, K-feldspar and subordinate muscovite, as well as accessory zircon, garnet, apatite and opaque minerals (Fig. 25). Only small number of zircon grains were extracted from this sample and these are highly variable in size, with lengths between ca. 70 and 190 µm and widths between ca. 60 and 130 µm. The grains vary between light and dark pink and orange in colour, and are ovoid or elongate in shape. Cathodoluminescence (CL) images of the zircons (Fig. 26) reveal mostly faint patterns of predominantly sector zoning and subordinate oscillatory zoning. Only few grains show relics of crystal faces. Most of the grains are highly fractured and contain inclusions.

Out of the 22 zircon grains dated, 19 yielded concordant U-Pb dates. Some of the grains were analyzed twice, and in the cases when both analysis gave the same age, only one of them were used in the spectrum. The corresponding age spectrum (Fig. 27) shows a majority of data forming a peak around ca. 2.10 Ga, as well as individual data at ca. 1.10, 1.45, 1.65 and between ca. 1.75 and 3.05 Ga.

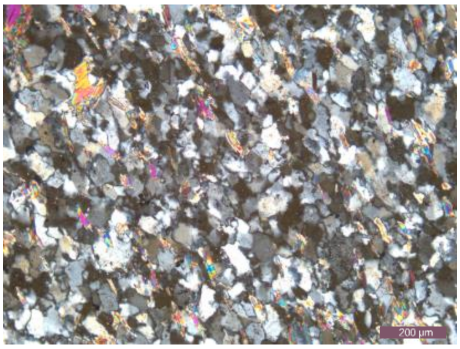

Fig. 25. Photomicrograph of the sample BA22 with crossed polarized light (XPL) and magnification 10x.

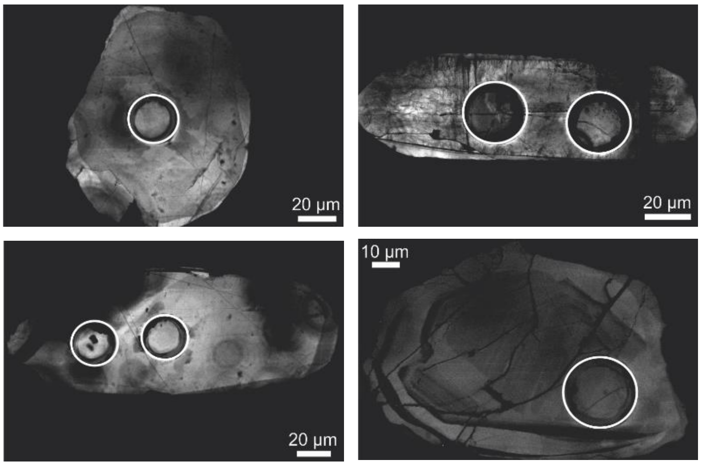

Fig. 26. Cathodoluminescence images of representative detrital zircon grains in the sample BA22. The circles represent the analyzed spots.

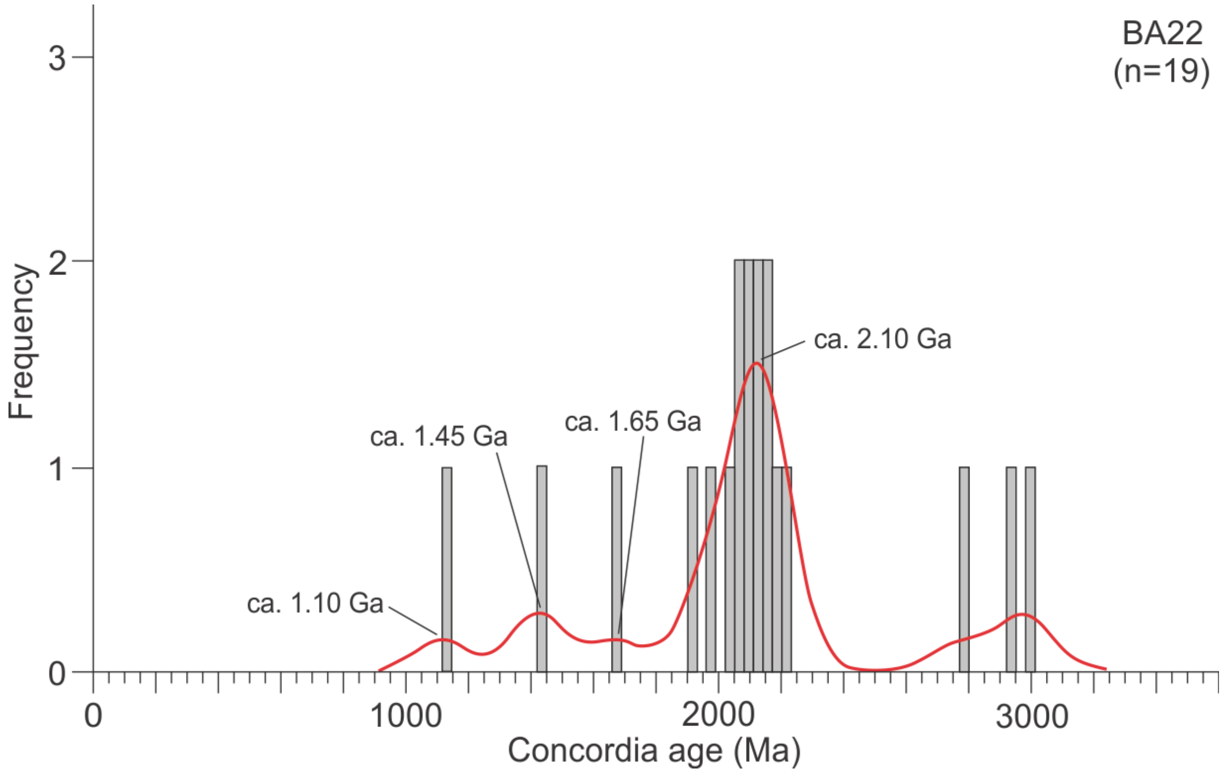

Fig. 27. Kernel density plot and histogram of detrital zircon age data from the sample BA22. The data show one peak at ca. 2.10 Ga, as well as individual ages at ca. 1.10, 1.45 and 1.65 Ga and between ca. 1.75-3.05 Ga.

4 Discussion

4.1 Detrital zircon age patterns of the studied rock samples

Based on the detrital U-Pb zircon data obtained for the metasedimentary rock samples in the Brusque Metamorphic Complex (Figs. 12, 15, 18, 21 and 24), three different age patterns can be observed. The first age pattern is represented by the sample BB08 (Fig. 12), where the distribution of ages is bimodal with one Paleoproterozoic age group with maxima at ca. 2.20 and 2.15 Ga and another Neoproterozoic age group with maxima at ca. 675, 625 and 565 Ma. The dates of ca. 375 and 85 Ma are interpreted as possible contamination, because the field relationships confirm Neoproterozoic age of deformation and metamorphism of the sample.

The second age pattern appears in the samples BB10-B (Fig. 15) and BB14-A (Figs. 18), where the zircons are predominantly Meso- and Paleoproterozoic within the interval of ca. 1.00-2.20 Ga. However, the age spectrum for the sample BB14-A shows more distinct peaks than compared to the distribution of ages observed in the sample BB10-B. Despite this difference, the samples BB10-B and BB14-A are considered as being derived from the same source(s). The xenocrystic zircons in the volcanic rock sample BA22 (Fig. 27) revealed similar age distribution as that observed in the samples BB10-B and BB14-A.

The third age pattern is represented by the samples BB22 (Fig. 21) and BA23 (Figs. 24), where majority of the zircons are Paleoproterozoic and show ages between ca. 2.00 and 2.20 Ga. However, in the sample BB22 most of the data occur as a narrow peak at ca. 2.20 Ga, while in the sample BA23 a broader peak of data appears around 2.00 Ga. The detrital zircons in the samples BB22 and BA23 were most likely derived from the same source(s), due to their similarities in the age signals.

The dates obtained for zircons in the samples BB10-B and BB14-A differ from those in the samples BB22 and BA23 by the significant suppression of Mesoproterozoic dates in the latter age pattern. The sample BB08 stands out because of the presence of Neoproterozoic zircons, which are absent in all other samples. When considering the detrital zircon age patterns of the Brusque Metamorphic Complex as a whole, the predominance of Paleoproterozoic dates is evident.

4.2 Comparison with existing detrital zircon data

The detrital U-Pb zircon dates recorded in the studied rock samples can be compared with existing data from metasedimentary rocks of the Brusque Metamorphic Complex presented in the section 1.1.

The quartzite sample of Hartmann et al. (2003) yielded dates between ca. 2.22 and 2.02 Ga with maxima around 2.17, 2.14 and 2.10 Ga, which is comparable with the age pattern recorded in the quartzite sample BB22, except that the 2.14 Ga peak is not observed in this study and the 2.05 Ga peak is absent in the quartzite of Hartmann et al. (2003) (Fig. 28a).

The garnet-biotite schist sample of Basei et al. (2006), which contained zircons between ca. 1.90 and 1.00 Ga with maxima at ca. 1.85, 1.50 and 1.05, is only partly comparable with the quartzite samples BB10-B and BB14-A (Figs. 15 and 18). The detrital zircon data in the samples of this study spans a wider range than the sample of Basei et al. (2006), and the ca. 1.05 Ga peak in the sample of Basei et al. (2006) is missing in the samples BB10-B and BB14-A. Another dated metasedimentary rock of Basei et al. (2006), which yielded ca. 2.20-1.80 Ga detrital zircon grains (no maxima emphasized), is very similar to the quartzite sample BA23 (Fig. 24) based on the time interval.

The zircon dates obtained for a mica schist and a garnet-biotite schist of Basei et al. (2008b), yielded pooled ages between ca. 2.25 and 1.10 Ga and between ca. 570 and 540 Ga. However, Basei et al. (2018) considered the ca. 570 and 540 Ma as possibly reflecting a Pb-loss. In that case, the age interval of the samples (ca. 2.25-1.10 Ga) resembles the data yielded for the sample BB14-A, whereas the position of maxima is more similar to those observed in the sample BB10-B (Fig. 28b). An exception is an additional peak at ca. 1.40 Ga in the samples of Basei et al. (2008b) and the lack of the ca. 2.25 Ga peak in the sample BB10-B.

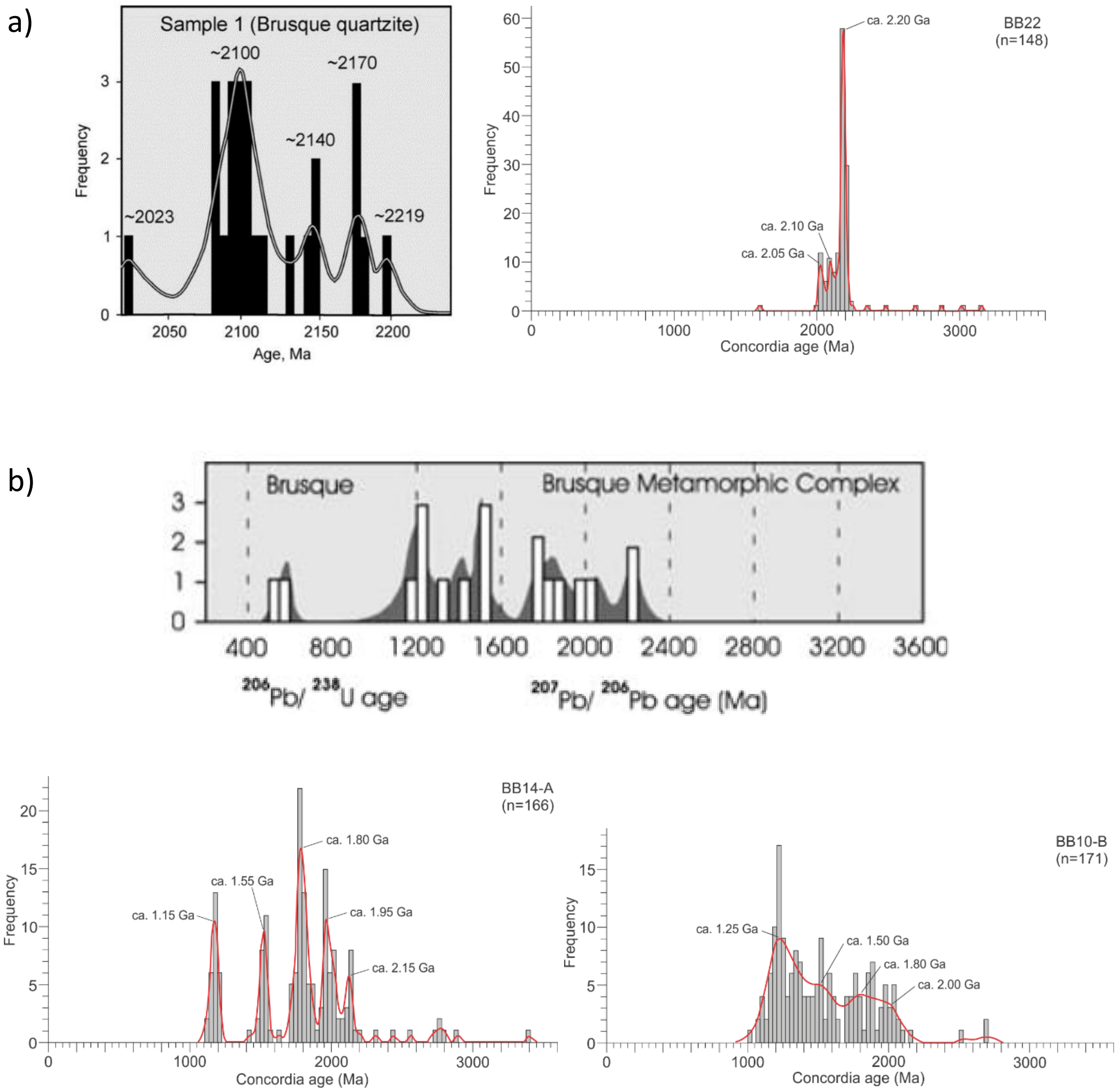

Fig. 28. Comparison of the detrital U-Pb zircon dates obtained for the studied samples and existing data. a) The quartzite sample of Hartmann et al. (2003) (left) and the sample BB22 of this study (right); b) The mica schist and garnet-biotite schist samples of Basei et al. (2008b) (top) and the samples BB14-A and BB10-B (bottom).

In the works of Hartmann et al. (2003) and Basei et al. (2008b), a number of 27 and 22 detrital zircons grains were dated for their metasedimentary samples, respectively. These are small numbers compared to the about 100-170 zircons grains dated for each of the metasedimentary rock samples in this study. As mentioned in section 2.2.2, a number of around 100 grains are suggested to be analyzed in order to avoid loss of minor zircon populations. Therefore, more geochronological studies with higher amount of analyzed zircon grains is necessary in order to make more conclusive correlations of the detrital zircon ages in the studied samples and in other metasedimentary rocks of the Brusque Metamorphic

Complex. The interval of 1.99-2.14 Ga, which Basei et al. (2008a) pointed out as a typical age signal for zircons in the metasedimentary rocks of the Brusque Metamorphic Complex, is present in all samples dated in this study and thus confirms their statement.

4.3 Possible source regions for the metamorphosed clastic sedimentary succession in the Brusque Metamorphic Complex

Based on reconstructions of the pre-collisional tectonic evolution in the Kaoko-Damara-Gariep-Dom Feliciano orogenic belts (e.g. Porada, 1989), the possible source regions that provided the detrital material for sedimentation in the Brusque paleobasin are the Río de la Plata Craton, Luís Alves Microplate and Congo Craton, as well as the pre-Neoproterozoic rocks of the Coastal-Punta del Este Terrane. Voluminous Neoproterozoic granitoid rocks of the Florianópolis Batholith adjacent to the Brusque Metamorphic Complex and the São João Batista, Valsungana and Nova Trento suites within the complex, as well as the granitoids intruding the Coastal Terrane in the Kaoko Belt, are considered as possible sources for the sedimentary protolith of the sample BB08. Available protolith data obtained for magmatic and high-grade metamorphic rocks in the above-mentioned units are presented below and shown as black bars in Fig. 29.

Protolith data for the basement rocks of the Río de la Plata Craton have been obtained by Leite et al. (2000), Hartmann et al. (2000b, 2001), Santos et al. (2003), Rapela et al. (2007), Mallmann et al. (2007) and Gaucher et al. (2011). These studies revealed Mesoproterozoic, Paleoproterozoic and Archean ages clustering around 1.44, 1.75, 2.07, 2.14 and 3.20 Ga. Available protolith data for the Luís Alves Microplate basement rocks show Paleoproterozoic and Archean ages of ca. 2.11, 2.20, 2.33 and 2.70 Ga (Hartmann et al., 2000a; Basei et al., 2009; Passarelli et al., 2018 and references therein). Protolith data for the basement rocks of the Congo Craton in northern Namibia, obtained by Seth et al. (1998, 2003), Franz et al. (1999), Kröner et al. (2004, 2010) and Luft et al. (2011), reveal Mesoproterozoic, Paleoproterozoic and Archean ages of ca. 1.50, 1.68, 1.77, 1.97 and 2.60 Ga. When comparing the protolith ages for the Río de la Plata Craton, Luís Alves Microplate and Congo Craton, the former and latter cratons reveal several similarities in their zircon protolith ages. This suggests that the Río de la Plata and Congo cratons may have represented one coherent cratonic block at the time when the Neoproterozoic rifting of the supercontinent Rodinia started, and may support the previous suggestion that South America and Africa were never completely separated during the rifting (Porada, 1989).

Konopásek et al. (2014, 2017) suggested that the Mesoproterozoic zircons in the clastic metasedimentary rocks of the Kaoko Belt, that yielded ages younger than about 1.45 Ga, probably derived from a presumed (now-eroded) Mesoproterozoic volcano-sedimentary cover of the Congo Craton. Remnants of this cover (the Okapuka Formation) overlies the Epupa gneisses of the Congo Craton (Fig. 3), in which a felsic schist has been dated at ca. 1.32 Ga (Kröner and Rojas-Agramonte, 2017). Numerous Mesoproterozoic granitoid rocks intruding the Epupa gneisses, and associated with the Okapuka Formation volcano-sedimentary cover, have been dated between ca. 1.17 and 1.53 Ga (Kröner and Rojas-Agramonte, 2017). There is no evidence for an equivalent to the Okapuka Formation in the northern part of the Dom Feliciano Belt and one can only speculate if such Mesoproterozoic volcano-sedimentary succession also covered the Río de la Plata Craton. However, since the Río de la Plata and Congo cratons possibly have represented one coherent block prior to the Neoproterozoic rifting, one cannot disregard the possibility that such Mesoproterozoic cover existed also on the South American side of the developing rift system. The presumed (now-eroded) Mesoproterozoic volcano-sedimentary cover of the Congo Craton, and possibly the Río de la Plata Craton, is regarded as a possible source for the Mesoproterozoic detrital zircons in the metasedimentary rocks of the Brusque Metamorphic Complex.

In addition to the Okapuka Formation, Konopásek et al. (2014, 2017) suggested the Mesoproterozoic Namaqua Metamorphic Belt, rimming the Kalahari Craton in central and northern Namibia (Fig. 3) (Becker et al., 2006), as a possible source for the Mesoproterozoic zircons in the Kaoko Belt. However, the Namaqua Metamorphic Belt is not considered here as a possible source region, because the belt is only exposed along the Kalahari Craton (Becker et al., 2006) and is distant to the Brusque Metamorphic Complex.

Protolith ages obtained for the Coastal-Punta del Este Terrane differ significantly compared to those obtained for the Río de la Plata Craton, Luís Alves Microplate and Congo Craton. In the Coastal-Punta del Este Terrane, Archean-Paleoproterozoic rocks are missing and the zircon dating revealed Neo- to Mesoproterozoic protolith ages between ca. 630 and 830 Ma and between ca. 970 Ma and 1.30 Ga, with a dominance of ages in the intervals of ca. 630-650 Ma and ca. 770-800 Ma (Seth et al., 1998; Preciozzi et al., 2003; Oyhantçabal et al., 2009; Lenz et al., 2011; Basei et al., 2011b; Masquelin et al., 2012; Konopásek et al., in press). Dating of granitoids in the Florianópolis Batholith and Angra Fria Magmatic Complex, at the opposite margins of the South Atlantic Ocean, revealed ages between ca. 630 and 575 Ma (Basei et al., 2000; da Silva et al., 2005a; Konopásek et al., 2016). The São João Batista, Valsungana and Nova Trento suites in the Brusque Metamorphic Complex have between dated between ca. 610 and 590 Ma (da Silva et al., 2005b; Basei et al., 2011a; Florisbal et al., 2012b), while the magmatic activity in the Boundary Igneous Complex in the Kaoko Belt is slightly younger and has been dated by Seth et al. (1998) and Konopásek et al. (2008) between ca. 580 and 550 Ma.

4.4 Possible source regions for the studied rock samples

Pooled U-Pb detrital zircon data for the five metasedimentary rock samples in this study are shown in Fig. 29. To interpret the source regions for the detrital zircon populations, the age data have been compared with the known zircon protolith ages in the possible source regions (see section 4.3) within the typical uncertainty for LA-ICP-MS analysis.

4.4.1 Samples BB10-B and BB14-A

Pooled U-Pb detrital zircon data for the samples BB10-B and BB14-A (Fig. 29a) show mainly Paleo- to Mesoproterozoic ages with maxima at ca. 2.15, 1.95, 1.80, 1.50, 1.35 and 1.20 Ga. The maxima at ca. 2.15 Ga corresponds well with the protolith age of ca. 2.14 Ga obtained for the Río de la Plata Craton, whereas the maxima at ca. 1.95, 1.80 and 1.50 Ga are comparable with the protolith ages of ca. 1.97, 1.77 and 1.50 Ga obtained for the Congo Craton. Zircons with ages around 1.35 and 1.20 Ga fall within the 1.53-1.17 Ga age interval of the Mesoproterozoic granitoid rocks intruding the Epupa gneisses of the Congo Craton basement. The maximum at ca. 1.35 Ga matches well the ca. 1.32 Ga age obtained for the presumed metavolcanic rock of the Mesoproterozoic cover of the Congo Craton (Okapuka Formation;

Kröner and Rojas-Agramonte, 2017). The Mesoproterozoic cover of the Congo Craton (the Okapuka Formation) nowadays represents only a small relic along the southwestern edge of the Congo Craton in Namibia. However, detrital zircon signals from the oldest Neoproterozoic cover of the Congo Craton at many localities of the Kaoko Belt (Konopásek et al., 2014, 2017) always show large proportion of Mesoproterozoic ages. This suggests, that the extent of the "Okapuka-like" Mesoproterozoic cover must have been large, but it was eroded away during initial stages of the Neoproterozoic rifting.

Even though no relics of the "Okapuka-like" Mesoproterozoic cover have been observed at the South American side, the presence of a large proportion of Mesorpoterozoic detrital zircon grains in the sample BB10-B and BB14-A suggest that Mesoproterozoic rocks could also have been covering the Río de la Plata Craton and Luís Alves Microplate. If the Mesoproterozoic cover, regardless whether in African and/or South America, provided the sedimentation of the samples BB10-B and BB14-A, the Paleoproterozoic detrital zircons most likely represent a second-cycle zircons already deposited in the Mesoproterozoic sedimentary rocks.

4.4.2 Samples BB22 and BA23

In Fig. 29b, the pooled U-Pb detrital zircon data for the samples BB22 and BA23 reveal predominantly Paleoproterozoic ages with maxima at ca. 2.20, 2.10, 2.05 and 1.95 Ga. The maxima at ca. 2.20 and 2.10 Ga are almost identical with the protolith ages of 2.20 and 2.11 Ga for the Luís Alves Microplate, whereas the maxima at ca. 2.05 and 1.95 Ga corresponds well with the protlith ages of 2.07 for the Río de la Plata Craton and 1.97 Ga for the Congo Craton, respectively. The notable suppression of Mesoproterozoic zircons in the samples BB22 and BA23, compared to the samples BB10-B and BB14-A, suggests a significant change in the source region(s) and most likely reflect the fact that at the time of sedimentation, the Mesoproterozoic cover of the source region has been already eroded and the samples reflect erosion of the cratonic basement.

4.4.3 Sample BB08

The distribution of zircon ages in the sample BB08 (Fig. 29c) is presented in section 4.1, and as mentioned, it is the only sample in this study that yielded zircons with Neoproterozoic ages. The maximum at ca. 2.20 Ga is compatible with the ca. 2.20 Ga protolith age obtained for the Luís Alves Microplate, while the maximum at ca. 2.15 is comparable with the ca. 2.14 protolith age obtained for the Río de la Plata Craton. Regarding the possible source(s) for the Neoproterozoic zircons, the Río de la Plata Craton, Luís Alves Microplate and Congo Craton are ruled out because zircons younger than Mesoproterozoic cannot represent the basement rocks. The Neoproterozoic zircons around 675 Ma may be sourced in the Coastal-Punta del Este Terrane, as the Neoproterozoic granitoids of the Florianópolis Batholith could not provide zircon grains older than ca. 630 Ma. For the zircons with ages around 625 and 565 Ma, the Florianópolis Batholith/Angra Fria Magmatic Complex and Boundary Igneous Complex are suggested as possible sources, respectively. However, the ca. 565 Ma old zircons are also comparable with the youngest zircons of the Florianópolis Batholith, which is a more likely source than the Boundary Igneous Complex because the former is situated in proximity to the Brusque Metamorphic Complex.

The Paleoproterozoic-Archean zircons in the sample BB08 probably represent a second-cycle grains derived from a source dominated by Neoproterozoic rocks. The Paleoproterozoic-Archean zircons could thus represent xenocrysts, whereas the Neoproterozoic zircon grains represent magmatic grains. The Brusque Metamorphic Complex is intruded by granitoids of the São João Batista, Valsungana and Nova Trento suites and some of them are as old as ca. 610 Ma, which indicates that the sample BB08 must be younger than the rest of the Brusque Metamorphic Complex as the youngest detrital zircon in the sample is around 540 Ma (see Appendix A). The age signal of the sample BB08 is similar to some sandstone samples of the Itajaí Basin obtained by Guadagnin et al. (2010), which suggest that the sample BB08 could be a part of the Itajaí sediments. The location of the sample BB08 in proximity to the Itajaí Basin (Fig. 4) supports the possibility that the sample is associated with the Itajaí Basin, rather than being a part of the Brusque Metamorphic Complex.

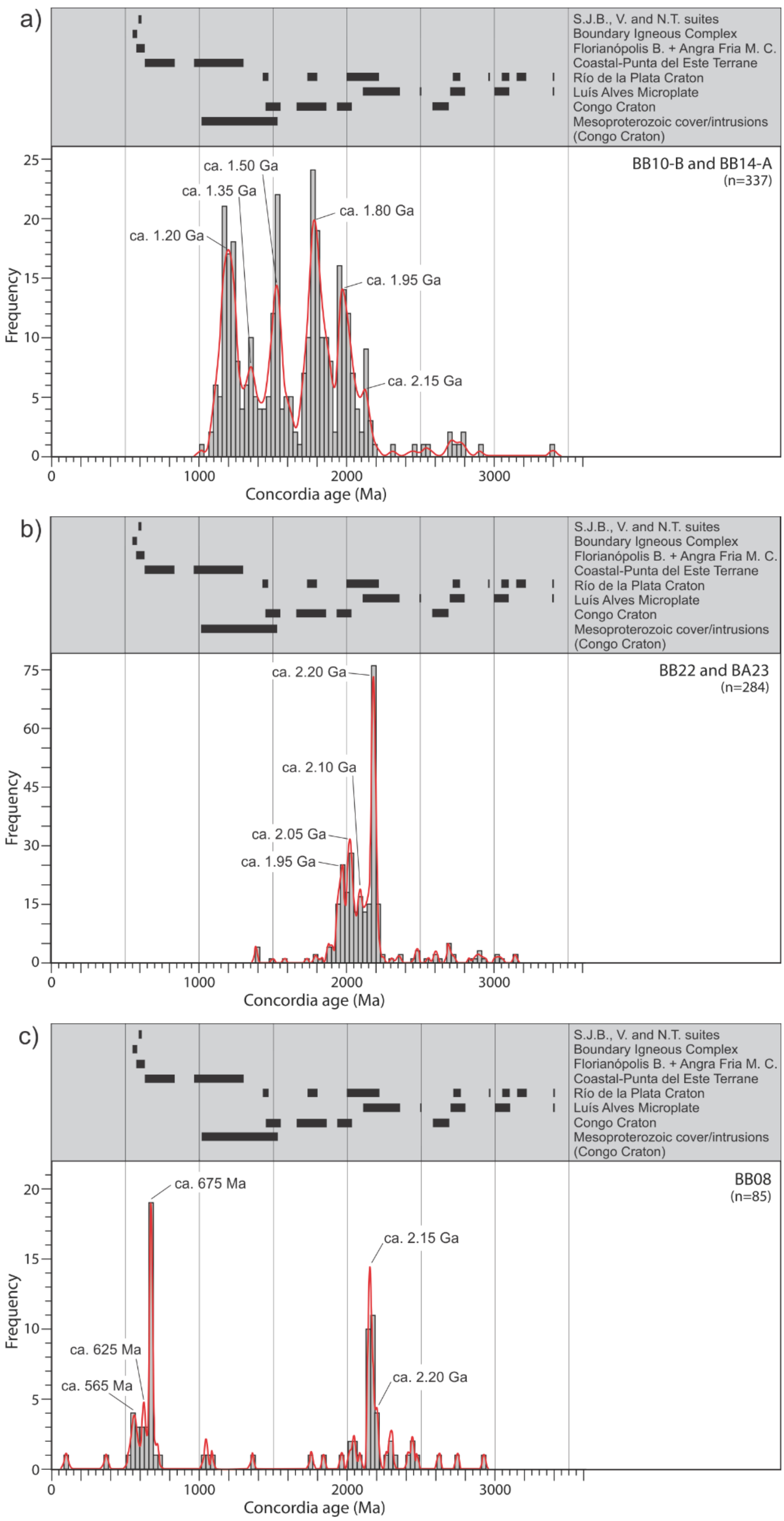

Fig. 29. Pooled U-Pb detrital zircon data for the studied metasedimentary rock samples. a) BB10-B and BB14-A; b) BB22 and BA23; c) BB08. The black bars represent the protolith ages for the possible source regions for the detrital material in the Brusque Metamorphic Complex, presented in section 4.3.

4.4.4 Sample BA22

The Mesoproterozoic-Archean zircon grains in the felsic volcanic rock sample BA22 most likely represent xenocrysts, trapped either during melting of the source, or during the movement of the magma through or along the surrounding (meta)sedimentary rocks of the Brusque Metamorphic Complex. Because only the xenocrysts were dated, the emplacement age of this igneous rock is not known.

4.5 Lithostratigraphy of the Brusque Metamorphic Complex

The volcano-sedimentary succession of the Brusque Metamorphic Complex was metamorphosed and deformed in the Neoproterozoic, and the original stratigraphic position of the lithological units is not well preserved (Basei et al., 2011a). However, as mentioned in the section 1.2.1.1, Basei et al. (2011a) made a division of the Brusque Metamorphic Complex into the Rio do Oliveira, Botuverá and Rio da Areia formations, which according to their interpretation represent the lower, intermediate and upper part of the succession, respectively. The formations were further subdivided into lithostratigraphic units, based on regional studies and previous geological mapping of the complex. Lithostratigraphic subdivisions of the Brusque Metamorphic Complex have also been carried out by authors like Chemale et al. (1995) and Philipp et al. (2004), where a more detailed division were made for restricted areas. In this study, however, an overall lithostratigraphy of the Brusque Metamorphic Complex is of interest. Based on the work of Basei et al. (2011a), as well as the detailed geological mapping of Basei et al. (2014a, b) and Wildner et al. (2014), a lithostratigraphic subdivision of the Brusque Metamorphic Complex is made (Fig. 30).

Because the Dom Feliciano and Kaoko belts are suggested to have formed in the same rift basin (Konopásek et al., in press), it should be possible to correlate the sedimentary successions of the Brusque Metamorphic Complex and the Central/Eastern Kaoko Zone. Konopásek et al. (2017) studied an uninterrupted lithostratigraphic profile of the low-grade southeastern part of the Central Kaoko Zone, where the stratigraphic position of their samples are shown along the profile (Fig. 31). The samples collected from the lower stratigraphic level (samples NL 20 and NL 24B of Konopásek et al., 2017 and sample NI 117 of Konopásek et al., 2014), associated with the early Neoproterozoic rifting period, yielded predominantly Meso- and Paleoproterozoic detrital zircon ages ranging between ca. 1.00 and 2.20 Ga. The source of the sedimentary protolith of their samples was suggested to be the Congo Craton and its inferred Mesoproterozoic volcano-sedimentary cover. The samples NL 20, NL 24B and NI 117 of Konopásek et al. (2014, 2017) reveal a similar age distribution as the samples BB10-B and BB14-A of this study, and thus suggest that the samples BB10-B and BB14-A most likely represent the lowermost sedimentary unit in the Brusque Metamorphic Complex.

Konopásek et al. (2017) also dated metasedimentary rocks in the intermediated part of the sedimentary succession of the Central Kaoko Zone (samples NL 21, NL 25, NL 26 and MDB-6), related to the later stage of the rifting. In these samples, they observed a disappearance of Mesoproterozoic zircons and a predominance of Paleoproterozoic zircons. This change in the detrital zircon age signal is also observed in the samples BB22 and BA23 of this study, which suggest that the samples BB22 and BA23 could represent the upper part of the sedimentary succession of the Brusque Metamorphic Complex. However, whereas the detrital zircons in the samples of Konopásek et al. (2017) predominantly range between ca. 1.70 and 1.85 Ga typical for the Congo Craton, the zircons in the samples BB22 and BA23 are somewhat older and between ca. 1.90 and 2.20 Ga typical for the Río de la Plata Craton and Luís Alves Microplate. Despite the difference in the sedimentary source for the samples of Konopásek et al. (2017) and of this study, the detrital zircon age signals only reflect, in both cases, an erosion of the local cratonic basement.

The detrital zircons in the metasedimentary rocks in the upper part of the sedimentary succession in the Central Kaoko Zone (samples NL 27, MDB-5, HKB-1 and NL 29 of Konopásek et al., 2017) revealed a bimodal age distribution and were interpreted as not related to rifting, but instead representing early orogenic flysch with source mainly in the Coastal-Punta del Este Terrane. Also, the sample NM 32 of Konopásek et al. (2017), collected from the upper unit of the Eastern Kaoko Zone, revealed a bimodal character and was suggested to represent molasse sediments sourced in the Granite Belt/Angra Fria Magmatic Complex and the Coastal-Punta del Este Terrane. Even though the bimodal distribution of the detrital zircon grains in the samples of Konopásek et al. (2017) and the sample BB08 of this study differ, the sample BB08 should also indicate a late orogenic sedimentary rock (molasses) due to the presence of late Neoproterozoic detrital zircon grains.

Based on the assumption that the sedimentary successions on both sides of the developing rift system between the South American and African continents should reveal similar evolutionary trends of detrital zircon age signals through the successive stratigraphic levels, the age spectra along the lithostratigraphic profile of the Brusque Metamorphic Complex and the Central/Eastern Kaoko Zone should reveal the same changes from the bottom to top of the basin (Figs. 30 and 31). However, as this is not the case, a new lithostratigraphic subdivision of the Brusque Metamorphic Complex is proposed and is based on the similarities in the detrital zircon age signals in the samples of this study and of Konopásek et al. (2017), as well as field observations.

In the new proposed lithostratigraphic subdivision of the Brusque Metamorphic Complex (Fig. 32), the lower basic metavolcanic unit is merged with the upper equivalent unit. In that case, the samples BB22 and BA23 represent the upper part of the Brusque Metamorphic Complex. Due to the similar detrital zircon age distribution in the samples BB22 and BA23, it is unlikely that they represent two units in completely different stratigraphic levels. As the samples BB22 and BA23 are quartzites, they are suggested to belong to the quartzite unit above the basic metavolcanic unit. As discussed above, the sample BB08 most likely belongs to the molasse sedimentary rocks of the Itajaí Basin rather than the Brusque Metamorphic Complex. Therefore, the metapelite-quartzite unit, from where the sample BB08 was collected, has been placed above the units of the the Rio do Olivera, Botuverá and Rio da Areia formations and a possible erosional unconformity is proposed to mark the boundary between the Brusque and Itajaí sedimentary rocks.

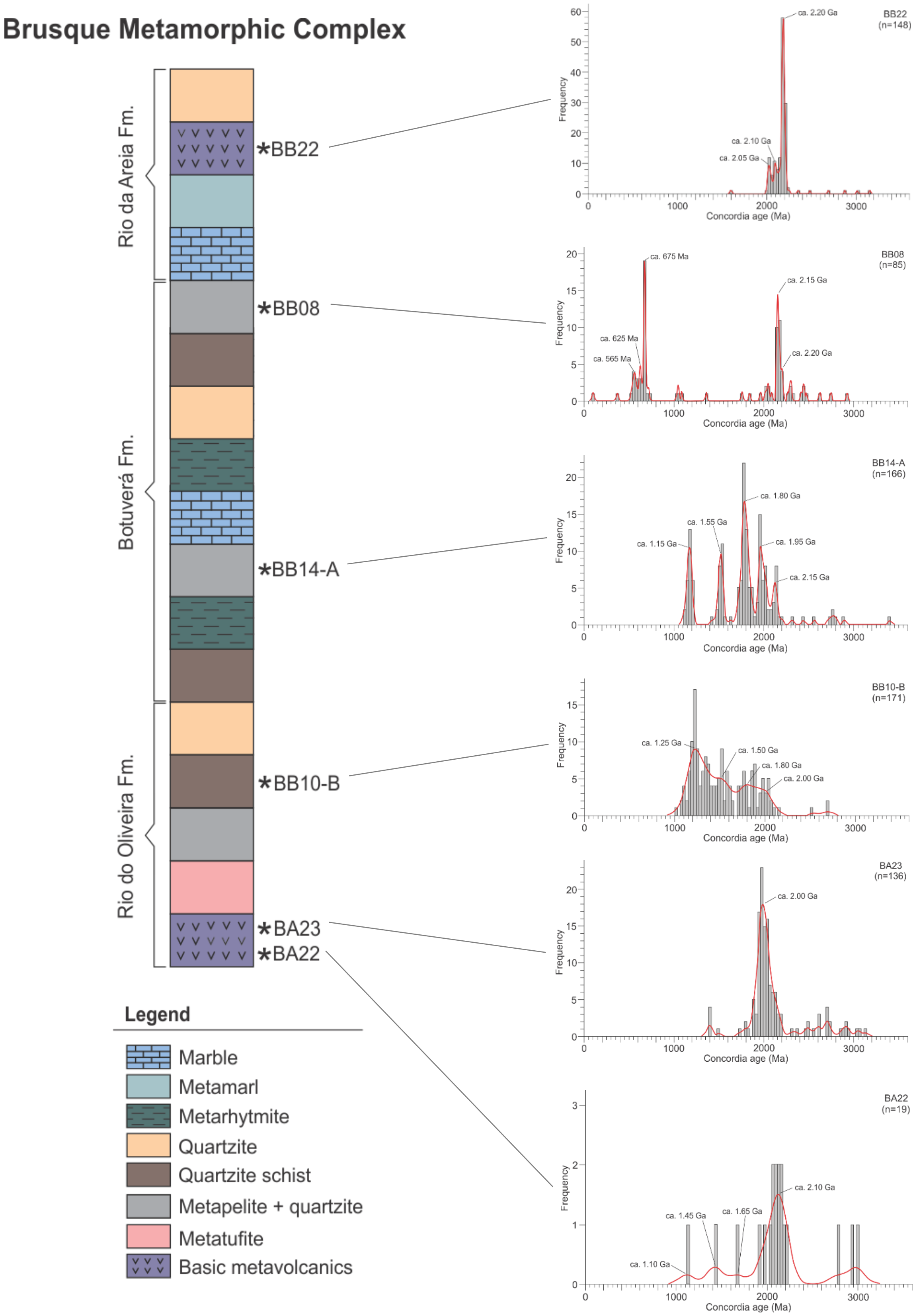

Fig. 30. Lithostratigraphic subdivision of the Brusque Metamorphic Complex, based on the work of Basei et al. (2011a, 2014a, b) and Wildner et al. (2014). The stratigraphic position of the studied samples is marked by asterisks and the corresponding age spectra are shown (see Figs. 12, 15, 18, 21, 24 and 27).

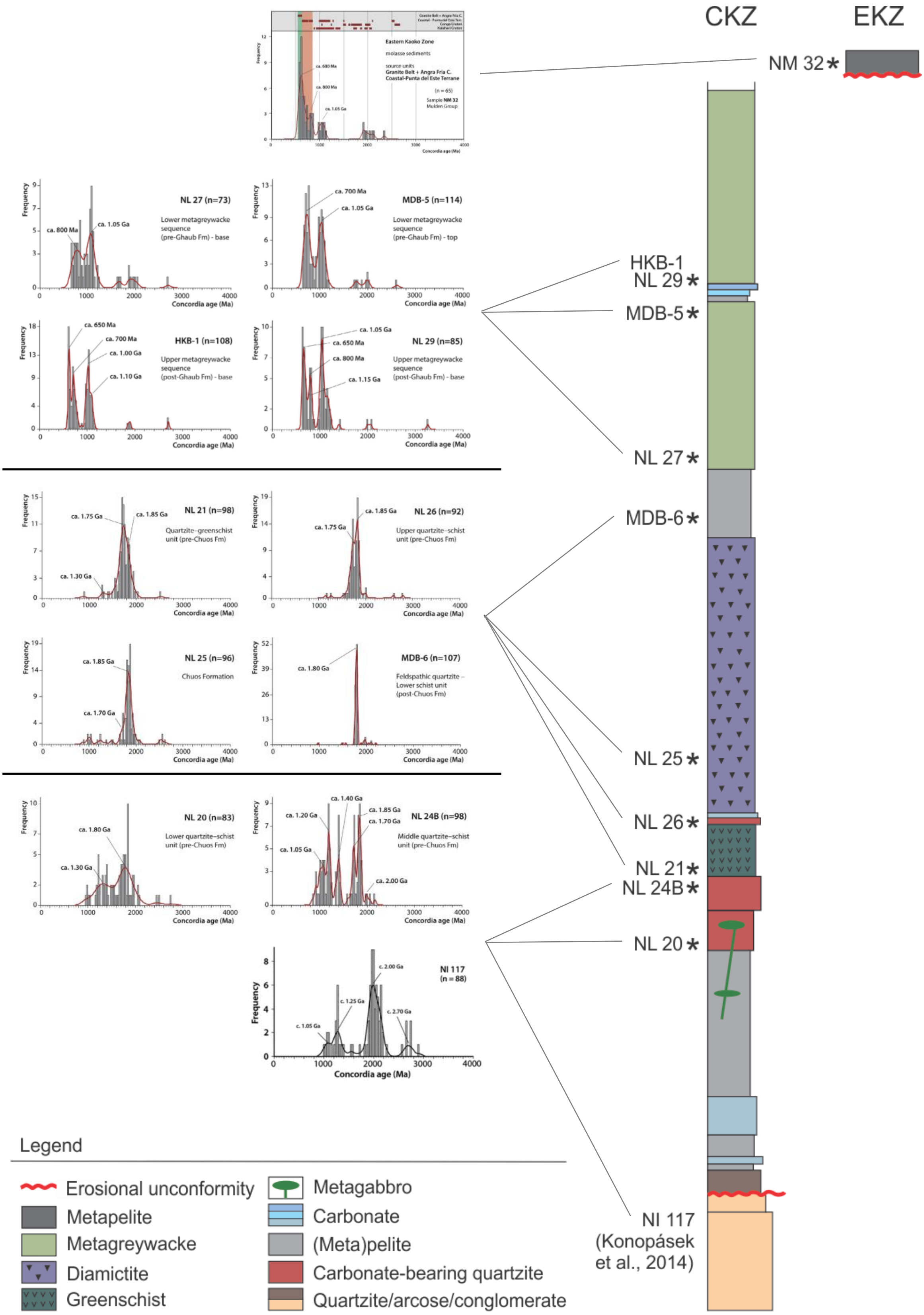

Fig. 31. Lithostratigraphic subdivision of the low-grade southeastern part of the Central Kaoko Zone (CKZ), as well as the uppermost unit of the Eastern Kaoko Zone (EKZ). The stratigraphic position of the studied samples of Konopásek et al. (2017), as well as the sample NI 117 of Konopásek et al. (2014), is marked by asterisks. The corresponding age spectra are shown (see Fig. 5 in Konopásek et al., 2017 and Fig. 4c in Konopásek et al., 2014). Modified after Konopásek et al. (2014, 2017).

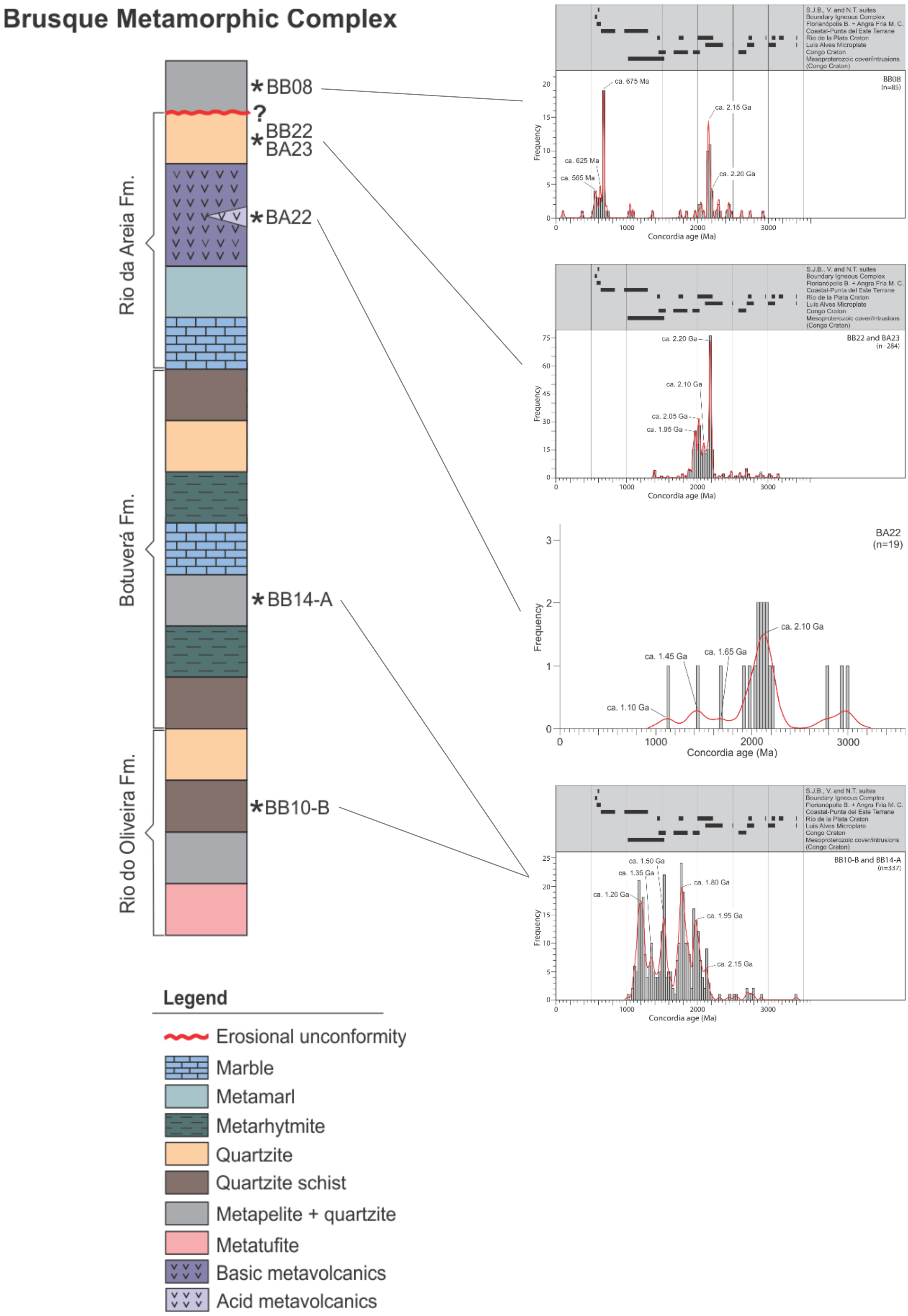

Fig. 32. Proposed lithostratigraphic subdivision of the Brusque Metamorphic Complex. The stratigraphic position of the studied samples is marked by asterisks and the corresponding age spectra are shown (see Figs. 27 and 29). The question mark represents the uncertainty regarding wether an erosional unconformity marks the boundary between the Brusque rocks and the unit of the sample BB08 (Itajaí molasse sedimentary rocks).

4.6 Tectonic evolution of the northern Dom Feliciano Belt and Kaoko Belt

Tectonic evolution of the Kaoko-Gariep-Dom Feliciano orogenic belts has been a matter of debate, particularly regarding the presence and later subduction of a hypothetical oceanic domain that has developed after the continental rifting stage. While Basei et al. (2000) suggested an eastward subduction of the Neoproterozoic ocean beneath Africa, Chemale et al. (2012) suggested that the ocean was subducted underneath South America. Multiple subduction zones, both eastward and westward, has also been proposed (Frimmel et al., 2011). However, Konopásek et al. (in press) questioned if an ocean existed at all and suggested that the Neoproterozoic rifting developed in a continental back-arc region. The suture zone between the South American and African continents is poorly defined, and very little oceanic crust is preserved (Goscombe and Gray, 2008). This makes the history of the hypothetical oceanic domain highly enigmatic.

A model of the possible tectonic evolution of the northern Dom Feliciano Belt and Kaoko Belt is proposed in Fig. 33, and is based on previous opinions regarding this topic. The model emphasizes the evolution of the Brusque sedimentary rocks and is suggested in the context of the detrital zircon age signals obtained for the studied samples.

Continental rifting stage at ca. 840-660 Ma

Rift-related volcanism dated along the margins of the eastern Río de la Plata Craton and the western Congo/Kalahari Craton, as well as in the Coastal-Punta del Este Terrane, suggest a time interval of ca. 840-710 Ma for the rifting between the South American and African continents (Frimmel et al., 1996, 2001; Basei et al., 2008a; Konopásek et al., 2008, 2014, in press; Oyhantçabal et al., 2009; Lenz et al., 2011; Saalmann et al., 2011). However, the rifting is suggested to have ended at ca. 660 Ma and is based on sedimentological data from the Otavi Platform (Fig. 6b) obtained by Hoffman and Halverson (2008).

As discussed in the section 4.5, the samples BB10-B and BB14-A probably represent clastic material in the lower part of the succession of the Brusque Metamorphic Complex, associated with the early Neoproterozoic rifting period (Fig. 33a). These two samples, like the samples NI 117, NL 20 and NL 24B of Konopásek et al. (2014, 2017) from the lower part of the succession of the Central Kaoko Zone, yielded predominantly Mesoproterozoic-Paleoproterozoic detrital zircon grains. The proportion of Mesoproterozoic zircons is large in both the South American and African samples, which suggests a wide extent of a Mesoproterozoic ("Okapuka-like") cover of the Paleoproterozoic–Archean cratonic basement. While the detrital zircon grains in the samples BB10-B and BB14-A reveal affinity to both the South American and African cratonic units, those in the samples of Konopásek et al. (2014, 2017) are apparently sourced only in Africa.

As the developing rift between the South American and African continents widened, the rift basin was further filled with volcanic rocks and sediments (Fig. 33b). At some point, the Mesoproterozoic cover of the Congo Craton, and possibly the Río de la Plata Craton and Luís Alves Microplate, was eroded away and has no longer served as a source for the basin sediments. This change in sediment source is evident by the suppression of Mesoproterozoic detrital zircons in the samples BB22 and BA23 of this study and the samples NL 21, NL 25, NL 26 and MDB-6 of Konopásek et al. (2017) from the Central Kaoko Zone. While the samples of Konopásek et al. (2017) represents the middle part of the succession of the Central Kaoko Zone, the samples of this study are interpreted as representing the upper part of the succession of the Brusque Metamorphic Complex. The volcanic rock sample BA22 was, based on the maps of Basei et al. (2014a, b) and Wildner et al. (2014), collected from the same lithostratigraphic unit as the sample BA23 (see section 4.5). It is thus suggested that the sample BA22 was collected from an igneous suite within the sedimentary unit from where the samples BB22 and BA23 were collected (Fig. 33b).

The age signals of the samples BB10-B, BB14-A, BB22 and BA23 show that the contribution of detrital zircon grains with African affinity decreases toward the top of the Brusque paleobasin (Fig. 32). This could be due to the increased distance between the Brusque paleobasin and the Congo Craton as the rifting proceeded. A significant amount of detrital zircon grains with affinity to the Luís Alves Microplate in the samples from the upper sedimentary succession (BB22 and BA23) may suggest that, at some point, the microplate was uplifted relative to the Río de la Plata Craton rocks.

Collisional stages at ca. 650-630 and 580-550 Ma

During the long-lived amalgamation of western Gondwana, which began at ca. 650 Ma and lasted until ca. 530 Ma (Goscombe and Gray, 2008), the main collisional stage occurred earlier in the northern Dom Feliciano Belt (ca. 650 Ma) than in the Kaoko Belt (ca. 580 Ma) (Goscombe et al., 2003b; Florisbal et al., 2012b).

During the collisional period in the northern Dom Feliciano Belt (Fig. 33c), the Brusque volcano-sedimentary rocks were affected by several metamorphism and deformation phases (Basei et al., 2011a). These phases were probably caused by burial of the Brusque rocks under the Coastal-Punta del Este Terrane. There is reason to believe that the collisional episode led to a topographic height at the South American side of the orogeny, which was subsequently eroded and provided molasse sediments of the developing Itajaí Basin. At about the same time as the main collisional period in the Brusque Metamorphic Complex, first syn-orogenic sediments start to be deposited on the African side of the orogeny (Fig. 33c). These sediments are represented by the samples NL 27, MDB-5, NL 29 and HKB-1 of Konopásek et al. (2017) from the upper succession of the Central Kaoko Zone, which was interpreted as representing flysch sediments sourced in the Coastal-Punta del Este Terrane.

During the collisional period in the Kaoko Belt (Fig. 33d), the Coastal Terrane was thrust over the Congo Craton margin (i.e. the Central Kaoko Zone and Orogen Core) and the boundary between the Coastal Terrane and Orogen Core was intruded by granitoids of the Boundary Igneous Complex. At this point, molasse sediments were deposited in the Eastern Kaoko Zone, and are represented by the sample NM 32 of Konopsek et al. (2017). During the post-collisional period in the northern Dom Feliciano Belt, granitoids intruded the Brusque Metamorphic Complex. Also, granitoids of the Florianópolis Batholith intruded the southeastern border of the complex. The erosion of the Brusque Metamorphic Complex probably caused an unconformity with respect to the overlying metamorphosed molasse sediments (Fig. 33d). However, the present day erosional level most likely reveals only relics of the molasse (Itajaí-type) sedimentary cover of the Brusque Metamorphic Complex in its northernmost part, from where the sample BB08 was collected (Fig. 4). As discussed in the section 4.4.3, the sample BB08 are considered as being part of the Itajaí sediments.

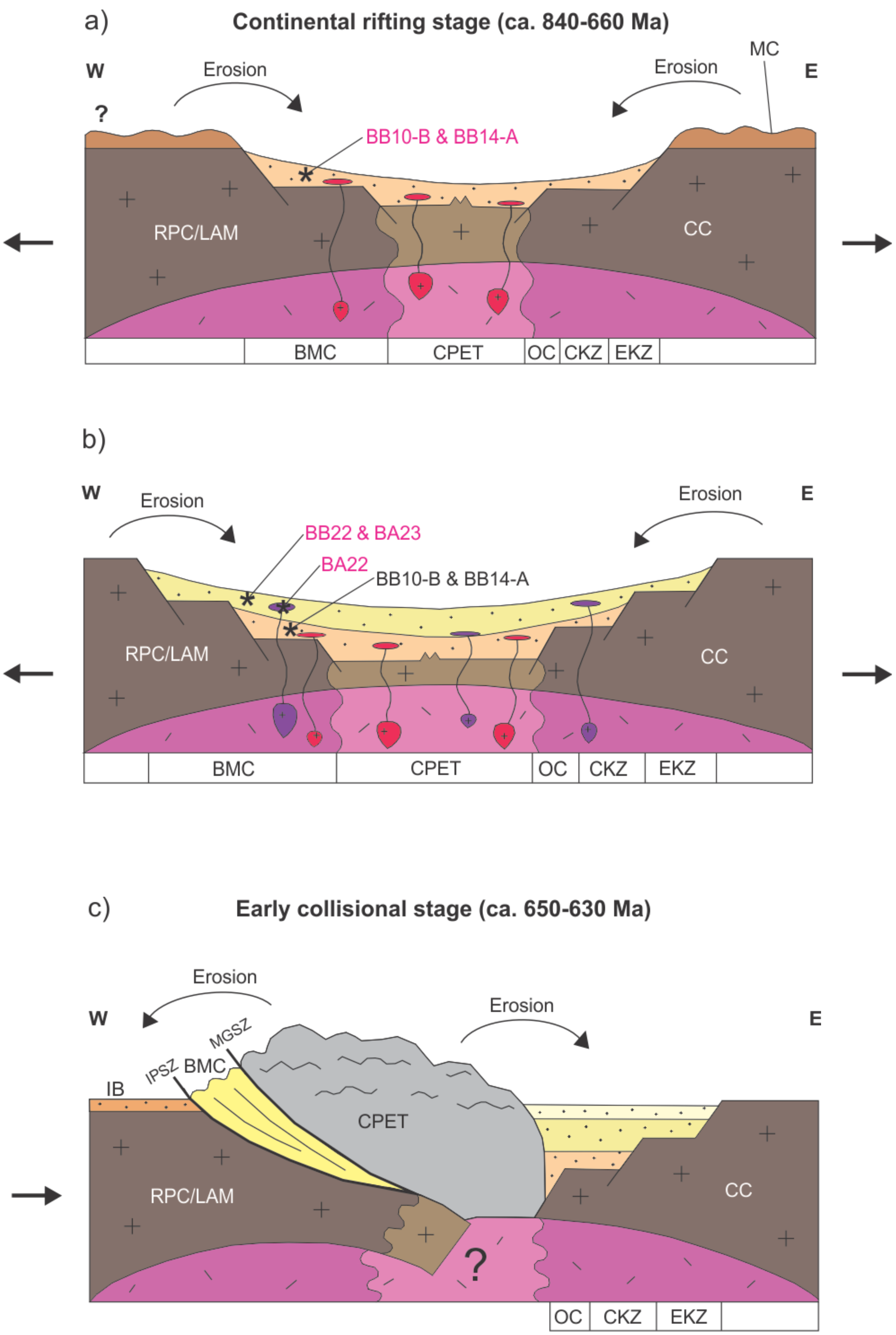
a)
Continental rifting stage (ca. 840-660 Ma)
W
Erosion
?
Erosion
MC
E
BB10-B & BB14-A
RPC/LAM
CC
BMC
CPET
OC
CKZ
EKZ
b)
W
Erosion
Erosion
E
BB22 & BA23
BA22
BB10-B & BB14-A
RPC/LAM
CC
BMC
CPET
OC
CKZ
EKZ
c)
Early collisional stage (ca. 650-630 Ma)
Erosion
W
MGSZ
IPSZ
BMC
IB
Erosion
E
CPET
RPC/LAM
CC
?
OC
CKZ
EKZ

Continued.

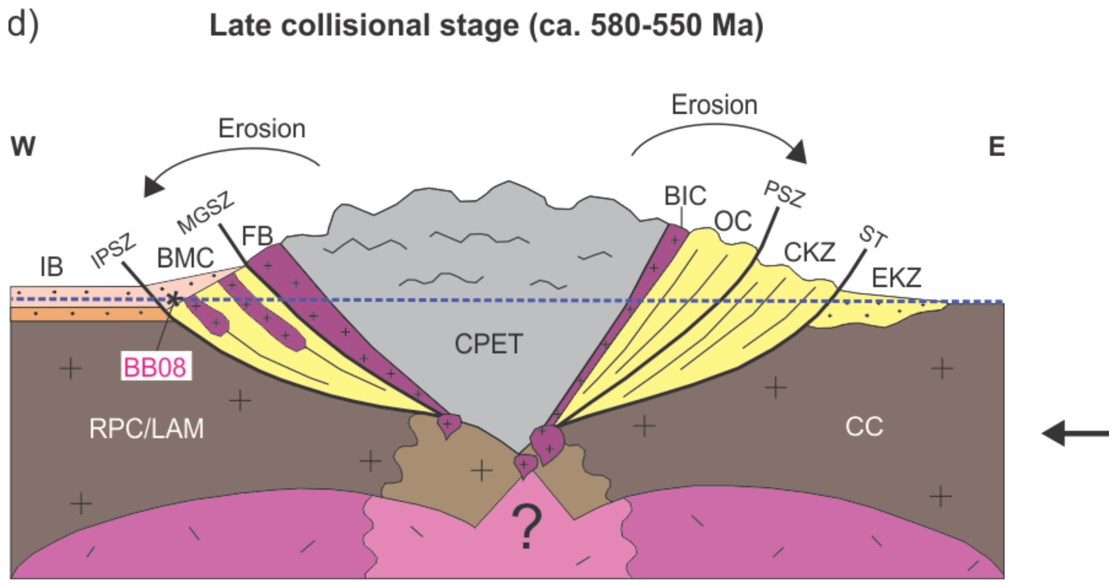

Fig. 33. Simplified model (not to scale) of the tectonic evolution of the northern Dom Feliciano Belt and the Kaoko Belt from early continental rifting stage (ca. 840 Ma) to late collisional stage (ca. 580-550 Ma). a) Erosion of the cratonic units and an inferred Mesoproterozoic volcano-sedimentary cover provide detritus for the lower sedimentary succession of the BMC, represented by the samples BB10-B and BB14-A. b) The Mesoproterozoic cover is eroded away and only the cratonic units provide sedimentation for the upper sedimentary succession of the BMC, represented by the samples BB22 and BA23. The sample BB22 occur as an igneous suite within the succession. c) Collision at the South American side results in burial of the Brusque rocks, and early molasse sediments are deposited in the developing IB. At the African side, flysch sediments are deposited in the uppermost succession in the CKZ. d) During the collision at the African side, the Coastal Terrane is thrust over the CC margin and provide molasse sediments in the EKZ. At the South American side, late molasse sediments are deposited in the IB, as well as on top of the BMC. The blue dotted line illustrate the present day erosion level. Question mark refers to the uncertainty regarding subduction of a hypothetical oceanic domain. RPC – Río de la Plata Craton; LAM – Luís Alves Microplate; CC – Congo Craton. CPET – Coastal-Punta del Este Terrane. MC – Mesoproterozoic cover. BMC – Brusque Metamorphic Complex; OC – Orogen Core; CKZ – Central Kaoko Zone; EKZ – Eastern Kaoko Zone; IB - Itajaí Basin. FB – Florianópolis Batholith; BIC – Boundary Igneous Complex. IPSZ - Itajaí-Perimbó Shear Zone; MGSZ - Major Gercino Shear Zone; PSZ - Purros Shear Zone; ST - Sesfontein Thrust.

5 Conclusions

This study has provided new insight into the provenance of metamorphosed clastic sediments in the Brusque Metamorphic Complex, and the following conclusions are:

- The quartzite samples BB10-B and BB14-A contained mostly Mesoproterozoic and Paleoproterozoic detrital zircon grains, which point to the Congo and Río de la Plata cratons, as well as an inferred Mesoproterozoic volcano-sedimentary cover, as possible source regions. The samples most likely represent the lower part of the sedimentary succession of the Brusque Metamorphic Complex, related to early Neoproterozoic rifting.
- The quartzite samples BB22 and BA23 revealed a predominance of Paleoproterozoic detrital zircon grains, whereas the proportion of Mesoproterozoic zircon grains is small. The lack of Mesoproterozoic detrital zircon grains suggests that the inferred Mesoproterozoic volcano-sedimentary cover was already eroded away at the time of sedimentation. The Congo and Río de la Plata cratons, as well as the Luís Alves Microplate, are suggested as possible sources for the Paleoproterozoic detrital zircons in these samples. The samples most likely represent the upper part of the sedimentary succession of the Brusque Metamorphic Complex, related to early–middle Neoproterozoic rifting.
- The phyllite sample BB08 yielded detrital zircon grains with mainly Neoproterozoic ages, which are suggested to be sourced in the Coastal-Punta del Este Terrane, Brusque Metamorphic Complex and Florianópolis Batholith. The Paleoproterozoic zircon grains probably represent a second cycle population. The sample most likely belongs to the molasse sedimentary rocks of the Itajaí Basin, rather than the Brusque Metamorphic Complex.
- Similarities in the detrital zircon age signals of the studied samples and those of Konopásek et al. (2017) from the low-grade part of the Central/Eastern Kaoko Zone, make it possible to propose a new lithostratigraphy of the Brusque Metamorphic Complex.

References

Basei, M.A.S, Siga, Jr.O., Masquelin, H., Harara, O.M., Reis Neto, J.M. & Preciozzi, F., 2000. *The Dom Feliciano Belt (Brazil-Uruguay) and its foreland (Rio de la Plata Craton): framework, tectonic evolution and correlations with similar terranes of southwestern Africa.* In: Cordani, U.G., Milani, E.J., Thomaz Filho, A., Campos, D.A. (Eds.), Tectonic Evolution of South America, pp. 311-334 (Rio de Janeiro).

Basei, M.A.S., Frimmel, H.E, Nutman, A. & Preciozzi, F., 2006. *Provenance and depositional age of the Dom Feliciano Belt supracrustals units, Brazil — Uruguay: correlations with SW Africa.* South American Symposium on Isotope Geology, V, Punta del Este, 2006: Short Papers, pp. 45–48.

Basei, M.A.S., Nutman, A., Grasso, C.B., Vlach, S., Siga, Jr.O. & Osako, L., 2008a. *The cryogenian rift-related granitogenesis of the Dom Feliciano Belt, Southern Brazil*. Abstracts volume, 4th international SHRIMP workshop, Saint Petersburg, Russia, pp. 24-26.

Basei, M.A.S., Frimmel, H.E., Nutman, A.P. & Preciozzi, F., 2008b. *West Gondwana amalgamation based on detrital zircon ages from Neoproterozoic Ribeira and Dom Feliciano belts of South America and comparison with coeval sequences from SW Africa*. Geological Society, London, Special Publications 294, pp. 239-256.

Basei, M.A.S., Nutman, A.P., Siga, Jr.O., Passarelli, C.R. Drukas, Cesar O, 2009. *The Evolution and tectonic setting of the Luis Alves Microplate of southeastern Brazil: An exotic terrane during the assembly of Western Gondwana*. Developments in Precambrian Geology 16, pp. 273-291.

Basei, M.A.S., Neto, M.C.C., Castro, N.A., Nutman, A.P., Wemmer, K., Yamamoto, Hueck, M., Osako, L. Siga. O. & Passarelli, C.R., 2011a. *Tectonic evolution of the Brusque Group, Dom Feliciano belt, Santa Catarina, Southern Brazil*. Journal of South American Earth Sciences 32, pp. 324-350.

Basei, M.A.S., Peel, E., Bettucci, L.S., Preciozzi, F. & Nutman, A.P., 2011b. *The basement of the Punta del Este Terrane (Uruguay): an African Mesoproterozoic fragment at the eastern border of the South American Río de la Plata Craton.* International Journal of Earth Sciences 100, pp. 289-304.

Basei, M.A.S., Drukas, C.O., Nutman, A.P., Wemmer, K., Dunyi, L., Santos, P.R.D., Passarelli, C.R. Neto, M.C.C. Siga, O.Jr. & Osako, L., 2011c. *The Itajaí foreland basin: a tectono-sedimentary record of the Ediacaran period, southern Brazil*. International Journal of Earth Sciences 100, pp. 543-569.

Basei, M.A.S., Neto, M.C.C., Lopes, A.P., Nutman, A.P., Liu, D. & Sato, K., 2013. *Polycyclic evolution of Camboriú Complex migmatites, Santa Catarina, Southern Brazil: integrated Hf isotopic and U-Pb age zircon evidence of episodic reworking of a Mesoarchean juvenile crust*. Brazilian Journal of Geology, 43, pp. 427-443.

Basei M.A.S., Campos N.M.C., Castro N.E., Santos P.R. & Siga Jr.O., 2014a. *Brusque sheet, 1:100.000.*

Basei M.A.S., Campos Neto M.C., Castro N.E., Santos P.R. & Siga Jr.O., 2014b. *Vidal Ramos sheet, 1:100.000.*

Basei, M.A.S., Frimmel, H.E., Neto, M.C.C., Araujo, C.E.G., Castro, N.A. & Passarelli, C.R., 2018. *The tectonic history of the Southern Adamastor Ocean based on a correlation of the Kaoko and Dom Feliciano belts.* In: Siegesmund, S., Basei, M., Oyhantçabal, P., Oriolo, S. (Eds.), Geology of Southwest Gondwana. Regional Geology Reviews. Springer, Cham. pp. 63-85.

Becker, T., Schreiber, U., Kampunzu, A.B. & Armstrong., 2006. *Mesoproterozoic rocks of Namibia and their plate tectonic setting.* Journal of African Earth Sciences 46, pp. 112-140.

Bitencourt, M.D.F. & Nardi, L.V.S., 2000. *Tectonic setting and sources of magmatism related to the southern Brazilian shear belt.* Revista Brasileira de Geociências 30, pp. 186-189.

de Campos, R.S., Philipp, R.P., Massonne, H.J., Chemale, F.Jr. & Theye, T., 2012. *Petrology and isotope geology of mafic to ultramafic metavolcanic rocks of the Brusque Metamorphic Complex, southern Brazil*. International Geology Review 54, pp. 686-713.

Chemale, Jr.F., Hartmann, L.A. & Silva, L.C.D., 1995. *Stratigraphy and tectonism of the Brasiliano Cycle in southern Brazil.* Communications of the Geological Survey of Namibia 10, pp. 153-168.

Chemale, Jr.F., Mallmann, G., Bitencourt, M.F. & Kawashita, K., 2012. *Time constraints on magmatism along the Major Gercino Shear Zone, southern Brazil: implications for West Gondwana reconstruction.* Gondwana Research 22, pp. 184-199.

Chisholm, E.I., Sircombe, K.N. and DiBugnara, D.L., 2014. *Handbook of Geochronology Mineral Separation Laboratory Techniques.* Record 2014/46. Geoscience Australia, Canberra.

Darke, S.A. & Tyson, J.F., 1993. *Interaction of laser radiation with solid materials and its significance to analytical spectrometry.* Journal of Analytical Atomic Spectrometry 8, pp. 145-209.

Deer, W.A., Howie, R.A. & Zussman, J., 2013. *An Introduction to the Rock Forming Minerals, 3rd Edition.* London: Mineralogical Society, pp. 12-14.

Evans, D.A.D., 2009. *The palaeomagnetically viable, long-lived and all-inclusive Rodinia supercontinent reconstruction.* Geological Society, London, Special Publications 327, pp. 371-404.

Florisbal, L.M., Janasi, V.A., Bitencourt, M.F., Nardi, L.V.S. & Heaman, L.M., 2012a. *Contrasted crustal sources as defined by whole-rock and Sr–Nd–Pb isotope geochemistry of neoproterozoic early post-collisional granitic magmatism within the Southern Brazilian Shear Belt, Camboriú, Brazil*. Journal of South American Earth Sciences 39, pp. 24-43.

Florisbal, L.M., Janasi, V.A., Bitencourt, M.F., Nardi, L.V.S. & Heaman, L.M., 2012b. *Space–time relation of post-collisional granitic magmatism in Santa Catarina, southern Brazil: U–Pb LA-MC-ICP-MS zircon geochronology of coeval mafic–felsic magmatism related to the Major Gercino Shear Zone*. Precambrian Research 216-219, pp. 132-151.

Franz, L., Romer, R.L. & Dingeldey, D.P., 1999. *Diachronous Pan-African granulite-facies metamorphism (650 Ma and 550 Ma) in the Kaoko belt, NW Namibia*. European Journal of Mineralogy 11, pp. 167-180.

Frimmel, H.E., Klötzli, U.S. & Siegfried, P.R., 1996. *New Pb-Pb single zircon age constraints on the timing of Neoproterozoic glaciation and continental break-up in Namibia*. The Journal of Geology 104, pp. 459-469.

Frimmel, H.E., Zartman, R.E. & Späth, A., 2001. *The Richtersveld igneous complex, South Africa: U-Pb zircon and geochemical evidence for the beginning of Neoproterozoic continental breakup*. The Journal of Geology 109, pp. 493-508.

Frimmel, H.E., Basei, M.A.S. and Gaucher, C., 2011. *Neoproterozoic geodynamic evolution of SW-Gondwana: a southern African perspective.* International Journal of Earth Sciences 100, pp. 323-354.

Gaucher, C., Boggiani, P.C., Sprechmann, P., Sial, A.N. & Fairchild, T., 2003. *Integrated correlation of the Vendian to Cambrian Arroyo del Soldado and Corumbá Groups (Uruguay and Brazil): palaeogeographic, palaeoclimatic and palaeobiologic implications.* Precambrian Research 120, pp. 241-278.

Gaucher, C., Frei, R., Chemale Jr. F., Frei, D., Bossi, J., Martínez, G., Chiglino, L. & Cernuschi, F., 2011. *Mesoproterozoic evolution of the Río de la Plata Craton in Uruguay: at the heart of Rodinia?* International Journal of Earth Sciences 100, pp. 273-288.

Goscombe, B., Hand, M. & Gray, D., 2003a. *Structure of the Kaoko Belt, Namibia: progressive evolution of a classic transpressional orogen.* Journal of Structural Geology 25, pp. 1049-1081.

Goscombe, B., Hand, M., Gray, D. & Mawby, J., 2003b. *The metamorphic architecture of a transpressional orogen: the Kaoko Belt, Namibia*. Journal of Petrology 44, pp. 679-711.

Goscombe, B., Gray, D., Armstrong, R., Foster, D.A. & Vogl, J., 2005a. *Event geochronology of the Pan-African Kaoko Belt, Namibia.* Precambrian Research 140, 103.e1-103.e41.

Goscombe, B., Gray, D. & Hand, M., 2005b. *Extrusional Tectonics in the Core of a Transpressional Orogen; the Kaoko Belt, Namibia.* Journal of Petrology 46, pp. 1203–1241.

Goscombe, B.D. & Gray, D.R., 2007. *The Coastal Terrane of the Kaoko Belt, Namibia: outboard arc-terrane and tectonic significance.* Precambrian research 155, 139-158.

Goscombe, B.D. & Gray, D.R., 2008. *Structure and strain variation at mid-crustal levels in a transpressional orogen: a review of Kaoko Belt structure and the character of West Gondwana amalgamation and dispersial.* Gondwana Research 13, pp. 45-85.

Guadagnin, F., Chemale, Jr.F., Dussin, I.A., Jelinek, A.R., Santos, M.N., Borba, M.L., Justino, D., Bertotti, A.L. & Alessandretti, L., 2010. *Depositional age and provenance of the Itajaí Basin, Santa Catarina State, Brazil: implications for SW Gondwana correlation*. Precambrian Research 180, pp. 156-182.

Günther, D. & Hattendorf, B., 2005. *Solid sample analysis using laser ablation inductively coupled plasma mass spectrometry.* Trends in Analytical Chemistry 24, pp. 355-265.

Hartmann, L.A., Santos, J.O.S., McNaughton, N.J., Vasconcellos, M.A.Z. & Silva, L.C.D., 2000a. *Ion microprobe (SHRIMP) dates complex granulite from Santa Catarina, southern Brazil.* Anais da Academica Brasileira de Ciências 72, pp. 559-572.

Hartmann, L.A., Piñeyro, D., Bossi, J., Leite, J.A.D. & McNaughton, N.J., 2000b. *Zircon U-Pb SHRIMP dating of Palaeoproterozoic Isla Mala granitic magmatism in Rio de la Plata Craton, Uruguay.* Journal of South American Earth Sciences 13, pp. 105-113.

Hartmann, L.A., Campal, N., Santos, J.O.S., McNaughton, N.J., Bossi, J., Schipilov, A. & Lafon, J.-M., 2001. *Archean crust in the Rio de la Plata Craton, Uruguay – SHRIMP U-Pb zircon reconnaissance geochronology.* Journal of South American Earth Sciences 14, pp. 557-570.

Hartmann, L.A., Bitencourt, M.F., Santos., J.O.S., McNaughton, N.J., Rivera, C.B. & Betiollo, L., 2003. *Prolonged Paleoproterozoic magmatic participation in the Neoproterozoic Dom Feliciano Belt, Santa Catarina, Brazil, based on zircon U-Pb SHRIMP geochronology.* Journal of South American Earth Sciences 16, pp. 477-492.

Hartnady, C., Joubert, P. & Stowe, C., 1985. *Proterozoic crustal evolution in southwestern Africa.* Episodes 8, pp. 236-244.

Hoffman, P.P., Hawkins, D.P., Isachsen, C.E. & Bowring, S.A., 1996. *Precise U-Pb zircon ages for early Damaran magmatism in the Summas Mountains and Welwitschia Inlier, northern Damara Belt, Namibia*. Communications of the Geological Survey of Namibia 11, pp. 49-53.

Hoffman, P.F. & Halverson, G.P., 2008. *Otavi Group of the western Northern Platform, the Eastern Kaoko Zone and the western Northern Margin Zone*. In: Miller, R.McG. (Ed) The Geology of Namibia, vol. 2. Geological Survey of Namibia, Windhoek, pp. 13-69 - 13-136.

Hueck, M., Basei, M.A.S. & Castro, N.A., 2016. *Origin and evolution of the granitic intrusions in the Brusque Group of the Dom Feliciano Belt, south Brazil: Petrostructural analysis and whole-rock/isotope geochemistry.* Journal of South American Earth Sciences 69, pp. 131-151.

Jackson, S.E., Pearson, N.J., Griffin, W.L. & Belousova, E.A., 2004. *The application of laser ablation-inductively coupled plasma-mass spectrometry to in situ U-Pb zircon geochronology.* Chemical Geology 211, pp. 47-69.

Jung, S., Brandt, S., Nebel, O., Hellebrand, E., Seth, B. & Jung, C., 2014. *The P–T–t paths of high-grade gneisses, Kaoko Belt, Namibia: Constraints from mineral data, U–Pb allanite and monazite and Sm–Nd/Lu–Hf garnet ages and garnet ion probe data*. Gondwana Research 25, pp. 775-796.

Konopásek, J., Košler, J., Tajčmanová, L., Ulrich, S. & Kitt, S.L., 2008. *Neoproterozoic igneous complex emplaced along major tectonic boundary in the Kaoko Belt (NW Namibia): ion probe and LA-ICP-MS dating of magmatic and metamorphic zircons*. Journal of the Geological Society, London 165, pp. 153-165.

Konopásek, J., Košler, J., Sláma, J. & Janoušek, V., 2014. *Timing and sources of pre-collisional Neoproterozoic sedimentation along the SW margin of the Congo Craton (Kaoko Belt, NW Namibia).* Gondwana Research 26, pp. 386-401.

Konopásek, J., Sláma, J. & Košler, J., 2016. *Linking the basement geology along the Africa-South America coasts in the South Atlantic*. Precambrian Research 280, pp. 221-230.

Konopásek, J., Hoffmann, K.-H., Sláma, J. & Košler J., 2017. *The onset of flysch sedimentation in the Kaoko Belt (NW Namibia) – Implications for the pre-collisional evolution of the Kaoko-Dom Feliciano-Gariep orogen.* Precambrium Research 298, pp. 220-234.

Konopásek, J., Janoušek, V., Oyhantçabal, P., Sláma, J., Ulrich, S., (in press): *Did the circum-Rodinia subduction trigger the Neoproterozoic rifting along the Congo-Kalahari Craton margin?* International Journal of Earth Sciences, DOI: 10.1007/s00531-017-1576-4.

Košler, J., Fonneland, H., Sylvester, P., Tubrett, M. & Pedersen, R.-B., 2002. *U-Pb dating of detrital zircons for sediment provenance studies – a comparison of laser ablation ICPMS and SIMS techniques*. Chemical Geology 182, pp. 605-618.

Košler, J. & Sylvester, P.J., 2003. *Present trends and the future of zircon in geochronology: laser ablation ICPMS. Reviews in mineralogy and geochemistry* 53, pp. 243-275.

Košler, J., Sláma, J., Belousova, E., Corfu, F., Gehrels, G.E., Gerdes, A., Horstwood, M.S.A., Sircombe, K.N., Sylvester, P.J., Tiepolo, M., Whitehouse, M.J. & Woodhead, J.D., 2013. *U-Pb detrital zircon analysis – results of an inter-laboratory comparison.* Geostandards and Geoanalytical Research 37, pp. 243-259.

Kröner, S., Konopásek, J., Kroner, A., Passchier, C.W., Poller, U., Wingate, M.T.D. & Hofmann, K.H., 2004. *U-Pb and Pb-Pb zircon ages for metamorphic rocks in the Kaoko Belt of Northwestern Namibia: A Palaeo-to Mesoproterozoic basement reworked during the Pan-African orogeny*. South African Journal of Geology 107, pp. 455-476.

Kröner, A., Rojas-Agramonte, Y., Hegner, E., Hoffmann, K-H. & Wingate, M.T.D., 2010. *SHRIMP zircon dating and Nd isotopic systematics of Palaeoproterozoic migmatitic orthogneisses in the Epupa Metamorphic Complex of northwestern Namibia*. Precambrian Research 183, pp. 50-69.

Kröner, A. & Rojas-Agramonte, Y., 2017. *Mesoproterozoic (Grenville-age) granitoids and supracrustal rocks in Kaokoland, northwestern Namibia.* Precambrian Research 298, pp. 572-592.

Leite, J.A.D., Hartmann, L.A, Fernandes, L.A.D., McNaughton, N.J., Soliani, Ê.Jr., Koester, E., Santos, J.O.S. & Vasconcellos, M.A.Z., 2000. *Zircon U-Pb SHRIMP dating of gneissic basement of the Dom Feliciano Belt, southernmost Brazil.* Journal of South American Earth Sciences 13, pp. 739-750.

Lenz, C., Fernandes, L.A.D., McNaughton, N.J., Porcher, C.C. & Masquelin, H., 2011. *U-Pb SHRIMP ages for the Cerro Bori Orthogneisses, Dom Feliciano Belt in Uruguay: evidences of a ca. 800 Ma magmatic and ca. 650 Ma metamorphic event.* Precambrian Research 185, pp. 149-163.

Li, Z.X., Bogdanova, S.V., Collins, A.S., Davidson, A., de Waele, B., Ernst, R.E., Fitzsimons, I.C.W., Fuck, R.A., Gladkochub, D.P., Jacobs, J., Karlstrom, K.E., Lu, S., Natapov, L.M., Pease, V., Pisarevsky, S.A., Thrane, K. & Vernikovsky, V., 2008. *Assembly, configuration and break-up history of Rodinia: a synthesis*. Precambrian Research 160, pp. 179-210.

Link, P.K., Fanning, C.M. & Beranek, L.P., 2005. *Reliability and longitudinal change of detrital zircon age spectra in the Snake River system, Idaho and Wyoming: an example of reproducing the bumpy barcode.* Sedimentary Geology 182, pp. 101-142.

Ludwig, K.R., 2012. *Isoplot 3.75. A geochronological toolkit for Microsoft Excel.* Berkley Geochronology Center Special Publication No. 5.

Luft Jr. J.L. & Chemale Jr., F., 2011. *Evidence of 1.7- to 1.8-Ga collisional arc in the Kaoko Belt, NW Namibia.* International Journal of Earth Sciences 100, pp. 305-321.

Mallmann, G., Chemale, F. Jr., Ávila, J.N., Kawashita, K. & Armstrong, R.A., 2007. *Isotope geochemistry and geochronology of the Nico Perez terrane, Rio de la Plata craton, Uruguay.* Gondwana Research 12, pp. 489-509.

Masquelin, H., Fernandes, L.A.D., Lenz, C., Porcher, C.C. & McNaughton, N.J., 2012. *The Cerro Olivo complex: a pre-collisional Neoproterozoic magmatic arc in Eastern Uruguay*. International Geology Review 54, pp. 1161-1183.

Meert, J.G. & Torsvik, T.H., 2003. *The making and unmaking of a supercontinent: Rodinia revisited*. Tectonophysics 375, pp. 261-288.

Miller, R.McG., 2008. *The Geology of Namibia, vol. 2.* Geological Survey of Namibia, Windhoek, pp. 13-10.

Orellana, F.A., Gálvez, C.G., Roldán, M.T. & García-Ruiz, C., 2013. *Applications of laser-ablation-inductively-coupled plasma-mass spectrometry in chemical analysis of forensic evidence.* Trends in Analytical Chemistry 42, pp. 1-34.

Oriolo, S., Oyhantçabal, P., Basei, M.A.S., Wemmer, K., Siegesmund, S., 2017. *Contemporaneous assembly of Western Gondwana and final Rodinia break-up: implications for the supercontinent cycle.* Geoscience Frontiers 8, pp. 1431-1445.

Oyhantçabal, P., Siegesmund, S., Wemmer, K., Presnyakov, S. & Layer, P., 2009. *Geochronological constraints on the evolution of the southern Dom Feliciano Belt (Uruguay).* Journal of the Geological Society, London 166, pp. 1075-1084.

Oyhantçabal, P., Siegesmund, S., Wemmer, K. & Layer, P., 2010. *The Sierra Ballena Shear Zone in the southernmost Dom Feliciano Belt (Uruguay): evolution, kinematics, and deformation conditions.* International Journal of Earth Sciences 99, pp. 1227-1246.

Oyhantçabal, P., Siegesmund, S., Wemmer, K. & Passchier, C.W., 2011. *The transpressional connection between Dom Feliciano and Kaoko belts at 580–550 Ma.* International Journal of Earth Sciences 100, pp. 379-390.

Passarelli, C.R., Basei, M.A.S., Siga, Jr. O. & Harara O.M.M., 2018. *The Luis Alves and Curitiba terranes: continental fragments in the Adamastor Ocean.* In: Siegesmund, S., Basei, M., Oyhantçabal, P., Oriolo, S. (eds) Geology of Southwest Gondwana. Regional Geology Reviews. Springer, pp. 189-215.

Philipp, R.P., Mallmann, G., Bitencourt, M.F., Souza, E.R., Souza, M.M.A., Liz, J.D., Wild, F., Arendt, S., Oliveira, A.S., Duarte, L., Riveira C.B. & Prado M., 2004. *Caracterização litológica e evolução metamórfica da porção leste do Complexo Metamórfico Brusque, Santa Catarina.* Revista Brasileira de Geociências 34, pp. 21-34.

Pisarevsky, S.A., Wingate, M.T.D., Powell, C.McA., Johnson, S. & Evans, D.A.D., 2003. *Models of Rodinia assembly and fragmentation*. Geological Society, London, Special Publications 206, pp. 35-55.

Porada, H., 1979. *The Damara-Ribeira orogen of the Pan-African – Brasiliano cycle in Namibia (Southwest Africa) and Brazil as interpreted in terms of continental collision*. Tectonophysics 57, pp. 237-265.

Porada, H., 1989. *Pan-African rifting and orogenesis in southern to equatorial Africa and eastern Brazil.* Precambrian Research 44, pp. 103-136.

Prave, A.R., 1996. *Tale of three cratons: Tectonostratigraphic anatomy of the Damara orogen in northwestern Namibia and the assembly of Gondwana*. Geology 24, pp. 1115-1118.

Preciozzi, F., Masquelin, H. & Basei, M.A.S., 1999. *The Namaqua/Grenville Terrane of eastern Uruguay*. II South American Symposium on Isotope Geology, Carlos Paz, pp. 1-3.

Preciozzi, F., Basei, M.A.S., Peel, E., Sánchez Bettucci, L., Cordani, U. & Oyhantçabal, P., 2003. *Punta del Este Terrane: Mesoproterozoic basement and Neoproterozoic cover*. IV South American Symposium on Isotope Geology, pp. 660-661.

Rapela, C.W., Pankhurst, R.J., Casquet, C., Fanning, C.M., Baldo, E.G., González-Casado, J.M., Galindo, C. & Dahlquist, J., 2007. *The Río de la Plata craton and the assembly of SW Gondwana*. Earth-Science Reviews 83, pp. 49-82.

Saalmann, K., Gerdes, A., Lahaye, Y., Hartmann, L.A., Remus, M.V.D. & Läufer, A., 2011. *Multiple accretion at the eastern margin of the Rio de la Plata Craton: the prolonged Brasiliano orogeny in southernmost Brazil*. International Journal of Earth Sciences 100, pp. 355-378.

Santos, J.O.S., Hartmann, L.A., Bossi, J., Campal, N., Schipilov, A., Piñeyro, D. & McNaughton, N.J., 2003. *Duration of the Trans-Amazonian Cycle and its correlation within South America based on U-Pb SHRIMP geochronology of the La Plata Craton, Uruguay*. International Geology Review 45, pp. 27-48.

Seth, B., Kröner, A., Mezger, K., Nemchin, A.A., Pidgeon, R.T. & Okrusch, M., 1998. *Archaean to Neoproterozoic magmatic events in the Kaoko belt of NW Namibia and their geodynamic significance.* Precambrian Research 92, pp. 341-363.

Seth, B., Armstrong, R.A., Brandt, S., Villa, I.M. & Kramers, J.D., 2003. *Mesoproterozoic U–Pb and Pb–Pb ages of granulites in NW Namibia: reconstructing a complete orogenic cycle*. Precambrian Research 126, pp. 147-168.

da Silva, L.C., McNaughton, N.J. & Fletcher, I.R., 2005a. *SHRIMP U-Pb zircon geochronology of Neoproterozoic crustal granitoids (Southern Brazil): A case for discrimination of emplacement and inherited ages.* Lithos 82, pp. 503-525.

da Silva, L.C., McNaughton, N.J., Armstrong, R., Hartmann, L.A. & Fletcher, I.R., 2005b. *The Neoproterozoic Mantiqueira Province and its African connections: a zircon-based U-Pb geochronologic subdivision for the Brasiliano/Pan-African systems of orogens.* Precambrian Research 136, pp. 203-240.

Sláma, J., Košler, J., Condon, D.J., Crowley, J.L., Gerdes, A., Hanchar, J.M., Horstwood, M.S.A., Morris, G.A., Nasdala, L., Norberg, N., Schaltegger, U., Schoene, B., Tubrett, N.M. & Whitehouse, M.J., 2008. *Plešovice zircon – a new natural reference material for U-Pb and Hf isotopic microanalysis.* Chemical Geology 249, pp. 1-35.

Ulrich, S., Konopásek, J., Jeřábek, P. & Tajčmanová, L., 2011. *Transposition of structures in the Neoproterozoic Kaoko Belt (NW Namibia) and their absolute timing*. International Journal of Earth Sciences 44, pp. 415-429.

Vermeesch, P., 2004. *How many grains are needed for a provenance study?* Earth and Planetary Science Letters 224, pp. 441-451.

Vermeesch, P., 2012. *On the visualisation of detrital age distributions*. Chemical Geology 312, pp. 190-194.

Wildner W., Camozzato E., Toniolo J.A., Binotto R.B., Iglesias C.M.F. & Laux J.H., 2014. *Geological map of Santa Catarina state (Brazil). 1:500.000.*

Wiedenbeck, M., Alle, P., Corfu, F., Griffin, W.L., Meier, M., Oberli, F., Vonquadt, A., Roddick, J.C. & Speigel, W., 1995. *3 natural zircon standards for U-Th-Pb, Lu-Hf, trace-element and REE analyses.* Geostandards Newsletter 19, pp. 1-23.

Appendix A – LA-ICP-MS data

* Dis. (6/38/7/6) = discordance of (^{206}Pb /^{238}U) / (^{207}Pb/^{206}Pb)

* Dis. (6/38/7/35) = discordance of (^{206}Pb /^{238}U) / (^{207}Pb/^{235}Pb)

Sample BB08																
Isotopic ratios								Concordia ages (Ma)								
Analysis	^{207}Pb /^{235}U	± 2σ	^{206}Pb /^{238}U	± 2σ	Rho	^{207}Pb/^{206}Pb	± 2σ	^{207}Pb /^{235}U	± 2σ	^{206}Pb /^{238}U	± 2σ	^{207}Pb/^{206}Pb	± 2σ	Dis. (6/38/7/6)	Dis. (6/38/7/35)
BB08_1	7.498	0.12	0.3997	0.0073	0.68085	0.1359	0.0015	2171	14	2165	34	2171	19	0.28	0.28
BB08_2	6.76	0.11	0.3847	0.0075	0.68031	0.1276	0.0015	2082	15	2098	34	2055	20	-2.09	-0.77
BB08_3	7.93	0.14	0.4219	0.0082	0.55779	0.1365	0.0018	2219	16	2265	37	2176	23	-4.09	-2.07
BB08_4	8.12	0.13	0.4214	0.0075	0.71234	0.1395	0.0013	2244	14	2265	34	2215	16	-2.26	-0.94
BB08_5	0.931	0.02	0.1099	0.0021	0.32728	0.0614	0.0013	665	12	672.1	12	617	48	-8.93	-1.07
BB08_6	0.936	0.02	0.1085	0.0026	0.69606	0.06241	0.001	668	12	664	15	671	35	1.04	0.60
BB08_7	6.34	0.17	0.3254	0.0083	0.69384	0.1414	0.0027	2020	23	1819	39	2236	32	18.65	9.95
BB08_8	7.43	0.13	0.3976	0.008	0.80922	0.1352	0.0012	2159	15	2157	37	2163	16	0.28	0.09
BB08_9	0.844	0.02	0.1011	0.0018	0.38034	0.0602	0.0011	619.5	10	620.7	11	585	41	-6.10	-0.19
BB08_10	7.719	0.12	0.4094	0.0073	0.55199	0.1366	0.0016	2195	14	2210	34	2175	20	-1.61	-0.68
BB08_11	7.942	0.12	0.4116	0.0075	0.64058	0.139	0.0014	2222	14	2222	35	2211	18	-0.50	0.00
BB08_12	7.71	0.12	0.4125	0.0076	0.58855	0.135	0.0016	2196	14	2227	35	2156	21	-3.29	-1.41
BB08_13	0.838	0.02	0.1019	0.002	0.35449	0.0595	0.0011	615.6	10	625.8	12	557	42	-12.35	-1.66
BB08_14	7.387	0.12	0.3966	0.0072	0.64272	0.1343	0.0015	2156	15	2151	33	2148	19	-0.14	0.23
BB08_15	10.18	0.18	0.4599	0.008	0.58098	0.1593	0.0019	2447	16	2439	36	2443	20	0.16	0.33
BB08_16	1.061	0.03	0.1104	0.0027	0.62771	0.0697	0.0013	732	12	675	15	911	37	25.91	7.79
BB08_17	5.28	0.19	0.308	0.014	0.68893	0.1261	0.0042	1860	31	1725	67	2027	59	14.90	7.26
BB08_18	6.531	0.12	0.3775	0.0071	0.48278	0.1248	0.0018	2046	16	2062	33	2015	26	-2.33	-0.78
BB08_19	5.73	0.24	0.327	0.016	0.78358	0.1283	0.0037	1937	34	1817	77	2063	49	11.92	6.20
BB08_20	8.08	0.14	0.3979	0.0076	0.58933	0.1462	0.0018	2237	16	2157	35	2298	21	6.14	3.58
BB08_21	0.964	0.02	0.1109	0.002	0.58867	0.06302	0.0008	684.8	9	677.6	12	700	28	3.20	1.05
BB08_22	0.965	0.02	0.1113	0.002	0.46538	0.06264	0.0009	684.9	9.1	680.7	12	680	31	-0.10	0.61
BB08_23	0.95	0.02	0.1099	0.002	0.33345	0.0622	0.0011	676.2	10	671.8	11	677	37	0.77	0.65
BB08_24	7.389	0.12	0.3967	0.0073	0.52931	0.1344	0.0017	2156	15	2152	34	2147	22	-0.23	0.19
BB08_25	7.83	0.13	0.4119	0.0077	0.57092	0.1373	0.0017	2209	15	2221	35	2187	21	-1.55	-0.54
BB08_26	8.08	0.13	0.4181	0.0073	0.58043	0.1391	0.0015	2239	14	2250	33	2210	18	-1.81	-0.49
BB08_27	16.35	0.33	0.5476	0.011	0.86405	0.2154	0.002	2893	20	2810	47	2943	15	4.52	2.87
BB08_28	7.11	0.13	0.3838	0.0074	0.6323	0.1341	0.0015	2125	16	2091	35	2145	20	2.52	1.60
BB08_29	2.853	0.05	0.2365	0.0044	0.71409	0.08696	0.0009	1366	13	1367	23	1353	19	-1.03	-0.07
BB08_30	7.6	0.17	0.3983	0.0076	0.4507	0.1375	0.0025	2183	20	2159	35	2185	32	1.19	1.10
BB08_31	0.715	0.02	0.0886	0.0017	0.42593	0.0579	0.0011	545.2	9.9	547	10	497	44	-10.06	-0.33
BB08_32	7.625	0.12	0.4066	0.0072	0.57442	0.1348	0.0015	2185	14	2198	33	2157	19	-1.90	-0.59
BB08_33	11.78	0.51	0.483	0.019	0.63799	0.1777	0.0055	2578	40	2534	80	2619	52	3.25	1.71
BB08_34	1.388	0.05	0.1231	0.0031	0.51862	0.0803	0.0021	881	19	748	18	1197	52	37.51	15.10
BB08_35	0.4528	0.01	0.05997	0.0011	0.37156	0.05435	0.0009	379	6.4	375.3	6.6	368	37	-1.98	0.98
BB08_36	0.735	0.02	0.0906	0.0017	0.38298	0.0586	0.0011	557.5	9.1	558.9	10	525	39	-6.46	-0.25
BB08_37	13.87	0.26	0.5215	0.011	0.60469	0.1913	0.0026	2740	18	2703	45	2744	23	1.49	1.35
BB08_38	0.675	0.02	0.0843	0.0016	0.41372	0.0579	0.0012	523	9.9	521.7	9.3	491	45	-6.25	0.25
BB08_39	0.806	0.01	0.0964	0.0018	0.58875	0.06025	0.0007	599.7	7.5	593.2	10	602	25	1.46	1.08
BB08_40	1.021	0.02	0.1166	0.0022	0.39188	0.0631	0.0011	712.6	11	710.7	13	685	37	-3.75	0.27
BB08_41	7.621	0.12	0.4061	0.0072	0.5479	0.135	0.0015	2185	14	2197	34	2157	19	-1.85	-0.55
BB08_42	0.707	0.01	0.0877	0.0016	0.45461	0.05832	0.0009	542.8	8	542	9.3	521	32	-4.03	0.15
BB08_43	7.524	0.12	0.4008	0.0073	0.5756	0.1353	0.0015	2173	15	2171	33	2162	20	-0.42	0.09
BB08_44	5.18	0.14	0.2912	0.0082	0.90785	0.1281	0.0014	1836	23	1641	41	2067	19	20.61	10.62
BB08_45	7.576	0.12	0.4036	0.0072	0.60374	0.1347	0.0014	2180	14	2186	33	2153	18	-1.53	-0.28
BB08_46	0.755	0.02	0.0923	0.0018	0.36452	0.059	0.0011	570.6	9.7	568.9	11	540	43	-5.35	0.30
BB08_47	0.847	0.02	0.1022	0.0019	0.25693	0.0599	0.0012	620.6	9.7	627.1	11	566	43	-10.80	-1.05
BB08_48	1.785	0.05	0.1726	0.0044	0.5574	0.0747	0.0016	1036	17	1025	24	1045	43	1.91	1.06
BB08_49	0.954	0.02	0.1103	0.0019	0.38228	0.06183	0.001	678.5	9.7	674.2	11	658	35	-2.46	0.63
BB08_50	4.896	0.08	0.3254	0.0058	0.55487	0.1087	0.0012	1799	14	1814	28	1767	21	-2.66	-0.83
BB08_51	0.83	0.02	0.0999	0.0021	0.33327	0.0598	0.0014	611	12	613.4	12	558	51	-9.93	-0.39
BB08_52	0.94	0.02	0.111	0.0021	0.47336	0.06111	0.001	671.4	9.9	678.8	12	629	34	-7.92	-1.10
BB08_53	0.943	0.02	0.1099	0.002	0.43112	0.0619	0.001	672.6	9.7	672.4	12	649	35	-3.61	0.03
BB08_54	1.725	0.04	0.1165	0.0023	0.64608	0.1067	0.0017	1012	15	709.7	13	1726	30	58.88	29.87
BB08_55	0.742	0.02	0.0909	0.0017	0.28742	0.0588	0.0011	561.5	8.8	560.7	10	532	41	-5.39	0.14
BB08_56	0.942	0.02	0.1097	0.0023	0.49536	0.06185	0.001	671.9	9.8	670	13	656	34	-2.13	0.28
BB08_57	10.15	0.17	0.4509	0.0087	0.61041	0.1621	0.0019	2447	15	2398	39	2477	20	3.19	2.00
BB08_58	6.29	0.19	0.3453	0.011	0.6085	0.1334	0.0036	2009	26	1908	52	2123	46	10.13	5.03
BB08_59	0.954	0.02	0.0849	0.0017	0.58408	0.0808	0.0013	678.5	11	524.9	10	1199	33	56.22	22.64
BB08_60	1.946	0.04	0.1835	0.0036	0.55028	0.0764	0.0012	1093	14	1085	19	1087	32	0.18	0.73
BB08_61	7.71	0.15	0.4063	0.0081	0.48029	0.1365	0.0022	2192	17	2197	37	2168	28	-1.34	-0.23
BB08_62	7.21	0.16	0.3821	0.0085	0.64268	0.1357	0.0021	2134	19	2083	40	2162	27	3.65	2.39
BB08_63	0.5116	0.01	0.05296	0.0011	0.59358	0.07008	0.001	419.1	6.7	332.6	6.5	918	29	63.77	20.64
BB08_64	9.12	0.18	0.4434	0.0082	0.57343	0.1484	0.0021	2349	17	2365	36	2314	24	-2.20	-0.68
BB08_65	2.318	0.08	0.0944	0.0021	0.26535	0.1773	0.005	1201	25	580.9	12	2597	51	77.63	51.63
BB08_66	0.884	0.02	0.1046	0.002	0.362	0.0611	0.0012	640.2	11	640.8	12	606	44	-5.74	-0.09

BB08_67	1.133	0.03	0.1121	0.0033	0.53804	0.0734	0.0018	767	16	685	19	1008	52	32.04	10.69
BB08_68	5.722	0.1	0.3426	0.0063	0.65155	0.1204	0.0013	1933	14	1897	30	1957	19	3.07	1.86
BB08_69	0.931	0.02	0.11	0.0022	0.36486	0.0614	0.0013	666	12	672.6	12	613	46	-9.72	-0.99
BB08_70	0.948	0.02	0.111	0.002	0.38724	0.06174	0.001	675	9.4	678.2	12	645	34	-5.15	-0.47
BB08_71	1.894	0.03	0.1833	0.0033	0.5529	0.0747	0.001	1077	12	1087	18	1048	28	-3.72	-0.93
BB08_72	8.48	0.24	0.396	0.013	0.84912	0.155	0.0024	2268	26	2139	59	2396	26	10.73	5.69
BB08_73	6.738	0.11	0.384	0.0067	0.61547	0.1268	0.0013	2075	14	2095	32	2047	18	-2.34	-0.96
BB08_74	0.773	0.02	0.0943	0.0018	0.36934	0.0592	0.0011	579	10	580.4	10	543	42	-6.89	-0.24
BB08_75	7.58	0.14	0.4074	0.0075	0.54476	0.1349	0.0018	2179	16	2200	34	2152	23	-2.23	-0.96
BB08_76	1.127	0.04	0.1078	0.0035	0.61978	0.0766	0.0022	767	20	659	20	1093	58	39.71	14.08
BB08_77	10.27	0.17	0.4643	0.0084	0.66252	0.1597	0.0017	2456	15	2458	38	2444	18	-0.57	-0.08
BB08_78	7.54	0.13	0.4039	0.0078	0.47457	0.1352	0.0019	2173	16	2184	36	2153	25	-1.44	-0.51
BB08_79	0.965	0.03	0.1124	0.0031	0.50654	0.0624	0.0016	683	15	686	18	664	58	-3.31	-0.44
BB08_80	8.42	0.14	0.422	0.0078	0.57816	0.1441	0.0017	2274	15	2267	35	2270	20	0.13	0.31
BB08_81	0.917	0.02	0.1094	0.0022	0.3561	0.0611	0.0014	658	12	669	13	595	51	-12.44	-1.67
BB08_82	0.0855	0	0.01318	0.0003	0.26323	0.0469	0.0014	83.2	2.6	84.4	1.8	40	63	-111.00	-1.44
BB08_83	0.942	0.02	0.1109	0.0021	0.37903	0.0613	0.0012	671.7	11	677.6	12	635	40	-6.71	-0.88
BB08_84	0.939	0.02	0.1104	0.0022	0.37029	0.0616	0.0013	669	11	674.8	13	630	45	-7.11	-0.87
BB08_85	0.941	0.03	0.109	0.0024	0.19902	0.0626	0.0017	673	13	666	14	679	57	1.91	1.04
BB08_86	7.637	0.11	0.4044	0.0071	0.65065	0.1363	0.0013	2186.6	13	2187	33	2178	17	-0.41	-0.02
BB08_87	5.184	0.08	0.3327	0.0059	0.70588	0.1127	0.0011	1849	14	1850	29	1835	18	-0.82	-0.05
BB08_88	8.28	0.25	0.413	0.011	0.55619	0.1469	0.0038	2261	29	2224	52	2297	45	3.18	1.64
BB08_89	1.045	0.03	0.1022	0.0025	0.45713	0.0746	0.0017	723	13	627	15	1028	45	39.01	13.28
BB08_90	0.908	0.02	0.1029	0.002	0.57855	0.06404	0.0009	655.7	9.4	630.9	12	731	31	13.69	3.78
BB08_91	1.013	0.02	0.1108	0.0021	0.43994	0.0661	0.0012	707.2	11	677.2	12	778	39	12.96	4.24
BB08_92	1.251	0.03	0.1173	0.0028	0.55295	0.0776	0.0015	822	13	715	16	1124	39	36.39	13.02
BB08_93	7.82	0.43	0.1523	0.0043	0.87949	0.358	0.01	2157	43	911	24	3710	42	75.44	57.77
BB08_94	1.028	0.03	0.1181	0.0025	0.55577	0.0631	0.0013	717	13	719	15	686	42	-4.81	-0.28
BB08_95	6.701	0.11	0.3743	0.0067	0.64248	0.1301	0.0013	2069	14	2050	31	2093	17	2.05	0.92
BB08_96	0.946	0.03	0.1104	0.0022	0.28172	0.0621	0.0016	671	13	674.4	13	625	55	-7.90	-0.51
BB08_97	6.49	0.14	0.3724	0.0088	0.84712	0.1257	0.0013	2040	19	2037	41	2033	19	-0.20	0.15
BB08_98	9.93	0.17	0.4587	0.0085	0.60471	0.1569	0.0019	2424	16	2433	38	2414	21	-0.79	-0.37
BB08_99	7.58	0.14	0.4103	0.0082	0.48139	0.1346	0.0021	2179	17	2212	37	2151	27	-2.84	-1.51
BB08_100	7.73	0.13	0.4045	0.0078	0.61767	0.1384	0.0017	2195	15	2189	35	2199	21	0.45	0.27
BB08_101	7.73	0.13	0.4129	0.0079	0.54385	0.1358	0.0019	2199	16	2228	35	2165	24	-2.91	-1.32

Sample BB10-B															
Isotopic ratios								Concordia ages (Ma)							
Analysis	^{207}Pb /^{235}U	± 2σ	^{206}Pb /^{238}U	± 2σ	Rho	^{207}Pb/^{206}Pb	± 2σ	^{207}Pb /^{235}U	± 2σ	^{206}Pb /^{238}U	± 2σ	^{207}Pb/^{206}Pb	± 2σ	Dis. (6/38/7/6)	Dis. (6/38/7/35)
BB10B_1	3.357	0.1	0.2595	0.0082	0.65983	0.0945	0.0023	1491	23	1479	41	1493	45	0.94	0.80
BB10B_2	2.411	0.06	0.2117	0.0051	0.65897	0.0835	0.0016	1244	16	1235	27	1270	38	2.76	0.72
BB10B_3	3.098	0.07	0.2471	0.0063	0.73927	0.0911	0.0017	1424	18	1422	33	1427	38	0.35	0.14
BB10B_4	1.929	0.04	0.181	0.0035	0.54879	0.0773	0.0014	1088	13	1071	19	1113	36	3.77	1.56
BB10B_5	3.3	0.08	0.2549	0.0064	0.71691	0.094	0.0017	1478	19	1460	33	1490	36	2.01	1.22
BB10B_6	3.52	0.12	0.2663	0.0088	0.72146	0.0963	0.0022	1518	27	1529	43	1518	43	-0.72	-0.72
BB10B_7	2.328	0.08	0.2023	0.0057	0.6578	0.0824	0.0021	1213	25	1186	31	1234	51	3.89	2.23
BB10B_8	2.476	0.06	0.2126	0.0055	0.60755	0.0849	0.0018	1259	18	1238	29	1305	40	5.13	1.67
BB10B_9	3.339	0.09	0.2571	0.0071	0.60368	0.094	0.0022	1485	22	1473	36	1492	44	1.27	0.81
BB10B_10	6.61	0.12	0.3771	0.0071	0.60753	0.1273	0.002	2060	16	2059	33	2054	29	-0.24	0.05
BB10B_11	4.73	0.12	0.3155	0.0087	0.72632	0.1089	0.0021	1766	21	1764	43	1775	36	0.62	0.11
BB10B_12	2.232	0.05	0.197	0.0043	0.55927	0.0823	0.0016	1187	15	1158	23	1233	38	6.08	2.44
BB10B_13	3.834	0.09	0.282	0.0063	0.69291	0.0983	0.0017	1593	18	1599	31	1576	33	-1.46	-0.38
BB10B_14	2.399	0.05	0.2104	0.005	0.64814	0.0833	0.0015	1238	15	1231	27	1264	37	2.61	0.57
BB10B_15	2.309	0.06	0.2095	0.004	0.42759	0.0803	0.0019	1212	17	1225	21	1183	47	-3.55	-1.07
BB10B_16	2.189	0.07	0.2016	0.0057	0.6193	0.0798	0.0019	1170	21	1180	30	1163	49	-1.46	-0.85
BB10B_17	6.23	0.13	0.3516	0.0073	0.6165	0.1283	0.0023	2002	18	1938	35	2067	32	6.24	3.20
BB10B_18	2.462	0.08	0.1845	0.0061	0.68796	0.0966	0.0022	1259	23	1095	34	1545	43	29.13	13.03
BB10B_19	2.4	0.05	0.2111	0.0045	0.55233	0.0829	0.0015	1236	15	1232	24	1245	34	1.04	0.32
BB10B_20	2.817	0.06	0.2329	0.0045	0.43683	0.0882	0.0019	1354	17	1348	23	1365	42	1.25	0.44
BB10B_21	5.55	0.1	0.3408	0.0049	0.58429	0.1181	0.0019	1904	15	1889	23	1915	28	1.36	0.79
BB10B_22	3.345	0.06	0.2542	0.0048	0.57143	0.095	0.0015	1488	14	1459	25	1517	30	3.82	1.95
BB10B_23	2.326	0.05	0.2071	0.0046	0.68118	0.082	0.0014	1218	16	1210	25	1234	32	1.94	0.66
BB10B_24	6.34	0.15	0.3632	0.0089	0.60067	0.1273	0.0024	2026	21	1993	42	2041	35	2.35	1.63
BB10B_25	1.607	0.03	0.1491	0.003	0.62317	0.0778	0.0012	971	12	895	17	1134	29	21.08	7.83
BB10B_26	6.41	0.13	0.3682	0.007	0.80238	0.1264	0.0014	2027	18	2019	32	2044	20	1.22	0.39
BB10B_27	6.556	0.1	0.3747	0.006	0.69249	0.1268	0.0014	2051	14	2049	28	2047	20	-0.10	0.10
BB10B_28	2.353	0.06	0.2096	0.0049	0.63157	0.0818	0.0015	1225	17	1226	27	1226	36	0.00	-0.08
BB10B_29	2.797	0.06	0.2305	0.0045	0.65846	0.0876	0.0016	1351	17	1336	24	1368	36	2.34	1.11
BB10B_30	6.01	0.12	0.3547	0.0071	0.65107	0.1233	0.002	1974	18	1952	34	1994	29	2.11	1.11
BB10B_31	5.877	0.1	0.3545	0.0062	0.68504	0.121	0.0021	1955	15	1959	31	1950	25	-0.46	-0.20
BB10B_32	4.48	0.13	0.3048	0.0085	0.73678	0.1066	0.0022	1722	25	1710	42	1732	38	1.27	0.70
BB10B_33	3.57	0.11	0.2638	0.0076	0.50157	0.0993	0.0026	1531	24	1504	39	1582	49	4.93	1.76
BB10B_34	3.99	0.12	0.2836	0.0078	0.6063	0.1022	0.0026	1619	25	1604	39	1642	45	2.31	0.93
BB10B_35	2.179	0.04	0.2026	0.0042	0.60644	0.0786	0.0014	1170	14	1190	23	1141	35	-4.29	-1.71
BB10B_36	2.827	0.06	0.2337	0.005	0.55546	0.0877	0.0016	1357	15	1351	26	1358	34	0.52	0.44
BB10B_37	5.12	0.12	0.3256	0.0069	0.77832	0.1133	0.0016	1833	20	1813	34	1845	27	1.73	1.09
BB10B_38	3.31	0.13	0.253	0.011	0.57111	0.0973	0.0034	1478	31	1449	57	1530	63	5.29	1.96
BB10B_39	2.917	0.06	0.2402	0.0049	0.69575	0.088	0.0014	1382	17	1385	26	1366	32	-1.39	-0.22
BB10B_40	3.564	0.07	0.2638	0.0053	0.71571	0.0971	0.0015	1538	16	1508	27	1559	29	3.27	1.95
BB10B_41	1.911	0.04	0.1814	0.0039	0.55979	0.077	0.0015	1082	15	1075	21	1110	39	3.15	0.65
BB10B_42	2.283	0.04	0.2072	0.004	0.59812	0.0797	0.0012	1206	12	1214	22	1175	32	-3.32	-0.66
BB10B_43	2.695	0.05	0.2266	0.0041	0.68287	0.0863	0.0011	1323	12	1315	21	1343	24	2.08	0.60
BB10B_44	3.577	0.1	0.276	0.008	0.58763	0.0944	0.0023	1540	22	1571	39	1491	46	-5.37	-2.01

BB10B_45	2.209	0.05	0.1977	0.004	0.68374	0.0807	0.0013	1182	15	1160	22	1201	34	3.41	1.86
BB10B_46	2.245	0.04	0.2005	0.0036	0.62824	0.081	0.0013	1191	14	1177	19	1214	32	3.05	1.18
BB10B_47	3.217	0.07	0.2551	0.0054	0.71076	0.0921	0.0014	1455	17	1461	28	1453	29	-0.55	-0.41
BB10B_48	2.055	0.04	0.1945	0.0044	0.48356	0.0771	0.0017	1135	15	1143	24	1092	42	-4.67	-0.70
BB10B_49	2.458	0.06	0.2175	0.0055	0.61557	0.0827	0.0019	1255	19	1265	29	1228	35	-3.01	-0.80
BB10B_50	2.361	0.07	0.2063	0.006	0.5394	0.0833	0.0021	1220	22	1204	32	1243	53	3.14	1.31
BB10B_51	6.48	0.16	0.3672	0.0092	0.72446	0.128	0.0022	2036	22	2010	43	2055	32	2.19	1.28
BB10B_52	1.95	0.11	0.1768	0.0054	0.4302	0.0796	0.0039	1083	36	1048	30	1117	99	6.18	3.23
BB10B_53	3.485	0.1	0.2642	0.0083	0.59628	0.096	0.0025	1518	23	1519	43	1509	47	-0.66	-0.07
BB10B_54	1.749	0.04	0.1749	0.0035	0.50882	0.0727	0.0014	1024	13	1038	19	1006	40	-3.18	-1.37
BB10B_55	3.199	0.06	0.2518	0.005	0.47295	0.0924	0.0016	1451	14	1444	26	1457	31	0.89	0.48
BB10B_56	5.58	0.13	0.3488	0.0073	0.6555	0.1156	0.0019	1911	19	1924	35	1879	32	-2.39	-0.68
BB10B_57	2.179	0.04	0.2002	0.0054	0.51114	0.0818	0.0027	1174	13	1173	29	1187	44	1.18	0.09
BB10B_58	4.697	0.09	0.3111	0.0061	0.56896	0.1098	0.0017	1768	17	1744	30	1787	30	2.41	1.36
BB10B_59	5.67	0.13	0.3507	0.0082	0.6164	0.1158	0.0022	1921	20	1935	39	1886	35	-2.60	-0.73
BB10B_60	6.2	0.15	0.3633	0.009	0.67763	0.1242	0.0024	2001	22	2002	43	1996	33	-0.30	-0.05
BB10B_61	2.545	0.06	0.2217	0.0056	0.6922	0.0832	0.0015	1279	18	1288	30	1262	35	-2.06	-0.70
BB10B_62	4.686	0.1	0.3219	0.0073	0.65237	0.1066	0.002	1763	17	1801	36	1724	34	-4.47	-2.16
BB10B_63	2.824	0.07	0.2381	0.0057	0.63959	0.0862	0.0016	1356	19	1382	30	1324	37	-4.38	-1.92
BB10B_64	5.46	0.16	0.342	0.01	0.66197	0.1175	0.0028	1885	26	1891	49	1886	41	-0.27	-0.32
BB10B_65	5.3	0.13	0.3455	0.0081	0.66731	0.1108	0.0021	1863	21	1916	39	1803	35	-6.27	-2.84
BB10B_66	2.709	0.06	0.2324	0.0055	0.69382	0.0842	0.0014	1325	18	1350	30	1285	32	-5.06	-1.89
BB10B_67	5.53	0.12	0.3466	0.0091	0.63688	0.1151	0.0023	1900	18	1924	43	1869	37	-2.94	-1.26
BB10B_68	5.59	0.16	0.3514	0.0099	0.61273	0.1163	0.0025	1904	24	1935	47	1898	41	-1.95	-1.63
BB10B_69	2.834	0.06	0.2349	0.0053	0.66399	0.0882	0.0015	1363	16	1357	28	1375	34	1.31	0.44
BB10B_70	9.4	1.1	0.362	0.011	0.83656	0.175	0.015	2223	88	1993	53	2390	120	16.61	10.35
BB10B_71	3.9	0.17	0.2683	0.0095	0.26092	0.1055	0.0046	1606	32	1529	49	1710	80	10.58	4.79
BB10B_72	6.44	0.2	0.358	0.013	0.38783	0.1335	0.0052	2025	27	1967	59	2091	54	5.93	2.86
BB10B_73	5.15	0.12	0.3224	0.0074	0.5833	0.1167	0.0025	1836	20	1800	37	1880	37	4.26	1.96
BB10B_74	2.742	0.08	0.2264	0.0066	0.55084	0.089	0.0024	1330	21	1315	34	1366	49	3.73	1.13
BB10B_75	2.719	0.06	0.2282	0.0051	0.69378	0.0861	0.0014	1330	15	1325	26	1329	31	0.30	0.38
BB10B_76	2.682	0.07	0.2232	0.005	0.6036	0.0882	0.0021	1315	19	1296	27	1360	47	4.71	1.44
BB10B_77	2.432	0.08	0.2159	0.0068	0.54657	0.0807	0.0021	1237	23	1254	36	1193	53	-5.11	-1.37
BB10B_78	4.51	0.17	0.301	0.012	0.68954	0.1106	0.0033	1718	31	1686	61	1779	53	5.23	1.86
BB10B_79	9.68	0.47	0.428	0.025	0.6595	0.1699	0.0082	2400	46	2280	110	2524	80	9.67	5.00
BB10B_80	4.92	0.14	0.3305	0.0097	0.63071	0.1091	0.0025	1797	26	1840	46	1772	44	-3.84	-2.39
BB10B_81	2.952	0.08	0.2415	0.0073	0.67194	0.0902	0.0019	1388	20	1388	38	1394	41	0.43	0.00
BB10B_82	2.225	0.04	0.1987	0.004	0.51324	0.0811	0.0015	1186	13	1167	22	1205	37	3.15	1.60
BB10B_83	1.951	0.04	0.1832	0.0036	0.59257	0.0772	0.0013	1098	13	1083	19	1124	33	3.65	1.37
BB10B_84	4.62	0.11	0.3076	0.0079	0.6266	0.1103	0.0023	1746	20	1721	39	1791	39	3.91	1.43
BB10B_85	1.855	0.04	0.1718	0.0035	0.61071	0.0784	0.0014	1062	13	1021	19	1140	35	10.44	3.86
BB10B_86	2.391	0.06	0.2107	0.0053	0.63675	0.0825	0.0017	1238	17	1232	27	1236	39	0.32	0.48
BB10B_87	5.06	0.11	0.3194	0.0069	0.56995	0.1146	0.0023	1826	19	1784	34	1862	36	4.19	2.30
BB10B_88	2.342	0.06	0.2107	0.0059	0.72525	0.0811	0.0015	1220	19	1231	31	1218	38	-1.07	-0.90
BB10B_89	2.226	0.05	0.2003	0.0053	0.7146	0.0808	0.0015	1186	15	1175	28	1205	36	2.49	0.93
BB10B_90	2.765	0.09	0.2342	0.0068	0.58105	0.0857	0.0021	1341	23	1350	35	1302	47	-3.69	-0.67
BB10B_91	3.47	0.08	0.2612	0.0061	0.61072	0.0961	0.0018	1518	17	1496	31	1538	33	2.73	1.45
BB10B_92	2.807	0.07	0.2337	0.0065	0.681	0.0878	0.0018	1349	18	1349	34	1357	39	0.59	0.00
BB10B_93	2.615	0.06	0.2249	0.0057	0.73435	0.0845	0.0014	1299	18	1304	30	1285	34	-1.48	-0.38
BB10B_94	3.977	0.09	0.2896	0.0067	0.67638	0.0998	0.0017	1623	18	1636	33	1609	32	-1.68	-0.80
BB10B_95	4.34	0.1	0.2992	0.0072	0.59216	0.1054	0.0021	1701	19	1689	36	1701	38	0.71	0.71
BB10B_96	3.114	0.07	0.2447	0.0053	0.71282	0.0921	0.0015	1432	17	1407	27	1468	27	4.16	1.75
BB10B_97	2.674	0.08	0.2243	0.0069	0.62638	0.0867	0.002	1310	21	1298	36	1337	43	2.92	0.92
BB10B_98	4.61	0.18	0.305	0.011	0.56068	0.1119	0.0035	1738	34	1703	55	1782	59	4.43	2.01
BB10B_99	2.682	0.06	0.2271	0.0053	0.55487	0.0854	0.0015	1319	16	1317	28	1309	36	-0.61	0.15
BB10B_100	2.328	0.05	0.2068	0.0047	0.64461	0.0819	0.0015	1221	16	1209	25	1238	37	2.34	0.98
BB10B_101	2.417	0.06	0.2142	0.0043	0.53756	0.0817	0.0017	1244	17	1249	23	1219	41	-2.46	-0.40
BB10B_102	2.262	0.05	0.2005	0.0042	0.70653	0.0817	0.0013	1195	15	1176	22	1231	32	4.47	1.59
BB10B_103	5.82	0.15	0.3423	0.0093	0.65636	0.1231	0.0024	1941	22	1902	43	1981	34	3.99	2.01
BB10B_104	2.581	0.08	0.2196	0.0069	0.68653	0.0855	0.0019	1284	22	1277	36	1312	40	2.67	0.55
BB10B_105	4.75	0.14	0.306	0.011	0.63581	0.1123	0.003	1771	24	1712	56	1818	51	5.83	3.33
BB10B_106	5.05	0.16	0.3139	0.0096	0.77443	0.116	0.0024	1821	27	1756	47	1885	37	6.84	3.57
BB10B_107	13.1	0.28	0.504	0.011	0.65381	0.187	0.0033	2681	20	2632	50	2713	30	2.99	1.83
BB10B_108	3.68	0.17	0.279	0.012	0.84848	0.0976	0.0026	1545	37	1572	62	1537	52	-2.28	-1.75
BB10B_109	3.223	0.06	0.2558	0.0051	0.59392	0.0921	0.0015	1465	16	1466	26	1469	32	0.20	-0.07
BB10B_110	2.212	0.04	0.1991	0.0039	0.70096	0.081	0.0011	1180	13	1168	21	1204	24	2.99	1.02
BB10B_111	2.41	0.04	0.2158	0.0033	0.54618	0.081	0.0011	1244	11	1258	18	1215	27	-3.54	-1.13
BB10B_112	2.13	0.13	0.1864	0.0098	0.65994	0.0831	0.0037	1142	44	1098	53	1255	89	12.51	3.85
BB10B_113	2.655	0.07	0.2252	0.0058	0.68396	0.0866	0.0017	1310	18	1308	30	1329	39	1.58	0.15
BB10B_114	3.551	0.06	0.2679	0.0046	0.65646	0.0957	0.0013	1534	14	1528	23	1530	25	0.13	0.39
BB10B_115	2.532	0.06	0.2226	0.0048	0.70799	0.084	0.0016	1277	16	1295	26	1261	34	-2.70	-1.41
BB10B_116	3.815	0.09	0.277	0.006	0.57694	0.0997	0.0019	1592	18	1573	30	1603	34	1.87	1.19
BB10B_117	5.37	0.15	0.341	0.0097	0.86713	0.1137	0.0017	1879	23	1885	46	1850	27	-1.89	-0.32
BB10B_118	13.34	0.29	0.52	0.012	0.64328	0.1856	0.0034	2692	21	2694	51	2698	31	0.15	-0.07
BB10B_119	3.756	0.1	0.277	0.0069	0.64342	0.0986	0.002	1572	21	1571	34	1577	37	0.38	0.06
BB10B_120	3.837	0.09	0.2761	0.0061	0.58557	0.1015	0.0019	1595	18	1572	30	1631	36	3.62	1.44
BB10B_121	2.253	0.05	0.2018	0.0045	0.61917	0.0823	0.0015	1193	14	1182	24	1238	34	4.52	0.92
BB10B_122	2.785	0.1	0.2241	0.0066	0.77359	0.0901	0.002	1344	26	1301	35	1422	41	8.51	3.20
BB10B_123	6.28	0.16	0.367	0.01	0.69263	0.1241	0.0023	2017	22	2015	50	2000	32	-0.75	0.10
BB10B_124	2.215	0.05	0.203	0.0047	0.54074	0.0792	0.0015	1182	15	1189	25	1172	41	-1.45	-0.59
BB10B_125	4.66	0.11	0.315	0.0084	0.63254	0.1086	0.0022	1760	20	1767	41	1751	36	-0.91	-0.40
BB10B_126	2.973	0.08	0.2448	0.006	0.61942	0.0895	0.0019	1397	20	1407	31	1389	40	-1.30	-0.72
BB10B_127	2.217	0.06	0.2036	0.0059	0.703	0.0791	0.0017	1186	19	1190	32	1146	43	-3.84	-0.34
BB10B_128	2.081	0.06	0.1719	0.0057	0.42686	0.0884	0.0029	1138	19	1021	31	1362	59	25.04	10.28

BB10B_129	2.153	0.06	0.1898	0.0044	0.53238	0.082	0.0019	1160	18	1119	24	1226	45	8.73	3.53
BB10B_130	1.958	0.05	0.1843	0.0049	0.57014	0.077	0.0018	1094	18	1095	27	1087	50	-0.74	-0.09
BB10B_131	3.298	0.07	0.2557	0.0048	0.59839	0.0931	0.0017	1473	17	1465	25	1470	35	0.34	0.54
BB10B_132	4.79	0.17	0.298	0.011	0.62246	0.1177	0.0034	1771	30	1668	55	1884	49	11.46	5.82
BB10B_133	4.9	0.14	0.3338	0.009	0.70311	0.107	0.0022	1788	24	1850	44	1733	36	-6.75	-3.47
BB10B_134	3.937	0.1	0.2847	0.0076	0.61085	0.1016	0.0024	1618	20	1609	38	1622	43	0.80	0.56
BB10B_135	3.024	0.09	0.2381	0.0078	0.57897	0.0928	0.0024	1404	22	1370	40	1441	50	4.93	2.42
BB10B_136	2.372	0.06	0.2094	0.0061	0.6225	0.0835	0.0019	1224	18	1224	33	1255	44	2.47	0.00
BB10B_137	3.805	0.1	0.284	0.0077	0.65118	0.0982	0.0021	1588	21	1604	38	1566	42	-2.43	-1.01
BB10B_138	3.601	0.09	0.2765	0.0074	0.59203	0.0957	0.002	1544	20	1570	38	1517	42	-3.49	-1.68
BB10B_139	4.084	0.09	0.2825	0.007	0.54553	0.1063	0.0024	1645	18	1603	36	1707	39	6.09	2.55
BB10B_140	2.997	0.09	0.2447	0.0078	0.61314	0.0895	0.0021	1394	24	1403	40	1399	47	-0.29	-0.65
BB10B_141	2.539	0.08	0.2117	0.0069	0.45348	0.0875	0.0029	1278	23	1242	37	1328	60	6.48	2.82
BB10B_142	5.23	0.13	0.3417	0.008	0.62153	0.1109	0.0021	1847	21	1891	39	1799	35	-5.11	-2.38
BB10B_143	3.27	0.11	0.2643	0.0093	0.69047	0.0909	0.0024	1457	26	1512	49	1409	52	-7.31	-3.77
BB10B_144	4.09	0.11	0.2975	0.0083	0.67777	0.1006	0.0021	1640	22	1678	41	1609	39	-4.29	-2.32
BB10B_145	2.181	0.06	0.1994	0.0062	0.60183	0.0807	0.0021	1168	21	1167	33	1168	52	0.09	0.09
BB10B_146	3.6	0.13	0.274	0.01	0.57979	0.0963	0.0031	1545	27	1552	53	1529	61	-1.50	-0.45
BB10B_147	4.29	0.14	0.297	0.011	0.72142	0.1055	0.0028	1680	28	1665	54	1695	50	1.77	0.89
BB10B_148	3.8	0.11	0.278	0.0083	0.62769	0.1	0.0024	1582	24	1576	42	1595	47	1.19	0.38
BB10B_149	3.39	0.12	0.2593	0.0092	0.66319	0.0969	0.0024	1486	29	1477	47	1535	51	3.78	0.61
BB10B_150	3.86	0.16	0.287	0.012	0.72185	0.0992	0.003	1591	35	1617	62	1581	59	-2.28	-1.63
BB10B_151	5.36	0.18	0.338	0.011	0.5656	0.1149	0.003	1855	29	1864	52	1858	48	-0.32	-0.49
BB10B_152	2.494	0.07	0.2158	0.0074	0.50195	0.0843	0.0025	1264	21	1256	39	1264	57	0.63	0.63
BB10B_153	6.04	0.14	0.3584	0.0092	0.65392	0.1228	0.0024	1971	20	1965	44	1988	34	1.16	0.30
BB10B_154	2.86	0.13	0.236	0.011	0.57009	0.0909	0.0034	1343	34	1355	58	1352	74	-0.22	-0.89
BB10B_155	2.373	0.1	0.1766	0.0083	0.56391	0.0987	0.0035	1221	30	1042	45	1539	71	32.29	14.66
BB10B_156	2.355	0.08	0.2063	0.0084	0.64718	0.0847	0.0027	1216	25	1202	44	1253	61	4.07	1.15
BB10B_157	5.97	0.28	0.353	0.017	0.58917	0.1271	0.0051	1934	42	1926	80	1964	74	1.93	0.41
BB10B_158	5.87	0.24	0.347	0.017	0.64369	0.1255	0.0049	1938	37	1907	79	1987	70	4.03	1.60
BB10B_159	5.92	0.32	0.333	0.017	0.54575	0.1292	0.006	1941	44	1842	82	2037	79	9.57	5.10
BB10B_160	4.75	0.2	0.316	0.013	0.62793	0.1112	0.0037	1744	38	1764	66	1758	63	-0.34	-1.15
BB10B_161	5.55	0.2	0.317	0.012	0.60606	0.1275	0.0033	1894	29	1761	57	2039	48	13.63	7.02
BB10B_162	3.17	0.11	0.25	0.0087	0.68605	0.0924	0.0024	1435	29	1428	45	1426	49	-0.14	0.49
BB10B_163	2.479	0.07	0.2181	0.006	0.64669	0.0832	0.0018	1258	21	1267	32	1240	43	-2.18	-0.72
BB10B_164	4.7	0.14	0.311	0.0099	0.68369	0.1107	0.0028	1753	27	1734	49	1763	47	1.64	1.08
BB10B_165	2.474	0.1	0.219	0.0085	0.74171	0.0828	0.0025	1241	30	1272	45	1222	58	-4.09	-2.50
BB10B_166	4.63	0.21	0.327	0.015	0.63403	0.1047	0.0036	1718	39	1808	72	1664	63	-8.65	-5.24
BB10B_167	6.01	0.19	0.358	0.011	0.68758	0.1228	0.0031	1961	28	1963	55	1964	47	0.05	-0.10
BB10B_168	2.299	0.09	0.2088	0.0083	0.67671	0.0812	0.0026	1204	27	1215	44	1168	65	-4.02	-0.91
BB10B_1	4.4	0.09	0.2982	0.005	0.65056	0.1072	0.0014	1711	16	1681	25	1747	24	3.78	1.75
BB10B_2	5.203	0.09	0.3309	0.0048	0.65635	0.1144	0.0012	1854	15	1841	23	1862	19	1.13	0.70
BB10B_3	2.35	0.04	0.2089	0.0032	0.73589	0.08167	0.0008	1226	14	1222	17	1230	20	0.65	0.33
BB10B_4	5.244	0.09	0.3303	0.0039	0.78185	0.11494	0.0007	1857.8	14	1840	18	1876	11	1.92	0.96
BB10B_5	2.4	0.06	0.2115	0.0042	0.56188	0.0826	0.0015	1239	17	1235	22	1246	35	0.88	0.32
BB10B_6	2.363	0.05	0.212	0.0037	0.59696	0.0807	0.0012	1227	15	1238	20	1203	30	-2.91	-0.90
BB10B_7	2.84	0.06	0.2355	0.0041	0.66705	0.0874	0.0012	1365	16	1362	21	1364	25	0.15	0.22
BB10B_8	3.06	0.06	0.2518	0.0041	0.87067	0.08772	0.0007	1421	16	1446	21	1370	16	-5.55	-1.76
BB10B_9	6.22	0.15	0.3683	0.0074	0.83246	0.1217	0.0014	1999	22	2016	35	1971	21	-2.28	-0.85
BB10B_10	5.981	0.11	0.3504	0.0057	0.71454	0.1238	0.0014	1972	17	1935	27	2006	20	3.54	1.88
BB10B_11	2.384	0.07	0.2103	0.0041	0.48627	0.0819	0.002	1233	21	1229	22	1214	48	-1.24	0.32
BB10B_12	2.465	0.06	0.2146	0.004	0.52146	0.083	0.0015	1260	16	1253	21	1263	34	0.79	0.56
BB10B_13	2.33	0.08	0.1955	0.0076	0.4865	0.0885	0.0042	1213	25	1153	39	1331	69	13.37	4.95
BB10B_14	6.97	0.15	0.3738	0.0075	0.86003	0.1349	0.0013	2102	20	2043	35	2157	17	5.29	2.81

Sample BB14-A															
Isotopic ratios								Concordia ages (Ma)							
Analysis	^{207}Pb /^{235}U	± 2σ	^{206}Pb /^{238}U	± 2σ	Rho	^{207}Pb/^{206}Pb	± 2σ	^{207}Pb /^{235}U	± 2σ	^{206}Pb /^{238}U	± 2σ	^{207}Pb/^{206}Pb	± 2σ	Dis. (6/38/7/6)	Dis. (6/38/7/35)
BB14A_1	5.04	0.17	0.33	0.012	0.5796	0.1126	0.0031	1816	28	1831	57	1815	49	-0.88	-0.83
BB14A_2	4.88	0.13	0.3183	0.0097	0.57776	0.1124	0.0025	1797	23	1775	47	1827	42	2.85	1.22
BB14A_3	2.352	0.07	0.2116	0.0066	0.6029	0.0822	0.0021	1220	21	1236	34	1204	49	-2.66	-1.31
BB14A_4	5.51	0.16	0.35	0.013	0.61298	0.1162	0.0028	1899	26	1925	60	1877	43	-2.56	-1.37
BB14A_5	7.05	0.22	0.393	0.013	0.62719	0.132	0.0034	2108	28	2121	60	2084	45	-1.78	-0.62
BB14A_6	6.23	0.18	0.38	0.013	0.54965	0.1221	0.0032	1999	27	2064	60	1950	46	-5.85	-3.25
BB14A_7	5.08	0.16	0.333	0.011	0.64723	0.1128	0.0027	1825	28	1847	57	1821	45	-1.43	-1.21
BB14A_8	6.1	0.19	0.364	0.012	0.57337	0.1234	0.0032	1990	27	1994	57	1958	47	-1.84	-0.20
BB14A_9	6.25	0.17	0.3677	0.011	0.66403	0.1237	0.0025	2003	25	2020	53	1998	37	-1.10	-0.85
BB14A_10	6.55	0.18	0.385	0.012	0.56063	0.1259	0.0031	2043	24	2088	58	2013	44	-3.73	-2.20
BB14A_11	4.97	0.15	0.3286	0.011	0.74664	0.1118	0.0024	1799	25	1825	51	1815	38	-0.55	-1.45
BB14A_12	3.572	0.1	0.2701	0.0088	0.68326	0.0965	0.0021	1531	23	1538	45	1546	43	0.52	-0.46
BB14A_13	6.09	0.17	0.361	0.013	0.66997	0.1237	0.003	1975	26	1987	60	1982	43	-0.25	-0.61
BB14A_14	6.54	0.17	0.3758	0.0097	0.628	0.126	0.0025	2044	22	2051	46	2024	36	-1.33	-0.34
BB14A_15	4.93	0.14	0.3173	0.009	0.52233	0.1125	0.0027	1794	24	1769	44	1822	44	2.91	1.39
BB14A_16	3.521	0.1	0.2654	0.0081	0.60532	0.0972	0.0023	1524	23	1511	41	1539	44	1.82	0.85
BB14A_17	2.304	0.08	0.2087	0.0063	0.45183	0.0808	0.0025	1200	24	1218	34	1166	62	-4.46	-1.50
BB14A_18	6.05	0.15	0.3578	0.01	0.65308	0.1241	0.0024	1975	22	1963	48	1997	35	1.70	0.61
BB14A_19	6.1	0.17	0.3627	0.01	0.65935	0.124	0.0025	1994	26	2000	48	1989	37	-0.55	-0.30
BB14A_20	5.26	0.13	0.3355	0.01	0.71945	0.1143	0.002	1853	22	1858	49	1862	33	0.21	-0.27
BB14A_21	2.311	0.07	0.2113	0.0067	0.57512	0.0796	0.002	1205	23	1231	35	1145	52	-7.51	-2.16
BB14A_22	6.28	0.16	0.3659	0.01	0.63737	0.1255	0.0026	2012	23	2006	48	2009	37	0.15	0.30
BB14A_23	4.99	0.12	0.3265	0.0093	0.57227	0.1115	0.0023	1813	21	1818	46	1814	37	-0.22	-0.28
BB14A_24	3.404	0.08	0.2645	0.0071	0.58176	0.0939	0.0018	1504	18	1508	36	1483	37	-1.69	-0.27
BB14A_25	2.263	0.06	0.2056	0.0056	0.50062	0.0802	0.0018	1194	18	1205	30	1171	46	-2.90	-0.92

BB14A_26	3.481	0.08	0.2672	0.0075	0.70295	0.0956	0.0017	1521	19	1525	39	1529	34	0.26	-0.26
BB14A_27	6.44	0.16	0.3645	0.0097	0.59017	0.129	0.0024	2025	22	1996	46	2068	32	3.48	1.43
BB14A_28	4.91	0.11	0.3253	0.0079	0.60131	0.1098	0.0021	1795	19	1811	38	1786	36	-1.40	-0.89
BB14A_29	3.443	0.08	0.267	0.0069	0.62987	0.0948	0.0017	1510	18	1521	35	1510	34	-0.73	-0.73
BB14A_30	3.57	0.08	0.2693	0.0064	0.68714	0.0958	0.0015	1540	18	1536	33	1528	30	-0.52	0.26
BB14A_31	4.92	0.13	0.3212	0.0092	0.66955	0.1113	0.002	1796	22	1792	45	1816	34	1.32	0.22
BB14A_32	7.03	0.15	0.401	0.01	0.59561	0.1278	0.0022	2112	19	2169	46	2062	30	-5.19	-2.70
BB14A_33	2.294	0.05	0.2078	0.005	0.70275	0.0802	0.0013	1205	17	1217	27	1180	32	-3.14	-1.00
BB14A_34	2.274	0.06	0.2042	0.0051	0.62163	0.0808	0.0015	1201	18	1195	27	1198	37	0.25	0.50
BB14A_35	4.606	0.1	0.3068	0.0066	0.65484	0.1088	0.0016	1745	17	1722	33	1768	28	2.60	1.32
BB14A_36	4.99	0.11	0.3212	0.0075	0.61266	0.1121	0.0019	1815	19	1791	37	1829	30	2.08	1.32
BB14A_37	2.227	0.04	0.2011	0.0044	0.63534	0.08	0.0011	1185	14	1181	24	1185	27	0.34	0.34
BB14A_38	6.45	0.13	0.3741	0.0077	0.6728	0.1253	0.0017	2037	18	2045	36	2022	24	-1.14	-0.39
BB14A_39	5.092	0.1	0.3374	0.0069	0.60672	0.1089	0.0015	1831	16	1871	33	1771	26	-5.65	-2.18
BB14A_40	2.271	0.05	0.2073	0.0045	0.62176	0.0792	0.0012	1200	15	1213	24	1169	31	-3.76	-1.08
BB14A_41	5.97	0.12	0.3568	0.0082	0.65591	0.1212	0.0019	1966	18	1962	39	1962	27	0.00	0.20
BB14A_42	3.445	0.08	0.2582	0.006	0.6751	0.0966	0.0015	1511	17	1478	30	1544	30	4.27	2.18
BB14A_43	4.855	0.09	0.3188	0.0063	0.56883	0.1105	0.0016	1789	16	1781	31	1795	26	0.78	0.45
BB14A_44	6.42	0.12	0.3737	0.0076	0.63989	0.1249	0.0017	2032	16	2043	35	2017	24	-1.29	-0.54
BB14A_45	2.255	0.04	0.2031	0.0043	0.57759	0.0805	0.0012	1197	13	1190	23	1198	30	0.67	0.58
BB14A_46	2.224	0.04	0.2002	0.004	0.64591	0.08	0.001	1185	13	1177	22	1186	26	0.76	0.68
BB14A_47	27.59	0.41	0.6911	0.012	0.63363	0.2891	0.0029	3403	15	3382	47	3408	16	0.76	0.62
BB14A_48	2.307	0.04	0.2062	0.0037	0.69711	0.08073	0.0008	1211.8	12	1207	20	1210	20	0.25	0.40
BB14A_49	4.547	0.09	0.3042	0.0059	0.59942	0.108	0.0015	1735	16	1710	29	1754	25	2.51	1.44
BB14A_50	5.302	0.1	0.3345	0.0067	0.62196	0.1141	0.0015	1867	16	1857	32	1858	24	0.05	0.54
BB14A_51	3.527	0.06	0.2692	0.0055	0.7011	0.0946	0.0011	1533	14	1537	28	1512	22	-1.65	-0.26
BB14A_52	2.164	0.05	0.1974	0.0038	0.5372	0.0787	0.0013	1165	14	1160	21	1157	33	-0.26	0.43
BB14A_53	6.13	0.1	0.3625	0.0069	0.68436	0.1226	0.0013	1994	16	1994	33	1990	19	-0.20	0.00
BB14A_54	11.53	0.21	0.4894	0.011	0.71251	0.1712	0.0022	2564	18	2562	47	2563	22	0.04	0.08
BB14A_55	3.592	0.08	0.2728	0.006	0.68493	0.0954	0.0014	1548	18	1555	30	1526	27	-1.90	-0.45
BB14A_56	4.92	0.11	0.3171	0.0074	0.64986	0.112	0.002	1800	20	1774	37	1815	32	2.26	1.44
BB14A_57	7.78	0.15	0.4056	0.0087	0.49028	0.1395	0.0023	2202	18	2190	40	2207	29	0.77	0.54
BB14A_58	9.43	0.19	0.4594	0.0097	0.57769	0.1483	0.0023	2376	18	2436	43	2317	27	-5.14	-2.53
BB14A_59	3.443	0.07	0.2592	0.0055	0.66232	0.0958	0.0014	1513	16	1484	28	1532	28	3.13	1.92
BB14A_60	6.54	0.14	0.3772	0.0093	0.66467	0.1255	0.0019	2051	18	2060	44	2025	27	-1.73	-0.44
BB14A_61	4.98	0.12	0.3268	0.0091	0.68691	0.1102	0.0019	1808	20	1816	44	1793	34	-1.28	-0.44
BB14A_62	4.474	0.11	0.3028	0.0078	0.67254	0.1078	0.0019	1727	20	1703	38	1756	32	3.02	1.39
BB14A_63	5.47	0.12	0.3409	0.0084	0.65467	0.1163	0.002	1895	19	1892	39	1885	31	-0.37	0.16
BB14A_64	4.604	0.09	0.3102	0.0068	0.69309	0.1068	0.0013	1748	17	1741	33	1739	23	-0.12	0.40
BB14A_65	4.896	0.11	0.3206	0.008	0.72901	0.1102	0.0015	1800	18	1787	39	1793	24	0.33	0.72
BB14A_66	4.62	0.11	0.3051	0.0079	0.69258	0.1092	0.0018	1744	21	1716	38	1773	29	3.21	1.61
BB14A_67	5.95	0.14	0.356	0.0089	0.5859	0.1209	0.0023	1965	21	1964	44	1962	33	-0.10	0.05
BB14A_68	15.7	0.41	0.544	0.015	0.54823	0.2096	0.0042	2853	24	2795	60	2899	33	3.59	2.03
BB14A_69	3.528	0.08	0.2678	0.0064	0.63585	0.0952	0.0017	1531	19	1526	33	1517	34	-0.59	0.33
BB14A_70	3.488	0.09	0.2655	0.0068	0.62099	0.0967	0.0018	1520	19	1514	35	1538	35	1.56	0.39
BB14A_71	4.79	0.13	0.3176	0.0094	0.69987	0.1094	0.0022	1777	22	1773	46	1771	37	-0.11	0.23
BB14A_72	5.12	0.13	0.3263	0.0099	0.64228	0.1141	0.0024	1834	21	1815	49	1840	40	1.36	1.04
BB14A_73	5.11	0.14	0.3338	0.0092	0.61711	0.1101	0.0022	1826	24	1849	44	1778	39	-3.99	-1.26
BB14A_74	4.93	0.13	0.3235	0.0085	0.52149	0.1103	0.0022	1806	21	1800	41	1789	39	-0.61	0.33
BB14A_75	6.86	0.15	0.3772	0.0093	0.50042	0.1333	0.0025	2089	19	2060	43	2125	32	3.06	1.39
BB14A_76	5.93	0.16	0.3547	0.01	0.63944	0.1217	0.0022	1961	23	1952	49	1972	33	1.01	0.46
BB14A_77	5.22	0.13	0.3447	0.0089	0.55907	0.1101	0.0022	1853	21	1905	42	1779	38	-7.08	-2.81
BB14A_78	4.51	0.14	0.2971	0.0096	0.70975	0.1095	0.0023	1726	26	1677	49	1781	39	5.84	2.84
BB14A_79	5.78	0.15	0.352	0.01	0.65024	0.1209	0.0026	1937	23	1940	49	1941	38	0.05	-0.15
BB14A_80	7.22	0.22	0.39	0.012	0.60764	0.1349	0.0033	2129	26	2122	56	2136	41	0.66	0.33
BB14A_81	5.03	0.16	0.33	0.012	0.72274	0.1107	0.0024	1812	27	1845	53	1780	41	-3.65	-1.82
BB14A_82	7.19	0.18	0.3925	0.011	0.65814	0.1327	0.0023	2129	23	2130	49	2121	30	-0.42	-0.05
BB14A_83	7.3	0.22	0.396	0.012	0.61997	0.1336	0.0028	2143	29	2158	59	2128	37	-1.41	-0.70
BB14A_84	5.94	0.16	0.3563	0.011	0.57991	0.122	0.0027	1961	25	1959	53	1967	40	0.41	0.10
BB14A_85	7.37	0.21	0.403	0.012	0.65388	0.1326	0.0028	2152	27	2180	57	2126	37	-2.54	-1.30
BB14A_86	2.218	0.06	0.2067	0.0061	0.61007	0.0789	0.0017	1184	19	1208	33	1149	43	-5.13	-2.03
BB14A_87	4.92	0.13	0.3236	0.0089	0.65368	0.1099	0.002	1794	22	1801	43	1779	35	-1.24	-0.39
BB14A_88	3.665	0.09	0.276	0.0072	0.61458	0.0964	0.0018	1558	19	1568	36	1537	36	-2.02	-0.64
BB14A_89	7.38	0.19	0.3944	0.011	0.70768	0.1347	0.0024	2152	24	2141	49	2152	32	0.51	0.51
BB14A_90	4.541	0.1	0.311	0.0075	0.69887	0.1055	0.0016	1734	18	1741	37	1711	29	-1.75	-0.40
BB14A_91	3.567	0.09	0.2722	0.0066	0.66172	0.0942	0.0017	1533	19	1551	34	1494	34	-3.82	-1.17
BB14A_92	5.314	0.11	0.3357	0.0078	0.63646	0.1151	0.0018	1868	19	1865	38	1865	29	0.00	0.16
BB14A_93	3.165	0.08	0.2517	0.0062	0.62395	0.091	0.0016	1448	18	1447	33	1431	34	-1.12	0.07
BB14A_94	7.44	0.17	0.4044	0.0096	0.5775	0.1339	0.0025	2159	20	2183	44	2129	33	-2.54	-1.11
BB14A_95	5.83	0.13	0.3521	0.0085	0.68918	0.1207	0.0019	1948	19	1939	41	1962	28	1.17	0.46
BB14A_96	7.17	0.15	0.3938	0.0088	0.57743	0.1309	0.002	2130	18	2142	41	2101	28	-1.95	-0.56
BB14A_97	4.572	0.1	0.3128	0.007	0.58161	0.1062	0.0018	1740	18	1751	34	1724	31	-1.57	-0.63
BB14A_98	4.702	0.1	0.3145	0.0074	0.59514	0.1092	0.0018	1761	17	1758	36	1775	30	0.96	0.17
BB14A_99	2.278	0.04	0.2058	0.0047	0.57517	0.0802	0.0013	1204	13	1204	25	1191	30	-1.09	0.00
BB14A_100	4.992	0.09	0.3306	0.0071	0.51726	0.1089	0.0015	1813	16	1841	35	1779	28	-3.49	-1.54
BB14A_101	3.532	0.07	0.2718	0.0062	0.60704	0.0947	0.0014	1530	16	1547	31	1503	29	-2.93	-1.11
BB14A_102	5.17	0.14	0.345	0.01	0.55895	0.1097	0.0025	1838	23	1907	50	1778	42	-7.26	-3.75
BB14A_103	7.22	0.14	0.3965	0.0088	0.64187	0.1327	0.0019	2136	18	2158	42	2120	25	-1.79	-1.03
BB14A_104	5.87	0.12	0.3544	0.0078	0.6006	0.1211	0.0019	1953	19	1955	36	1965	28	0.51	-0.10
BB14A_105	3.623	0.08	0.2706	0.0062	0.66129	0.0974	0.0015	1550	17	1540	32	1565	29	1.60	0.65
BB14A_106	4.77	0.11	0.317	0.0072	0.52257	0.1099	0.0022	1771	20	1771	35	1776	37	0.28	0.00
BB14A_107	2.233	0.05	0.2051	0.0047	0.53938	0.0793	0.0015	1187	16	1203	25	1162	38	-3.53	-1.35
BB14A_108	3.614	0.08	0.2755	0.006	0.46306	0.0957	0.0018	1549	17	1566	30	1525	34	-2.69	-1.10
BB14A_109	2.216	0.04	0.2032	0.0042	0.59724	0.0795	0.0011	1185	13	1191	23	1174	28	-1.45	-0.51

BB14A_110	4.907	0.09	0.324	0.0064	0.64974	0.1104	0.0014	1799	15	1807	31	1796	23	-0.61	-0.44
BB14A_111	2.221	0.04	0.2035	0.0043	0.57746	0.0793	0.0012	1185	13	1193	23	1168	30	-2.14	-0.68
BB14A_112	3.558	0.07	0.2739	0.0057	0.68726	0.0946	0.0012	1536	14	1558	29	1515	24	-2.84	-1.43
BB14A_113	6.18	0.12	0.3683	0.0081	0.77174	0.1223	0.0013	1999	18	2017	38	1990	20	-1.36	-0.90
BB14A_114	14.73	0.26	0.5494	0.012	0.65771	0.1953	0.0026	2795	17	2823	49	2780	22	-1.55	-1.00
BB14A_115	5.003	0.11	0.3303	0.0071	0.6584	0.1107	0.0017	1814	17	1836	34	1801	28	-1.94	-1.21
BB14A_116	10.24	0.18	0.466	0.0089	0.56186	0.1603	0.0021	2451	16	2465	40	2449	22	-0.65	-0.57
BB14A_117	1.966	0.04	0.1861	0.0038	0.7018	0.07748	0.001	1101	12	1099	20	1123	24	2.14	0.18
BB14A_118	6	0.12	0.3587	0.0079	0.67661	0.1218	0.0016	1969	17	1974	37	1969	24	-0.25	-0.25
BB14A_119	2.178	0.05	0.2006	0.0044	0.48622	0.0797	0.0015	1170	15	1181	24	1172	37	-0.77	-0.94
BB14A_120	13.87	0.25	0.5251	0.011	0.76108	0.1924	0.0021	2738	17	2721	47	2757	18	1.31	0.62
BB14A_121	4.692	0.1	0.3119	0.0071	0.54883	0.1101	0.0019	1761	17	1747	35	1793	31	2.57	0.80
BB14A_122	7.18	0.16	0.3941	0.0094	0.59506	0.1343	0.0023	2126	21	2139	43	2140	30	0.05	-0.61
BB14A_123	2.189	0.05	0.2016	0.0049	0.65511	0.0799	0.0014	1175	16	1182	26	1177	33	-0.42	-0.60
BB14A_124	5.24	0.12	0.336	0.0083	0.70912	0.1144	0.0018	1855	19	1862	40	1856	29	-0.32	-0.38
BB14A_125	4.65	0.11	0.3101	0.0073	0.59761	0.1094	0.002	1748	20	1740	36	1771	34	1.75	0.46
BB14A_126	5.804	0.11	0.35	0.0076	0.7187	0.121	0.0016	1941	16	1931	36	1962	24	1.58	0.52
BB14A_127	5.73	0.12	0.3484	0.0085	0.62067	0.1203	0.0018	1931	18	1921	40	1950	27	1.49	0.52
BB14A_128	5.85	0.12	0.3531	0.0085	0.65581	0.1211	0.0019	1949	18	1947	40	1960	29	0.66	0.10
BB14A_129	3.31	0.13	0.2491	0.0078	0.38163	0.0966	0.0036	1474	30	1431	40	1532	72	6.59	2.92
BB14A_130	3.476	0.06	0.2692	0.0056	0.60997	0.095	0.0013	1519	14	1534	28	1516	25	-1.19	-0.99
BB14A_131	2.236	0.04	0.2036	0.0044	0.66562	0.0802	0.001	1191	13	1193	23	1199	26	0.50	-0.17
BB14A_132	4.419	0.09	0.3074	0.0065	0.65398	0.1062	0.0016	1712	16	1725	32	1721	27	-0.23	-0.76
BB14A_133	1.938	0.04	0.1851	0.0038	0.59623	0.0766	0.0011	1093	12	1095	21	1106	29	0.99	-0.18
BB14A_134	7.265	0.12	0.3969	0.0082	0.59807	0.1335	0.0017	2141	15	2156	39	2137	24	-0.89	-0.70
BB14A_135	14.53	0.26	0.5374	0.011	0.61251	0.199	0.0028	2782	17	2766	47	2806	23	1.43	0.58
BB14A_136	4.619	0.11	0.3169	0.008	0.70563	0.1065	0.0017	1745	20	1770	39	1731	30	-2.25	-1.43
BB14A_137	5.897	0.11	0.3611	0.0075	0.64995	0.1191	0.0015	1956	16	1984	36	1936	23	-2.48	-1.43
BB14A_138	4.85	0.1	0.3263	0.0078	0.67264	0.1098	0.0017	1788	17	1816	38	1784	28	-1.79	-1.57
BB14A_139	3.904	0.09	0.2603	0.007	0.75754	0.1098	0.0018	1611	20	1494	37	1784	29	16.26	7.26
BB14A_140	4.585	0.09	0.3109	0.0069	0.57328	0.1084	0.0017	1741	17	1741	34	1759	29	1.02	0.00
BB14A_141	2.208	0.05	0.2037	0.0048	0.5928	0.0794	0.0014	1180	16	1193	25	1163	35	-2.58	-1.10
BB14A_142	5.9	0.12	0.3562	0.008	0.64521	0.1214	0.0019	1957	18	1960	38	1966	27	0.31	-0.15
BB14A_143	4.906	0.1	0.3255	0.0074	0.5912	0.1105	0.0019	1797	18	1815	36	1790	30	-1.40	-1.00
BB14A_144	7.33	0.18	0.395	0.0098	0.64983	0.1358	0.0024	2142	21	2139	45	2161	31	1.02	0.14
BB14A_145	4.663	0.11	0.317	0.0078	0.73576	0.1079	0.0016	1760	18	1772	38	1752	28	-1.14	-0.68
BB14A_146	3.486	0.08	0.2683	0.0062	0.65972	0.0947	0.0014	1521	17	1532	31	1509	29	-1.52	-0.72
BB14A_147	4.442	0.1	0.3086	0.0073	0.61025	0.1056	0.0018	1715	18	1730	36	1708	31	-1.29	-0.87
BB14A_148	4.91	0.11	0.3211	0.008	0.70415	0.1124	0.0018	1800	20	1790	39	1821	30	1.70	0.56
BB14A_149	3.482	0.07	0.2674	0.0063	0.65762	0.0951	0.0015	1519	17	1527	32	1523	30	-0.26	-0.53
BB14A_150	6.23	0.14	0.3603	0.0091	0.66266	0.1273	0.0021	2008	20	1977	42	2046	29	3.37	1.54
BB14A_151	2.265	0.04	0.2078	0.0041	0.63415	0.07981	0.001	1198.8	12	1216	22	1182	25	-2.88	-1.43
BB14A_152	2.29	0.04	0.2074	0.0043	0.69669	0.0807	0.001	1206	13	1214	23	1204	24	-0.83	-0.66
BB14A_153	4.903	0.09	0.3259	0.0069	0.66779	0.11	0.0014	1800	16	1815	34	1796	24	-1.06	-0.83
BB14A_154	4.178	0.07	0.3019	0.0057	0.59165	0.1008	0.0012	1667	15	1701	28	1633	23	-4.16	-2.04
BB14A_155	11.13	0.21	0.4383	0.0096	0.73878	0.1838	0.0024	2529	18	2339	43	2685	21	12.89	7.51
BB14A_156	5.934	0.11	0.3575	0.0075	0.64404	0.1215	0.0016	1962	16	1967	36	1971	23	0.20	-0.25
BB14A_157	13.63	0.24	0.5258	0.01	0.65833	0.1885	0.0022	2721	16	2725	45	2722	20	-0.11	-0.15
BB14A_158	2.028	0.04	0.1901	0.0039	0.60703	0.0783	0.0011	1121	13	1121	21	1136	29	1.32	0.00
BB14A_159	6.29	0.12	0.3649	0.0074	0.57431	0.1258	0.0017	2012	16	2002	35	2026	25	1.18	0.50
BB14A_160	6.346	0.11	0.3737	0.0075	0.54923	0.124	0.0016	2022	15	2043	35	2004	24	-1.95	-1.04
BB14A_161	4.758	0.09	0.3221	0.0065	0.65274	0.1074	0.0014	1774	15	1797	32	1742	24	-3.16	-1.30
BB14A_162	6.131	0.11	0.3682	0.0073	0.6579	0.1205	0.0014	1992	15	2018	34	1957	21	-3.12	-1.31
BB14A_163	5.38	0.15	0.3275	0.0093	0.70009	0.1193	0.0022	1878	24	1824	45	1938	34	5.88	2.88
BB14A_164	4.883	0.1	0.3233	0.0068	0.57264	0.1101	0.0017	1797	17	1803	33	1786	29	-0.95	-0.33
BB14A_165	4.911	0.08	0.3238	0.0063	0.62238	0.1105	0.0014	1802	14	1808	30	1799	22	-0.50	-0.33
BB14A_166	4.943	0.1	0.3179	0.0071	0.67765	0.1124	0.0016	1806	17	1779	35	1828	25	2.68	1.50
BB14A_167	4.928	0.09	0.3191	0.0065	0.62389	0.1127	0.0015	1803	15	1783	32	1835	24	2.83	1.11
BB14A_168	2.296	0.04	0.2094	0.0039	0.54933	0.0795	0.001	1208	12	1225	21	1173	25	-4.43	-1.41

Sample BB22															
Isotopic ratios								Concordia ages (Ma)							
Analysis	$^{207}Pb/^{235}U$	± 2σ	$^{206}Pb/^{238}U$	± 2σ	Rho	$^{207}Pb/^{206}Pb$	± 2σ	$^{207}Pb/^{235}U$	± 2σ	$^{206}Pb/^{238}U$	± 2σ	$^{207}Pb/^{206}Pb$	± 2σ	Dis. (6/38/7/6)	Dis. (6/38/7/35)
BB22_1	7.743	0.12	0.4066	0.004	0.48034	0.1378	0.0011	2199.9	14	2198	18	2195	14	-0.14	0.09
BB22_2	7.34	0.15	0.3915	0.0068	0.6671	0.1358	0.0019	2154	19	2128	31	2170	24	1.94	1.21
BB22_3	7.005	0.11	0.3862	0.0037	0.45405	0.1307	0.0011	2110.3	14	2105	17	2103	15	-0.10	0.25
BB22_4	7.783	0.12	0.4099	0.004	0.47492	0.137	0.0011	2204.1	14	2214	18	2187	15	-1.23	-0.45
BB22_5	7.303	0.12	0.3947	0.0041	0.53547	0.1338	0.0013	2147.2	15	2143	19	2142	17	-0.05	0.20
BB22_6	7.734	0.12	0.4054	0.0041	0.43566	0.1374	0.0012	2198.2	14	2193	19	2193	16	0.00	0.24
BB22_7	7.071	0.11	0.3869	0.0039	0.44534	0.1319	0.0012	2118.1	14	2108	18	2118	16	0.47	0.48
BB22_8	7.582	0.11	0.4016	0.0039	0.4636	0.1363	0.0011	2181.8	13	2175	18	2175	15	0.00	0.31
BB22_9	6.711	0.1	0.3772	0.0035	0.59033	0.12869	0.0009	2072.8	13	2063	16	2076	12	0.63	0.47
BB22_10	8.192	0.13	0.4152	0.0042	0.46509	0.1424	0.0013	2250	14	2237	19	2250	16	0.58	0.58
BB22_11	7.358	0.11	0.3948	0.0038	0.49651	0.1349	0.0011	2154.8	14	2145	18	2157	14	0.56	0.45
BB22_12	7.81	0.13	0.4112	0.0046	0.46918	0.1372	0.0014	2206.6	15	2219	21	2188	17	-1.42	-0.56
BB22_13	7.739	0.12	0.4072	0.0042	0.517	0.1371	0.0012	2198.7	14	2201	19	2184	15	-0.78	-0.10
BB22_14	7.228	0.12	0.3934	0.0049	0.84786	0.13281	0.0008	2137	15	2136	23	2132	11	-0.19	0.05
BB22_15	7.718	0.13	0.4069	0.0041	0.3556	0.1371	0.0014	2197.8	15	2200	19	2185	19	-0.69	-0.10
BB22_16	6.764	0.12	0.3806	0.0055	0.87591	0.12832	0.0009	2078	16	2077	26	2072	12	-0.24	0.05
BB22_17	7.654	0.12	0.4038	0.0039	0.553	0.1366	0.0011	2190.1	14	2186	18	2182	15	-0.18	0.19
BB22_18	7.92	0.14	0.413	0.0045	0.45161	0.1386	0.0016	2220	16	2228	21	2202	20	-1.18	-0.36
BB22_19	7.56	0.11	0.3999	0.0037	0.55126	0.13644	0.001	2178.5	13	2168	17	2180	12	0.55	0.48
BB22_20	7.564	0.11	0.401	0.0037	0.56526	0.1361	0.001	2178.9	13	2173	17	2174	12	0.05	0.27

BB22_21	7.473	0.13	0.3961	0.0047	0.5388	0.1361	0.0015	2167	16	2152	22	2173	19	0.97	0.69
BB22_22	6.441	0.11	0.3676	0.004	0.45229	0.1267	0.0013	2035.9	15	2017	19	2046	19	1.42	0.93
BB22_23	7.528	0.11	0.3951	0.004	0.54165	0.1378	0.0011	2175.2	14	2145	18	2196	14	2.32	1.39
BB22_24	7.435	0.11	0.3911	0.0037	0.60679	0.13742	0.001	2164.2	13	2128	17	2191	12	2.88	1.67
BB22_25	7.534	0.11	0.4009	0.0038	0.51364	0.1357	0.001	2175.4	14	2175	17	2168	13	-0.32	0.02
BB22_26	7.604	0.12	0.3958	0.004	0.52165	0.1388	0.0012	2183.6	14	2150	19	2205	16	2.49	1.54
BB22_27	6.326	0.09	0.3656	0.0035	0.63222	0.12505	0.0008	2020.6	13	2010	17	2026	11	0.79	0.52
BB22_28	8.839	0.14	0.4243	0.0041	0.584	0.1505	0.0012	2319	14	2279	18	2349	13	2.98	1.72
BB22_29	7.474	0.12	0.3968	0.004	0.48622	0.1361	0.0013	2167.5	14	2153	18	2173	16	0.92	0.67
BB22_30	16.29	0.27	0.5702	0.0063	0.84111	0.2068	0.0012	2890	16	2906	26	2878.3	9.2	-0.96	-0.55
BB22_31	7.6	0.11	0.402	0.0037	0.47029	0.1365	0.001	2183.3	13	2179	17	2181	13	0.09	0.20
BB22_32	7.573	0.12	0.3988	0.004	0.47674	0.1373	0.0013	2179	15	2162	19	2188	17	1.19	0.78
BB22_33	6.22	0.13	0.357	0.0067	0.89118	0.1265	0.0012	2006	19	1966	32	2046	16	3.91	1.99
BB22_34	7.499	0.12	0.3944	0.0037	0.56544	0.1371	0.001	2171	14	2142	17	2190	13	2.19	1.34
BB22_35	7.316	0.13	0.39	0.0045	0.61795	0.1355	0.0014	2148	16	2122	21	2165	18	1.99	1.21
BB22_36	7.726	0.11	0.4057	0.0038	0.63059	0.1376	0.0009	2198.8	14	2196	18	2194	11	-0.09	0.13
BB22_37	7.823	0.13	0.4127	0.0044	0.47336	0.1373	0.0013	2210	14	2226	20	2187	17	-1.78	-0.72
BB22_38	6.328	0.12	0.3613	0.0059	0.57911	0.1269	0.0018	2020	17	1987	28	2049	25	3.03	1.63
BB22_39	7.695	0.13	0.4075	0.0052	0.86544	0.13648	0.0008	2192.9	15	2202	24	2181	10	-0.96	-0.41
BB22_40	7.97	0.15	0.4146	0.0056	0.63421	0.1394	0.0016	2226	18	2234	25	2213	21	-0.95	-0.36
BB22_41	7.422	0.12	0.3959	0.0042	0.55231	0.1359	0.0012	2162.3	14	2149	19	2169	15	0.92	0.62
BB22_42	7.872	0.13	0.4133	0.0042	0.39091	0.138	0.0014	2213.8	15	2229	19	2194	18	-1.60	-0.69
BB22_43	7.669	0.12	0.4054	0.0043	0.54873	0.1371	0.0012	2192.4	14	2192	20	2187	16	-0.23	0.02
BB22_44	6.889	0.1	0.3858	0.0037	0.54084	0.1295	0.001	2095.5	13	2102	17	2086	14	-0.77	-0.31
BB22_45	6.731	0.11	0.3591	0.0039	0.62787	0.1358	0.0011	2075.1	14	1977	19	2171	14	8.94	4.73
BB22_46	7.787	0.12	0.4062	0.0041	0.6036	0.1387	0.001	2204.9	14	2196	19	2207	13	0.50	0.40
BB22_47	7.674	0.12	0.4039	0.004	0.37059	0.1375	0.0013	2192.1	14	2186	18	2189	17	0.14	0.28
BB22_48	7.168	0.11	0.3816	0.0043	0.68376	0.13585	0.001	2131.3	14	2083	20	2172	13	4.10	2.27
BB22_49	7.465	0.12	0.3942	0.0047	0.83556	0.13701	0.0008	2167.9	15	2142	21	2187	10	2.06	1.19
BB22_50	7.852	0.13	0.4093	0.0043	0.55524	0.1386	0.0012	2213.6	14	2210	20	2206	15	-0.18	0.16
BB22_51	7.9	0.15	0.4239	0.0074	0.61879	0.1351	0.0018	2215	18	2277	33	2157	24	-5.56	-2.80
BB22_52	7.677	0.13	0.405	0.0049	0.68356	0.1374	0.0011	2192	15	2190	22	2192	15	0.09	0.09
BB22_53	7.603	0.14	0.407	0.0059	0.64751	0.1346	0.0015	2184	16	2201	27	2153	19	-2.23	-0.78
BB22_54	7.94	0.14	0.4199	0.006	0.86923	0.13716	0.0009	2222	17	2257	27	2190	11	-3.06	-1.58
BB22_55	6.43	0.09	0.3738	0.0035	0.55927	0.12442	0.0009	2035.7	13	2048	16	2017	12	-1.54	-0.60
BB22_56	6.94	0.12	0.3828	0.0042	0.36274	0.1314	0.0016	2101	15	2088	20	2106	22	0.85	0.62
BB22_57	6.386	0.1	0.3701	0.0039	0.55205	0.1254	0.0011	2029.6	14	2029	18	2029	16	0.00	0.03
BB22_58	13.15	0.2	0.5167	0.0053	0.60738	0.1844	0.0014	2688.9	14	2685	23	2690	12	0.19	0.15
BB22_59	8.111	0.13	0.4183	0.0044	0.50979	0.1406	0.0013	2241.8	15	2251	20	2230	16	-0.94	-0.41
BB22_60	6.915	0.1	0.3846	0.0037	0.58266	0.1303	0.0009	2098.9	13	2097	17	2099	12	0.10	0.09
BB22_61	6.812	0.1	0.3809	0.0037	0.60788	0.12938	0.0009	2086.4	13	2080	17	2086	12	0.29	0.31
BB22_62	8.11	0.15	0.4228	0.006	0.41261	0.1396	0.0021	2241	18	2271	27	2212	26	-2.67	-1.34
BB22_63	7.531	0.13	0.3979	0.0052	0.60452	0.1373	0.0014	2174	15	2157	24	2189	17	1.46	0.78
BB22_64	7.673	0.12	0.407	0.0039	0.60059	0.13665	0.001	2191.7	14	2200	18	2182	12	-0.82	-0.38
BB22_65	7.07	0.18	0.3893	0.008	0.86545	0.1313	0.0015	2106	24	2117	37	2108	19	-0.43	-0.52
BB22_66	7.962	0.12	0.4177	0.0041	0.5	0.1382	0.0012	2224.9	14	2249	19	2202	15	-2.13	-1.08
BB22_67	7.769	0.12	0.4088	0.0041	0.49099	0.1379	0.0012	2202.5	14	2208	19	2195	15	-0.59	-0.25
BB22_68	6.96	0.1	0.3833	0.0036	0.5514	0.13144	0.0009	2106.1	13	2091	17	2116	13	1.18	0.72
BB22_69	8.369	0.13	0.4359	0.0049	0.56185	0.1399	0.0012	2271.3	15	2331	22	2220	15	-5.00	-2.63
BB22_70	6.79	0.14	0.369	0.0052	0.58842	0.1338	0.0015	2081	18	2023	24	2142	21	5.56	2.79
BB22_71	7.323	0.11	0.3893	0.0041	0.68106	0.1364	0.001	2149.9	14	2119	19	2178	13	2.71	1.44
BB22_72	7.697	0.11	0.4073	0.0037	0.50345	0.13685	0.001	2194.7	13	2202	17	2187	12	-0.69	-0.33
BB22_73	6.75	0.18	0.3525	0.0061	0.6984	0.1387	0.0023	2075	24	1945	29	2205	29	11.79	6.27
BB22_74	6.865	0.13	0.3857	0.0043	0.30241	0.1289	0.0018	2090	16	2103	20	2078	24	-1.20	-0.62
BB22_75	7.613	0.12	0.4047	0.004	0.61959	0.13618	0.001	2184.7	14	2191	19	2175	12	-0.74	-0.29
BB22_76	6.331	0.1	0.3666	0.0033	0.59885	0.125	0.0008	2021.1	13	2014	16	2026	12	0.59	0.35
BB22_77	7.763	0.14	0.4062	0.0058	0.85957	0.13837	0.001	2202	16	2196	27	2204	12	0.36	0.27
BB22_78	7.611	0.11	0.4014	0.0038	0.61147	0.13751	0.0009	2186.2	13	2175	17	2193	11	0.82	0.51
BB22_79	7.903	0.12	0.4177	0.0039	0.49453	0.1373	0.001	2218.3	14	2249	18	2189	13	-2.74	-1.38
BB22_80	6.003	0.12	0.3187	0.005	0.92355	0.13653	0.0008	1973	17	1783	25	2181	9.7	18.25	9.63
BB22_81	7.842	0.11	0.4113	0.0037	0.52856	0.13823	0.0009	2211.7	13	2222	17	2201	12	-0.95	-0.47
BB22_82	7.881	0.13	0.4193	0.0044	0.46057	0.1363	0.0014	2215.3	15	2256	20	2175	18	-3.72	-1.84
BB22_83	7.685	0.11	0.4137	0.0038	0.49475	0.13448	0.001	2193.3	13	2231	17	2156	13	-3.48	-1.72
BB22_84	7.689	0.11	0.407	0.0037	0.56847	0.13686	0.0008	2194.7	13	2200	17	2185	11	-0.69	-0.24
BB22_85	6.467	0.12	0.3746	0.0042	0.35493	0.1253	0.0017	2038	16	2050	20	2022	23	-1.38	-0.59
BB22_86	7.655	0.12	0.4042	0.004	0.44616	0.1375	0.0013	2191.5	14	2187	19	2190	16	0.14	0.21
BB22_87	7.77	0.14	0.4142	0.0047	0.41252	0.1364	0.0017	2203	17	2233	21	2177	22	-2.57	-1.36
BB22_88	7.039	0.11	0.3601	0.0038	0.48834	0.1416	0.0012	2114.6	14	1982	18	2244	15	11.68	6.27
BB22_89	4.69	0.17	0.2768	0.0088	0.9075	0.1227	0.0017	1759	29	1573	44	1991	24	20.99	10.57
BB22_90	6.886	0.1	0.3842	0.0035	0.82666	0.12998	0.0007	2095.5	13	2095	16	2094.8	9.6	-0.01	0.02
BB22_91	8.07	0.16	0.4246	0.006	0.64758	0.1376	0.0016	2236	18	2280	27	2192	21	-4.01	-1.97
BB22_92	7.714	0.13	0.4116	0.0044	0.50556	0.1362	0.0013	2197.3	15	2223	20	2172	17	-2.35	-1.17
BB22_93	7.573	0.13	0.4025	0.0044	0.40027	0.1366	0.0017	2179	16	2179	20	2174	22	-0.23	0.00
BB22_94	7.783	0.12	0.411	0.0039	0.47569	0.1369	0.0011	2204.3	14	2220	18	2184	14	-1.65	-0.71
BB22_95	7.352	0.11	0.4001	0.0038	0.5808	0.13304	0.0009	2154.4	13	2169	18	2136	12	-1.54	-0.68
BB22_96	7.913	0.13	0.4178	0.0046	0.62308	0.1373	0.0012	2219.2	15	2249	21	2190	15	-2.69	-1.34
BB22_97	6.28	0.09	0.3669	0.0033	0.5512	0.12401	0.0008	2014.5	13	2014	16	2011	11	-0.15	0.02
BB22_98	7.092	0.11	0.3912	0.0039	0.52026	0.1316	0.0011	2122.6	13	2128	18	2114	15	-0.66	-0.25
BB22_99	6.287	0.1	0.3425	0.0037	0.47821	0.1332	0.001	2015.5	13	1898	18	2136	14	11.14	5.83
BB22_100	7.484	0.13	0.3952	0.0047	0.38067	0.1376	0.0017	2168	16	2145	22	2187	22	1.92	1.06
BB22_101	6.327	0.1	0.3585	0.0046	0.68246	0.128	0.0011	2020.7	14	1974	22	2067	15	4.50	2.31
BB22_102	7.736	0.11	0.41	0.0037	0.54022	0.13681	0.0009	2200.1	13	2214	17	2184	11	-1.37	-0.63
BB22_103	7.151	0.11	0.3815	0.0036	0.4975	0.1359	0.001	2128.8	13	2083	17	2171	13	4.05	2.15
BB22_104	7.569	0.11	0.4016	0.004	0.52105	0.1365	0.001	2179.6	13	2175	18	2180	13	0.23	0.21

BB22_105	7.638	0.13	0.4021	0.0047	0.39469	0.1383	0.0017	2188	16	2177	22	2198	21	0.96	0.50
BB22_106	20.81	0.5	0.6092	0.0096	0.41522	0.2481	0.0048	3121	23	3062	38	3160	31	3.10	1.89
BB22_107	6.16	0.12	0.3544	0.0057	0.88007	0.12595	0.0009	1997	17	1954	27	2039	12	4.17	2.15
BB22_108	7.54	0.15	0.3987	0.005	0.39552	0.1366	0.002	2174	18	2161	23	2179	26	0.83	0.60
BB22_109	10.65	0.17	0.4749	0.0051	0.45314	0.1625	0.0015	2490.6	15	2504	22	2479	16	-1.01	-0.54
BB22_110	7.728	0.13	0.4059	0.0046	0.38142	0.1381	0.0017	2197	16	2196	21	2196	21	0.00	0.05
BB22_111	7.489	0.12	0.4052	0.004	0.56186	0.134	0.0011	2169.6	14	2192	18	2147	14	-2.10	-1.03
BB22_112	7.022	0.11	0.3917	0.0038	0.61237	0.1302	0.0009	2113.3	13	2130	18	2097	12	-1.57	-0.79
BB22_113	8.16	0.13	0.4296	0.0046	0.48251	0.1379	0.0013	2246.4	14	2303	21	2194	16	-4.97	-2.52
BB22_114	7.689	0.13	0.4043	0.0041	0.37941	0.1379	0.0015	2192.4	15	2188	19	2193	18	0.23	0.20
BB22_115	7.622	0.12	0.4013	0.0038	0.64561	0.13747	0.001	2185.6	14	2175	17	2192	12	0.78	0.48
BB22_116	6.325	0.09	0.3675	0.0033	0.58429	0.12471	0.0008	2021.8	13	2017	15	2021	11	0.20	0.24
BB22_117	6.92	0.1	0.3817	0.0037	0.61708	0.13153	0.0009	2099.7	13	2083	17	2114	12	1.47	0.80
BB22_118	6.273	0.09	0.3665	0.0034	0.56441	0.1243	0.0008	2014.6	13	2013	16	2016	12	0.15	0.08
BB22_119	6.371	0.11	0.3579	0.0052	0.87679	0.12922	0.0008	2025	16	1970	24	2086	10	5.56	2.72
BB22_120	7.768	0.11	0.412	0.0039	0.59304	0.13659	0.0009	2203.1	13	2223	18	2182	11	-1.88	-0.90
BB22_121	7.694	0.12	0.4058	0.0041	0.57715	0.1375	0.0011	2193.6	14	2195	19	2191	14	-0.18	-0.06
BB22_122	7.67	0.11	0.4076	0.0038	0.47743	0.1362	0.001	2191.5	13	2204	17	2178	13	-1.19	-0.57
BB22_123	7.598	0.12	0.405	0.0041	0.40877	0.1362	0.0012	2182.7	14	2191	19	2173	15	-0.83	-0.38
BB22_124	4.681	0.11	0.2403	0.0054	0.93874	0.1419	0.0011	1756	20	1385	28	2246	13	38.33	21.13
BB22_125	6.313	0.09	0.3659	0.003	0.50926	0.1252	0.0007	2019.3	12	2009.9	14	2029	10	0.94	0.47
BB22_126	7.59	0.15	0.4017	0.0048	0.33963	0.1371	0.002	2181	17	2175	22	2183	26	0.37	0.28
BB22_127	6.638	0.11	0.3704	0.0039	0.47856	0.1299	0.0012	2062.8	14	2031	19	2096	16	3.10	1.54
BB22_128	7.451	0.14	0.4009	0.0047	0.3554	0.135	0.0018	2163	16	2171	22	2153	23	-0.84	-0.37
BB22_129	7.775	0.12	0.4069	0.0039	0.35283	0.1385	0.0013	2204.1	14	2200	18	2204	16	0.18	0.19
BB22_130	6.226	0.1	0.3633	0.0036	0.51035	0.1244	0.0011	2006.2	14	1997	17	2014	15	0.84	0.46
BB22_131	3.834	0.07	0.2821	0.0032	0.43075	0.0987	0.0013	1597	16	1601	16	1587	25	-0.88	-0.25
BB22_132	6.29	0.14	0.3507	0.0052	0.4756	0.1303	0.0022	2013	20	1937	25	2095	31	7.54	3.78
BB22_133	7.629	0.12	0.4074	0.0039	0.5103	0.136	0.001	2187.2	13	2202	18	2172	13	-1.38	-0.68
BB22_134	7.647	0.11	0.4063	0.0039	0.44706	0.1366	0.0011	2188.9	13	2197	18	2181	14	-0.73	-0.37
BB22_135	7.23	0.11	0.3853	0.0041	0.45798	0.1359	0.0012	2138.9	14	2100	19	2177	15	3.54	1.82
BB22_136	7.732	0.12	0.4075	0.0037	0.44335	0.1377	0.0011	2198.4	14	2203	17	2194	15	-0.41	-0.21
BB22_137	7.868	0.12	0.4151	0.0041	0.6173	0.13749	0.0009	2214.3	14	2237	19	2193	12	-2.01	-1.03
BB22_138	7.795	0.13	0.4091	0.0042	0.51474	0.1382	0.0015	2205.4	15	2210	19	2199	18	-0.50	-0.21
BB22_139	7.425	0.11	0.4028	0.0037	0.49366	0.1338	0.001	2162.3	13	2181	17	2144	13	-1.73	-0.86
BB22_140	7.633	0.12	0.4062	0.0039	0.22285	0.1363	0.0012	2186.6	14	2197	18	2175	16	-1.01	-0.48
BB22_141	7.885	0.12	0.4182	0.004	0.57807	0.13691	0.001	2216.2	14	2251	18	2184	13	-3.07	-1.57
BB22_142	7.81	0.12	0.4093	0.0038	0.55369	0.13833	0.001	2207.8	13	2211	18	2204	12	-0.32	-0.14
BB22_143	6.38	0.1	0.3738	0.0035	0.41501	0.1238	0.0011	2027.5	14	2046	17	2005	16	-2.04	-0.91
BB22_144	6.686	0.13	0.365	0.005	0.6174	0.1326	0.0015	2069	17	2005	24	2128	20	5.78	3.09
BB22_145	6.989	0.12	0.3806	0.0041	0.55379	0.1334	0.0013	2108	15	2078	19	2137	17	2.76	1.42
BB22_146	7.654	0.11	0.4066	0.004	0.55985	0.13663	0.001	2190.3	13	2198	18	2182	13	-0.73	-0.35
BB22_147	18.86	0.3	0.607	0.0069	0.69098	0.2253	0.0016	3033.4	15	3060	28	3017	12	-1.43	-0.88
BB22_148	6.573	0.1	0.3796	0.0035	0.44274	0.1256	0.001	2054.7	14	2074	16	2032	14	-2.07	-0.94
BB22_149	7.831	0.12	0.4112	0.0038	0.41497	0.138	0.0012	2210.7	13	2221	18	2197	15	-1.09	-0.47
BB22_150	7.877	0.12	0.418	0.0042	0.50078	0.1368	0.0011	2215.5	13	2252	19	2182	14	-3.21	-1.65
BB22_151	7.47	0.15	0.3959	0.0052	0.35963	0.1372	0.0022	2164	18	2148	24	2183	28	1.60	0.74
BB22_152	6.944	0.11	0.3966	0.0039	0.37612	0.1268	0.0012	2102.2	14	2152	18	2052	17	-4.87	-2.37
BB22_153	6.733	0.1	0.3855	0.0034	0.32808	0.1268	0.0011	2075.8	14	2101	16	2049	16	-2.54	-1.21
BB22_154	7.569	0.12	0.4055	0.0039	0.43316	0.1357	0.0012	2179.8	14	2193	18	2167	16	-1.20	-0.61

Sample BA23															
Isotopic ratios								Concordia ges (Ma)							
Analysis	$^{207}Pb/^{235}U$	± 2σ	$^{206}Pb/^{238}U$	± 2σ	Rho	$^{207}Pb/^{206}Pb$	± 2σ	$^{207}Pb/^{235}U$	± 2σ	$^{206}Pb/^{238}U$	± 2σ	$^{207}Pb/^{206}Pb$	± 2σ	Dis. (6/38/7/6)	Dis. (6/38/7/35)
BA23_1	4.25	0.07	0.2515	0.005	0.78802	0.1213	0.0012	1682	15	1445	26	1971	18	26.69	14.09
BA23_2	5.36	0.07	0.333	0.0055	0.66184	0.11519	0.001	1878.3	12	1852	27	1877	15	1.33	1.40
BA23_3	13.25	0.23	0.5056	0.0089	0.64412	0.1877	0.002	2696	16	2636	38	2722	18	3.16	2.23
BA23_4	15.7	0.23	0.5562	0.0097	0.6828	0.2024	0.0018	2858.8	14	2848	40	2841	15	-0.25	0.38
BA23_5	5.864	0.11	0.346	0.0069	0.6761	0.1209	0.0014	1952	17	1919	34	1965	22	2.34	1.69
BA23_6	5.98	0.09	0.3454	0.006	0.6384	0.1237	0.0012	1971	14	1911	29	2007	17	4.78	3.04
BA23_7	6.204	0.1	0.3575	0.0062	0.55705	0.1241	0.0013	2002.4	13	1969	29	2013	19	2.19	1.67
BA23_8	6.74	0.12	0.3842	0.008	0.85298	0.12581	0.001	2076	16	2095	38	2038	14	-2.80	-0.92
BA23_9	5.904	0.11	0.3457	0.0073	0.78211	0.1221	0.0013	1959	16	1912	35	1984	19	3.63	2.40
BA23_10	3.473	0.06	0.2646	0.0049	0.45043	0.094	0.0013	1518	14	1512	25	1500	26	-0.80	0.40
BA23_11	5.927	0.09	0.3532	0.006	0.63739	0.1204	0.0012	1963.2	13	1948	28	1959	17	0.56	0.77
BA23_12	6.479	0.11	0.3657	0.0069	0.78838	0.1269	0.0011	2040	15	2009	32	2052	16	2.10	1.52
BA23_13	6.536	0.1	0.3724	0.0064	0.48518	0.126	0.0015	2048	14	2041	31	2033	21	-0.39	0.34
BA23_14	13.38	0.22	0.517	0.0093	0.48156	0.1856	0.0023	2703	16	2684	40	2697	21	0.48	0.70
BA23_15	6.193	0.1	0.3644	0.0066	0.61126	0.1219	0.0014	2001	15	2001	31	1975	21	-1.32	0.00
BA23_16	6.353	0.1	0.3678	0.0067	0.62399	0.1243	0.0013	2023.8	13	2017	31	2011	19	-0.30	0.34
BA23_17	7.152	0.11	0.3861	0.0068	0.65446	0.1325	0.0012	2127.6	14	2103	31	2127	16	1.13	1.16
BA23_18	13.38	0.23	0.5169	0.01	0.71106	0.1864	0.0021	2707	16	2685	44	2704	19	0.70	0.81
BA23_19	5.863	0.09	0.3515	0.0062	0.64813	0.1196	0.0011	1953.9	13	1940	29	1943	17	0.15	0.71
BA23_20	5.935	0.1	0.3538	0.0067	0.53108	0.1207	0.0015	1964	14	1953	31	1956	23	0.15	0.56
BA23_21	13.56	0.28	0.5097	0.011	0.77204	0.19	0.0025	2715	19	2649	50	2736	21	3.18	2.43
BA23_22	6.264	0.1	0.3604	0.0064	0.63934	0.1249	0.0012	2012.2	13	1982	30	2024	18	2.08	1.50
BA23_23	6.1	0.2	0.353	0.012	0.90329	0.1237	0.0017	1983	28	1945	56	2006	25	3.04	1.92
BA23_24	5.566	0.08	0.3333	0.0056	0.5829	0.1201	0.0012	1908.1	13	1853	27	1952	18	5.07	2.89
BA23_25	5.38	0.14	0.3235	0.009	0.64885	0.1204	0.0024	1884	21	1804	44	1952	37	7.58	4.25
BA23_26	5.25	0.08	0.3278	0.0057	0.64788	0.1154	0.0011	1858.9	13	1826	28	1881	17	2.92	1.77
BA23_27	15.53	0.26	0.5344	0.01	0.64322	0.2088	0.0025	2847	17	2757	44	2893	19	4.70	3.16
BA23_28	5	0.08	0.3261	0.0055	0.6421	0.11019	0.001	1817.5	13	1818	27	1796	17	-1.22	-0.03
BA23_29	10.38	0.18	0.4576	0.0085	0.57008	0.1636	0.0021	2469	15	2426	38	2487	21	2.45	1.74

BA23_30	6.188	0.1	0.3559	0.0068	0.62681	0.1249	0.0015	2001	15	1961	32	2021	20	2.97	2.00
BA23_31	6.05	0.11	0.3573	0.0071	0.76222	0.1217	0.0012	1978	15	1969	34	1975	17	0.30	0.46
BA23_32	6.244	0.1	0.3652	0.0063	0.61985	0.1231	0.0013	2008	14	2005	30	1997	18	-0.40	0.15
BA23_33	6.117	0.1	0.3624	0.0069	0.7351	0.1211	0.0012	1988	15	1993	33	1966	18	-1.37	-0.25
BA23_34	5.88	0.1	0.3541	0.0066	0.71642	0.1194	0.0012	1956	15	1952	31	1942	18	-0.51	0.20
BA23_35	11.75	0.17	0.484	0.0082	0.59161	0.1745	0.0017	2583	14	2543	36	2601	16	2.23	1.55
BA23_36	6.914	0.12	0.3826	0.0077	0.71164	0.1302	0.0014	2100	15	2085	36	2095	20	0.48	0.71
BA23_37	7.2	0.14	0.3937	0.0081	0.63975	0.1322	0.0018	2134	19	2137	38	2124	24	-0.61	-0.14
BA23_38	2.97	0.07	0.2411	0.0047	0.55576	0.0886	0.0015	1395	16	1393	25	1384	32	-0.65	0.14
BA23_39	6.288	0.09	0.3662	0.0062	0.57414	0.1238	0.0012	2015.3	12	2010	29	2008	17	-0.10	0.26
BA23_40	6.75	0.13	0.3776	0.0076	0.57252	0.129	0.002	2074	17	2062	35	2072	27	0.48	0.58
BA23_41	6.771	0.1	0.3794	0.0067	0.64474	0.1291	0.0012	2081	14	2071	31	2081	17	0.48	0.48
BA23_42	6.233	0.09	0.3577	0.0062	0.57961	0.1257	0.0013	2008.1	13	1970	30	2034	18	3.15	1.90
BA23_43	6.466	0.09	0.3724	0.006	0.70152	0.12511	0.001	2040.1	12	2040	28	2026	14	-0.69	0.00
BA23_44	6.515	0.1	0.377	0.0065	0.67719	0.1248	0.0011	2045.3	13	2060	30	2022	15	-1.88	-0.72
BA23_45	6.37	0.12	0.3661	0.0074	0.65721	0.1254	0.0017	2024	17	2012	36	2027	24	0.74	0.59
BA23_46	16.68	0.32	0.558	0.012	0.6473	0.2159	0.003	2912	18	2853	49	2944	22	3.09	2.03
BA23_47	6.563	0.11	0.3654	0.0064	0.61326	0.1296	0.0014	2050	14	2007	31	2087	19	3.83	2.10
BA23_48	6.036	0.1	0.3589	0.0068	0.62635	0.1219	0.0013	1978	14	1974	32	1977	19	0.15	0.20
BA23_49	2.958	0.05	0.2399	0.0044	0.45576	0.0891	0.0012	1395	13	1385	23	1391	27	0.43	0.72
BA23_50	6.024	0.1	0.3501	0.0062	0.59003	0.1241	0.0015	1977	15	1936	30	2012	20	3.78	2.07
BA23_51	6.412	0.1	0.3666	0.0067	0.77721	0.1261	0.0011	2031	14	2018	33	2041	15	1.13	0.64
BA23_52	6.191	0.09	0.3667	0.006	0.5896	0.1219	0.0012	2001.9	13	2013	28	1980	17	-1.67	-0.55
BA23_53	6.39	0.13	0.3652	0.0075	0.638	0.1273	0.0018	2029	17	2005	35	2053	25	2.34	1.18
BA23_54	19.61	0.28	0.6103	0.01	0.66197	0.2317	0.002	3069.8	14	3068	41	3059	14	-0.29	0.06
BA23_55	6.094	0.09	0.3629	0.0061	0.55509	0.1216	0.0012	1987.1	13	1994	29	1975	17	-0.96	-0.35
BA23_56	10.54	0.15	0.4682	0.008	0.64295	0.1628	0.0014	2480.4	13	2473	35	2479	15	0.24	0.30
BA23_57	16.55	0.25	0.5688	0.0098	0.70408	0.2103	0.0018	2908	14	2900	40	2906	14	0.21	0.28
BA23_58	5.572	0.08	0.3438	0.0057	0.59168	0.1171	0.0011	1909.6	12	1904	27	1906	17	0.10	0.29
BA23_59	6.084	0.09	0.3664	0.0061	0.60103	0.1196	0.001	1986	12	2011	29	1948	16	-3.23	-1.26
BA23_60	6.302	0.09	0.3637	0.0059	0.66346	0.12494	0.001	2016.7	12	1999	28	2025	14	1.28	0.88
BA23_61	5.401	0.1	0.3396	0.0067	0.61486	0.1153	0.0015	1882	15	1884	33	1880	23	-0.21	-0.11
BA23_62	6.657	0.1	0.3817	0.0065	0.51056	0.1263	0.0013	2065.8	13	2083	30	2041	19	-2.06	-0.83
BA23_63	7.19	0.15	0.3881	0.0072	0.67874	0.134	0.0018	2133	18	2112	33	2145	23	1.54	0.98
BA23_64	4.761	0.08	0.2776	0.0051	0.54194	0.1245	0.0014	1775	14	1578	26	2013	20	21.61	11.10
BA23_65	7.48	0.14	0.3953	0.008	0.65764	0.137	0.0017	2169	16	2145	37	2183	22	1.74	1.11
BA23_66	6.047	0.1	0.3614	0.0062	0.54321	0.1214	0.0014	1980	14	1987	29	1971	20	-0.81	-0.35
BA23_67	6.055	0.09	0.3603	0.0064	0.59983	0.1215	0.0013	1982	13	1982	30	1971	19	-0.56	0.00
BA23_68	5.717	0.09	0.3482	0.0061	0.65036	0.119	0.0011	1931.1	13	1926	30	1936	17	0.52	0.26
BA23_69	6.905	0.11	0.3839	0.0066	0.63896	0.1305	0.0013	2099	14	2093	31	2097	18	0.19	0.29
BA23_70	18.97	0.29	0.6012	0.01	0.60787	0.2288	0.0023	3039	15	3031	42	3038	16	0.23	0.26
BA23_71	6.709	0.1	0.3765	0.0065	0.61907	0.129	0.0012	2071.3	13	2060	30	2083	16	1.10	0.55
BA23_72	5.687	0.08	0.3441	0.006	0.72166	0.1199	0.0011	1927	13	1905	29	1949	16	2.26	1.14
BA23_73	7.152	0.11	0.3903	0.0069	0.64867	0.1328	0.0013	2127	14	2122	32	2128	17	0.28	0.24
BA23_74	7.31	0.13	0.3948	0.0075	0.58945	0.1348	0.0018	2146	16	2145	35	2150	23	0.23	0.05
BA23_75	6.043	0.1	0.3605	0.0064	0.56929	0.122	0.0014	1980	14	1983	30	1979	21	-0.20	-0.15
BA23_76	4.613	0.07	0.3139	0.0055	0.57077	0.1064	0.0011	1748.7	13	1758	27	1730	20	-1.62	-0.53
BA23_77	6.288	0.11	0.3652	0.0066	0.38299	0.1249	0.0018	2012	15	2005	31	2014	26	0.45	0.35
BA23_78	6.297	0.1	0.3681	0.0062	0.54793	0.1245	0.0014	2017	14	2020	30	2016	19	-0.20	-0.15
BA23_79	7.632	0.12	0.4054	0.0071	0.52692	0.1371	0.0016	2186	14	2192	33	2181	20	-0.50	-0.27
BA23_80	5.989	0.09	0.361	0.0064	0.67392	0.1202	0.0011	1972	14	1985	30	1955	17	-1.53	-0.66
BA23_81	3.051	0.07	0.2481	0.0049	0.38046	0.0899	0.0019	1415	19	1427	25	1388	42	-2.81	-0.85
BA23_82	6.469	0.11	0.3685	0.0067	0.6676	0.1273	0.0013	2039	14	2020	31	2057	18	1.80	0.93
BA23_83	6.869	0.12	0.3811	0.0067	0.48868	0.1308	0.0017	2090	15	2079	31	2097	23	0.86	0.53
BA23_84	6.9	0.13	0.3756	0.0078	0.67655	0.1336	0.0017	2096	17	2053	37	2139	22	4.02	2.05
BA23_85	6.027	0.1	0.3607	0.0062	0.49161	0.1212	0.0015	1978	15	1986	30	1972	22	-0.71	-0.40
BA23_86	12.08	0.18	0.498	0.0085	0.61966	0.1759	0.0017	2607.7	14	2603	36	2609	16	0.23	0.18
BA23_87	6.525	0.1	0.3768	0.0063	0.65453	0.1255	0.0011	2046.7	13	2060	29	2034	15	-1.28	-0.65
BA23_88	5.881	0.09	0.3547	0.0061	0.64151	0.1205	0.0012	1956.6	13	1956	29	1958	17	0.10	0.03
BA23_89	8.63	0.14	0.4256	0.0079	0.73959	0.147	0.0013	2298	14	2283	35	2308	16	1.08	0.65
BA23_90	5.584	0.11	0.3384	0.007	0.68479	0.1202	0.0016	1910	16	1877	34	1954	23	3.94	1.73
BA23_91	6.158	0.1	0.3672	0.0065	0.8086	0.12154	0.0009	1995	14	2014	31	1974	14	-2.03	-0.95
BA23_92	6.011	0.09	0.3664	0.0064	0.54816	0.1197	0.0013	1976	14	2011	30	1942	20	-3.55	-1.77
BA23_93	5.25	0.14	0.3223	0.01	0.71735	0.1194	0.0026	1857	22	1798	49	1938	38	7.22	3.18
BA23_94	9.281	0.13	0.4447	0.0074	0.61647	0.152	0.0013	2364.7	13	2372	32	2364	14	-0.34	-0.31
BA23_95	5.81	0.13	0.3339	0.0074	0.81009	0.1258	0.0015	1943	19	1855	36	2033	21	8.76	4.53
BA23_96	5.258	0.09	0.3407	0.0063	0.64372	0.1122	0.0012	1860	14	1888	30	1827	20	-3.34	-1.51
BA23_97	6.2	0.09	0.3653	0.0063	0.51367	0.1234	0.0014	2003.5	13	2005	30	1998	20	-0.35	-0.07
BA23_98	6.48	0.14	0.3431	0.0074	0.68917	0.1369	0.0018	2037	18	1899	36	2180	23	12.89	6.77
BA23_99	5.755	0.09	0.3498	0.0062	0.61834	0.1192	0.0012	1937.6	13	1934	30	1937	18	0.15	0.19
BA23_100	5.912	0.09	0.354	0.0063	0.63689	0.1215	0.0012	1963.3	13	1952	30	1972	18	1.01	0.58
BA23_101	5.408	0.09	0.3406	0.0061	0.62853	0.1149	0.0012	1882	14	1888	29	1873	20	-0.80	-0.32
BA23_102	6.441	0.11	0.3722	0.0067	0.57129	0.1254	0.0014	2034	14	2037	32	2029	20	-0.39	-0.15
BA23_103	6.054	0.1	0.3617	0.0066	0.61456	0.1216	0.0014	1980	15	1988	31	1970	21	-0.91	-0.40
BA23_104	5.397	0.09	0.3352	0.0061	0.59357	0.1167	0.0013	1882	14	1866	30	1896	21	1.58	0.85
BA23_105	5.839	0.1	0.3552	0.0068	0.69503	0.1194	0.0012	1950	14	1957	32	1941	19	-0.82	-0.36
BA23_106	6.062	0.1	0.3608	0.0068	0.59358	0.122	0.0014	1981	14	1984	32	1978	20	-0.30	-0.15
BA23_107	13.28	0.19	0.5199	0.0091	0.59248	0.1849	0.0018	2698.5	14	2700	40	2693	16	-0.26	-0.06
BA23_108	5.811	0.09	0.3523	0.0066	0.61149	0.1199	0.0013	1945	14	1945	32	1945	20	0.00	0.00
BA23_109	6.143	0.1	0.3647	0.0069	0.6399	0.1227	0.0013	1995	14	2002	32	1990	19	-0.60	-0.35
BA23_110	6.012	0.1	0.3573	0.0066	0.60613	0.1218	0.0014	1973	15	1967	31	1974	21	0.35	0.30
BA23_111	5.49	0.15	0.3406	0.0093	0.64749	0.1171	0.0024	1894	23	1887	44	1901	37	0.74	0.37
BA23_112	6.778	0.12	0.3809	0.0072	0.66299	0.129	0.0014	2080	15	2078	34	2075	20	-0.14	0.10
BA23_113	16.94	0.28	0.5767	0.011	0.66032	0.2122	0.0025	2926	16	2940	44	2917	19	-0.79	-0.48

BA23_114	11.46	0.16	0.4871	0.0084	0.64268	0.17	0.0015	2559.7	13	2556	36	2554	15	-0.08	0.14
BA23_115	6.64	0.13	0.3737	0.0075	0.63675	0.1281	0.0015	2061	18	2046	36	2063	21	0.82	0.73
BA23_116	3.021	0.05	0.2482	0.0046	0.59248	0.08826	0.001	1411.4	12	1428	24	1385	22	-3.10	-1.18
BA23_117	13.45	0.2	0.5262	0.0097	0.69459	0.1854	0.0017	2710	15	2721	41	2696	16	-0.93	-0.41
BA23_118	7.218	0.12	0.3946	0.0073	0.57435	0.1328	0.0016	2137	14	2144	33	2127	21	-0.80	-0.33
BA23_119	6.043	0.09	0.3597	0.0065	0.59482	0.1214	0.0013	1979	14	1979	31	1972	19	-0.35	0.00
BA23_120	7.55	0.13	0.3978	0.0075	0.61195	0.1371	0.0017	2175	16	2156	35	2186	21	1.37	0.87
BA23_121	5.937	0.09	0.3535	0.0059	0.6058	0.1216	0.0011	1965.2	12	1950	28	1975	16	1.27	0.77
BA23_122	6.696	0.1	0.3808	0.0065	0.51771	0.1274	0.0014	2069.4	13	2078	31	2058	19	-0.97	-0.42
BA23_123	4.867	0.08	0.3216	0.0058	0.53441	0.1097	0.0013	1793	14	1796	28	1787	22	-0.50	-0.17
BA23_124	6.194	0.1	0.3691	0.0064	0.37733	0.1218	0.0016	2000	14	2023	30	1972	23	-2.59	-1.15
BA23_125	10.11	0.16	0.4545	0.0085	0.63499	0.1611	0.0017	2444	15	2413	38	2464	19	2.07	1.27
BA23_126	6.229	0.11	0.3642	0.0063	0.4958	0.1232	0.0016	2005	15	2002	30	1995	23	-0.35	0.15
BA23_127	6.11	0.12	0.3565	0.0081	0.59293	0.1247	0.002	1990	17	1963	38	2016	28	2.63	1.36
BA23_128	5.94	0.21	0.343	0.0094	0.52311	0.1252	0.0037	1961	31	1899	45	2017	52	5.85	3.16
BA23_129	7.31	0.13	0.3922	0.0073	0.52167	0.135	0.0019	2148	16	2131	33	2153	25	1.02	0.79
BA23_130	6.423	0.1	0.3733	0.0066	0.55025	0.1247	0.0014	2032	14	2043	31	2015	20	-1.39	-0.54
BA23_131	21.25	0.33	0.6335	0.011	0.6601	0.2436	0.0023	3148	15	3159	44	3139	15	-0.64	-0.35
BA23_132	6.833	0.11	0.3758	0.0067	0.60901	0.1314	0.0014	2088	14	2057	32	2111	20	2.56	1.48
BA23_133	11.88	0.19	0.485	0.0088	0.61931	0.1773	0.002	2592	15	2546	38	2619	19	2.79	1.77
BA23_134	5.838	0.09	0.356	0.0063	0.62036	0.1189	0.0012	1951	13	1961	30	1933	19	-1.45	-0.51
BA23_135	6.059	0.1	0.3633	0.0068	0.47621	0.1214	0.0016	1981	15	1998	31	1965	25	-1.68	-0.86
BA23_136	6.366	0.11	0.3673	0.0067	0.75147	0.1253	0.0012	2024	15	2021	32	2027	16	0.30	0.15
BA23_137	3.96	0.11	0.2577	0.0069	0.71566	0.1118	0.0019	1614	23	1473	35	1818	29	18.98	8.74
BA23_138	6.194	0.11	0.3582	0.0073	0.72967	0.1261	0.0014	2002	16	1975	35	2039	20	3.14	1.35
BA23_139	5.804	0.09	0.3442	0.0064	0.6132	0.1225	0.0014	1944	14	1905	30	1986	20	4.08	2.01
BA23_140	5.01	0.23	0.308	0.013	0.91881	0.1175	0.0021	1816	39	1724	65	1911	32	9.79	5.07

Sample BA22															
Isotopic ratios								Concordia ages (Ma)							
Analysis	$^{207}Pb/^{235}U$	± 2σ	$^{206}Pb/^{238}U$	± 2σ	Rho	$^{207}Pb/^{206}Pb$	± 2σ	$^{207}Pb/^{235}U$	± 2σ	$^{206}Pb/^{238}U$	± 2σ	$^{207}Pb/^{206}Pb$	± 2σ	Dis. (6/38/7/6)	Dis. (6/38/7/35)
BA22_1	2.456	0.06	0.1385	0.0029	0.37065	0.1277	0.0019	1256	17	836.1	16	2057	26	59.35	33.43
BA22_2	1.955	0.05	0.183	0.0043	0.66686	0.077	0.001	1099	17	1083	24	1120	25	3.30	1.46
BA22_3	6.828	0.14	0.3844	0.0078	0.60383	0.1282	0.0011	2087.9	18	2097	36	2068	15	-1.40	-0.44
BA22_4	7.28	0.17	0.3941	0.0089	0.6299	0.1327	0.0016	2143	21	2140	41	2130	22	-0.47	0.14
BA22_6	6.617	0.15	0.3664	0.009	0.00065	0.141	0.022	2061	21	2012	42	2097	27	4.05	2.38
BA22_7	6.97	0.19	0.3914	0.0094	0.63606	0.1294	0.0019	2104	24	2126	44	2078	26	-2.31	-1.05
BA22_8	1.118	0.04	0.1057	0.0027	0.37944	0.076	0.0017	761	17	648	16	1094	48	40.77	14.85
BA22_9	7.94	0.18	0.4184	0.0091	0.55511	0.1371	0.0016	2223	20	2251	41	2187	20	-2.93	-1.26
BA22_10	7.56	0.23	0.3983	0.0097	0.3208	0.1379	0.0035	2169	28	2160	46	2164	45	0.18	0.41
BA22_11	7.75	0.24	0.4113	0.011	0.36134	0.1371	0.0034	2194	28	2216	52	2162	45	-2.50	-1.00
BA22_12	3.167	0.07	0.2538	0.0052	0.46734	0.09013	0.0007	1448.2	16	1458	27	1424	14	-2.39	-0.68
BA22_13	3.151	0.07	0.2528	0.0052	0.64525	0.09019	0.0007	1445	16	1452	27	1426	14	-1.82	-0.48
BA22_15	6.5	0.18	0.3597	0.011	0.69432	0.1305	0.0024	2043	25	1978	54	2103	33	5.94	3.18
BA22_16	7.12	0.23	0.3736	0.012	0.53211	0.1402	0.0035	2117	28	2041	55	2206	45	7.48	3.59
BA22_17	9.12	0.29	0.3517	0.0083	0.54185	0.1877	0.004	2337	29	1940	39	2707	36	28.33	16.99
BA22_18	14.5	0.3	0.5435	0.011	0.74496	0.1936	0.0013	2782.1	20	2796	48	2770	11	-0.94	-0.50
BA22_19	6.429	0.15	0.3666	0.0078	0.49744	0.1266	0.0016	2033	20	2012	37	2042	22	1.47	1.03
BA22_20	5.63	0.15	0.3491	0.0076	0.54845	0.117	0.0018	1913	23	1928	36	1903	28	-1.31	-0.78
BA22_21	15.91	0.77	0.537	0.027	0.77825	0.2166	0.0066	2863	46	2760	110	2946	49	6.31	3.60
BA22_22	7.26	0.25	0.3982	0.01	0.23833	0.133	0.0041	2133	31	2158	48	2115	53	-2.03	-1.17
BA22_23	18.49	0.4	0.5952	0.013	0.68755	0.2241	0.002	3013.5	20	3007	51	3008	14	0.03	0.22
BA22_24	5.88	0.26	0.348	0.013	0.506	0.1225	0.0047	1951	39	1924	64	1975	69	2.58	1.38
BA22_25	4.1	0.16	0.2851	0.008	0.35271	0.1062	0.0036	1640	32	1615	40	1668	64	3.18	1.52
BA22_26	6.75	0.22	0.362	0.013	0.59537	0.1353	0.0037	2077	29	1989	63	2160	47	7.92	4.24
BA22_27	9.13	0.22	0.2976	0.0072	0.77229	0.2222	0.0023	2348	22	1678	36	2993	17	43.94	28.53
BA22_28	12.73	0.32	0.4175	0.011	0.55395	0.2208	0.0039	2658	24	2247	51	2981	28	24.62	15.46